Ternary and quaternary phases in the alkali-earth - rhenium - oxygen system

Vom Fachbereich Material- und Geowissenschaften
der Technischen Universität Darmstadt

zur
Erlangung des akademischen Grades eines
Doktor rer. nat.
genehmigte Dissertation

angefertigt von
Dipl.-Chem. Kirill G. Bramnik

Berichterstatter:	Prof. Dr. H. Fuess
Mitberichterstatter:	Prof. Dr. J. Galy
	Prof. Dr. H.M. Ortner

Tag der Einreichung: 09.05.2001
Tag der mündlichen Prüfung: 07.06.2001

Darmstadt 2001

D 17

Моим родителям

1 Introduction

The structural chemistry of complex rhenium oxides is very rich. The oxidation state of rhenium cations may be varied by a change of cation and/or anion composition as well as conditions of synthesis and can result in a formation of different structure types. In the formal oxidation state +7 rhenium occurs tetrahedrally or octahedrally coordinated as, for example, in Re_2O_7, where half of the rhenium atoms is situated in tetrahedra and another half has octahedral coordination [1]. Also a square pyramidal oxygen coordination is known for Re^{+7} [2]. An example of a 5-fold coordination for rhenium in the oxidation state +7 is the trigonal-bipyramidal oxygen environment in Na_3ReO_5 [3]. On the other hand, only 6-fold coordination is known for Re^{+6} in oxides. However, the octahedral environment varies from the perfect octahedron in ReO_3 [4] to the distorted one in Ca_3ReO_6 [5]. A decrease of the oxidation state of rhenium (<6) should lead to the formation of structures, containing cluster groups with different order of metallic Re-Re bonds. The Re_2O_{10} cluster is known for the average oxidation state of rhenium atoms between +4 and +5.5. The Re_2O_8 group on the contrary was found only in the compounds containing Re^{+4}. The oxidation state of rhenium in such double oxides will influence the charge carrier concentration and, consequently, the electrical and magnetic properties of these compounds. Nevertheless, there are only rare cases of careful structure-properties investigations in these systems. This fact can be explained by highly sophisticated preparation methods, which are required to synthesise single crystals suitable for diffraction experiments or single phase compounds with rhenium in the low oxidation states, *i.e.* less than +7, since rhenium in oxides is most stable in its highest oxidation state. Therefore, it is necessary to develop new synthetic techniques for synthesis of ternary rhenium oxides with desired cation composition and oxygen content.

Only one attempt to observe and build a phase diagram for the ternary rhenium oxides was carried out (BaO-Re-Re_2O_7) [6]. However, information for other alkali-earth - rhenium - oxygen systems is very scarce. Hence, it is impossible to discuss about tendencies of ternary rhenium oxides to adopt one or another structure

type because of the lack of available data. On the example of alkali-earth rhenium ternary oxides we propose to investigate the influence of different radii of alkali-earth elements on forming different structure types, and changing of physical properties.

The physical properties of most of the known compounds with rhenium in the low oxidation states were studied seldom even in the rare cases of thoroughly investigated compounds. The most interesting points of rhenium oxides physics are the superconductivity of rhenium bronzes [7] and metallic properties of ReO_3 [8]. It was predicted on the base of the strong electron-phonon coupling, that ReO_3 should be a superconductor at *ca*. 1.2 K, but this transition was not observed till 0.02 K [9]. But despite of these promising effects information about different magnetic and electric properties of ternary rhenium oxides and relationship to their structures is practically missing in the literature.

The aim of this work is to add to the structural knowledge in the systems containing alkali-earth elements and rhenium in low oxidation states and to investigate their magnetic properties.

2 Literature survey

2.1 Structural chemistry of ternary rhenium oxides

Rhenium may exhibit different oxidation states from +4 to +7 in oxides. At the present time only compounds containing Re (+7) are well studied, while the information about reduced Re-containing oxides ($V_{Re} < +7$) is very limited. In spite of the rich chemistry of rhenium in a low oxidation state the synthetic problems discourage the research in this field: Re cations with ($V_{Re} < +7$) are easily oxidised to Re^{+7} and, moreover, they have the strong tendency to disproportionate. Such compounds attract the attention of scientists in basic research for their various interesting physical properties. For example, rhenium bronzes A_xReO_3 (A = Li, K) exhibit superconducting properties at low temperatures [7] as mentioned above.

The formation of reduced Re-based oxides is often accompanied by the occurrence of Re-Re bonds in their structures. Two types of such clusters are known. The Re_2O_8 one with triple Re-Re bonding was found only in the compounds containing Re^{+4} (electron configuration d^3). An average Re-Re distance in this structural unit is 2.259 Å [11], thus significantly shorter than the same one in metallic rhenium (2.76 Å) [10]. This Re-Re distance value is very close to the metal-metal bonds distance in $Re_2Cl_8^{2-}$ units (2.24 Å) despite the difference in oxidation state of the Re atoms in these compounds. The formal oxidation state, +3, of rhenium in $Re_2Cl_8^{2-}$ and the diamagnetic behaviour of compounds with this group, gave rise to the suggestion of 4-fold Re-Re bonds [11]. Re_2O_8 clusters consist of two ReO_4 square pyramids with Re at the top, see Fig. 1. The Re-O distances are 1.915 Å, and the Re atom lies 0.42 Å above the basal plane of the square pyramid. These two ReO_4 groups, regarded as a Re_2O_8 unit , are connected with each other by a Re-Re bond in an eclipsed conformation, forming an elongated cube with two different O-O distances: eight distances of 2.642 Å and four of 3.099 Å [12].

The Re_2O_{10} cluster may be formed when the average oxidation state of rhenium atoms is in the range of +4 to +5.5. The Re-Re distance in the Re_2O_{10} group varies from 2.40 to 2.61 Å (see Table 1), corresponding to double bonds between

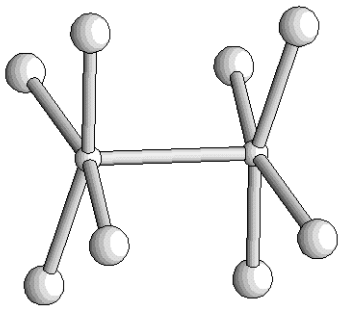

Fig. 1: Structure of the Re_2O_8 cluster.

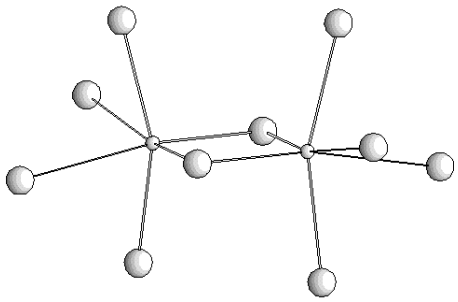

Fig. 2: Structure of the Re_2O_{10} cluster.

rhenium cations. The Re_2O_{10} units are built up by two distorted edge-sharing ReO_6 octahedra, see Fig. 2. The "ideal" Re_2O_{10} group was calculated based on the Re-O distance of 1.96 Å for the Re^{+5}. For such a unit a Re-Re distance of 2.77 Å is calculated if the Re atoms are located precisely in the centre of each octahedron. This distance corresponds precisely to that of metallic rhenium [13].

The Re_2O_8 group was found in the crystal structure of La_2ReO_5 [12]. It crystallises with tetragonal symmetry and may be formally considered as a fluorite-related structure (cell parameters $a \approx \sqrt{2}\, a_{\text{fluorite}}$, $c \approx a_{\text{fluorite}}$). All O atoms, forming a somewhat distorted primitive cubic oxygen arrangement, are on fluoride sites, while La atoms occupy four of five Ca sites and the fifth accommodates a pair of Re atoms with the Re-Re bond aligned parallel to the *c* axis.

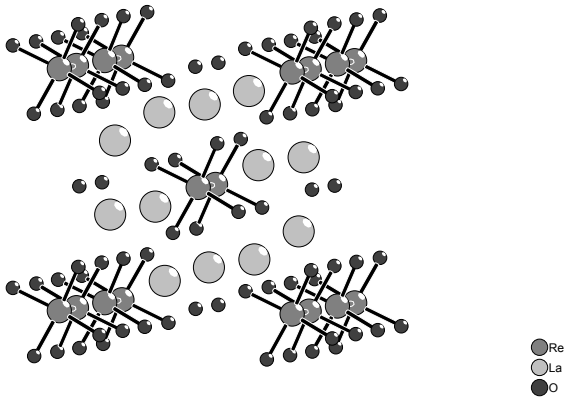

Fig. 3: The structure of La_2ReO_5.

The La_2ReO_5 structure consists of isolated Re_2O_8 clusters, which are linked together by La_4O tetrahedra (see Fig. 3). The formal oxidation state of Re is equal to +4, all three electrons are involved in the formation of the 3-fold metal-metal bonding and localised on the binuclear groups Re_2O_8. The Re-Re distance in this unit is 2.259(1)

Å. Compounds with this structure type are known for rare-earth elements from La to Gd. The Re_2O_8 unit looks different in the Ln_2ReO_5 compounds for *Ln* = Sm, Eu and Gd. Two ReO_4 groups, forming a Re_2O_8 unit, are connected with each other by a Re-Re bond in a staggered conformation in contrast to eclipsed conformation of this group in the structure type described above. The nearest oxygen atoms form an antiprismatic coordination for the Re-Re pairs [14]. The Re-Re distance of 2.251(1) Å in this unit is very close to the one in the La_2ReO_5 compound.

Table 1. Crystallographic data for the compounds with Re_2O_{10} units.

Compound	Space group	d(Re-Re), Å.	Bonding type of Re_2O_{10} units	Formal oxidation state of Re atoms	Ref.
$Nd_4Re_2O_{11}$	$P4_2/n$	2.421(1)	Isolated	+5.0	[17]
$La_4Re_6O_{19}$	$I23$	2.422(7)	3-dimensional network	+4.3	[23]
Sr_xReO_3 ($0.4 \le x \le 0.5$)	$Im\bar{3}$	2.429(7)	3-dimensional network	+5.0-5.2	[24]
$Pb_6Re_6O_{19}$	$Pn3$	2.455(2)	3-dimensional network	+4.3	[25]
$Tm_5Re_2O_{12}$	$C2/m$	2.455(1) 3.129(1)	Chains	+4.5	[18]
$La_6Re_4O_{18}$	$P\bar{1}$	2.456(5)	Isolated	+4.5	[15]
$La_3Re_2O_{10}$	$C2/m$	2.484(1)	Isolated	+5.5	[16]
$BiRe_2O_6$	$C2/m$	2.508(1)	Layers	+4.5	[20]
ß-ReO_2	$Pbcn$	2.61	3-dimensional network	+4.0	[22]
$PbRe_2O_6$	$R\bar{3}m$	3.102(1)	3-dimensional network	+5.0	[13]
Re_2O_{10} calculated.		2.77			[13]

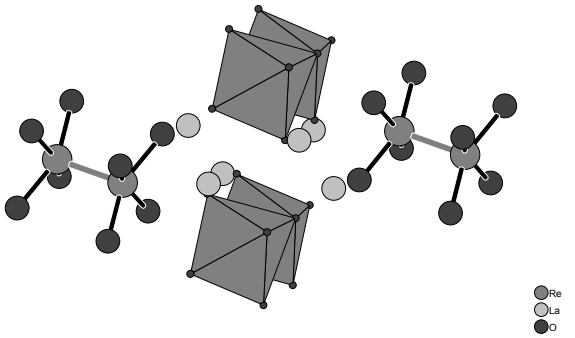

Fig. 4: The structure of the $La_6Re_4O_{18}$ compound.

Isolated Re_2O_8- and Re_2O_{10}- clusters exist in the $La_6Re_4O_{18}$ compound [15], which crystallises with triclinic symmetry. Therefore, $La_6Re_4O_{18}$ is more precisely described as $La_6[Re_2O_8][Re_2O_{10}]$ (see Fig. 4). The Re-Re distances in these groups are 2.235 Å and 2.456 Å, respectively. The Re_2O_8 and Re_2O_{10} groups are only linked by La atoms. The formal oxidation state of Re +4.5 in this compound suggest two different oxidation states: Re^{+4} in the Re_2O_8 unit and Re^{+5} in the Re_2O_{10} one.

There is a great variety of links between the Re_2O_{10} groups and, therefore, a large number of structure types exist with Re_2O_{10} as the main structural units: examples for compounds with isolated Re_2O_{10} groups are $Nd_4Re_2O_{11}$, $La_3Re_2O_{10}$ and $La_6Re_4O_{18}$. However, Re_2O_{10} groups can also be connected by corner-sharing, resulting in two-dimensional layers ($BiRe_2O_6$) and three-dimensional networks (β-ReO_2, $La_4Re_6O_{19}$, $PbRe_2O_6$) (see also Table 1) or by edge-sharing, forming infinite chains ($Tm_5Re_2O_{12}$).

The $Nd_4Re_2O_{11}$ and $La_3Re_2O_{10}$ crystal structures comprise the isolated Re_2O_{10} groups. Synthesis of the latter one was carried out by hydrothermal methods (700 ^{0}C, 3 kbar). The Re-Re bond length in the $La_3Re_2O_{10}$ structure is 2.484 Å [16]. This structure contains Re in the highest oxidation state observed of +5.5, which allows a metal-metal bonding. Each Re pair in $La_3Re_2O_{10}$ has two electrons available for Re-Re σ-bonding and an additional unpaired electron. The fact that all rhenium atoms are crystallographically equivalent shows that the unpaired electron cannot be assigned to a particular atom. However, the semiconducting behaviour of this compound indicates that this electron is localised within each Re_2O_{10} unit. Two crystallographically non-equivalent eight-coordinated lanthanum atoms interconnect the isolated Re_2O_{10} groups.

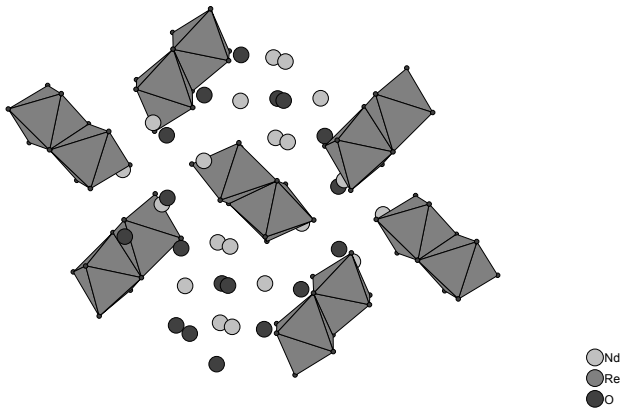

Fig. 5: The structure of the $Nd_4Re_2O_{11}$ compound.

The $Nd_4Re_2O_{11}$ crystal structure [17] differs significantly from the Nd_2ReO_5 one, which contains the Re_2O_8 groups and is isostructural to La_2ReO_5 described above, despite the similarity of chemical composition. There are isolated Re_2O_{10} clusters instead of Re_2O_8 ones in the $Nd_4Re_2O_{11}$ structure. These isolated units are linked together by Nd_4O (see Fig. 5). The Nd atoms have a 8-fold coordination of neighbouring oxygen atoms. The Nd-O distances lie in the range of 2.32-2.55 Å.

Another connectivity scheme of Re_2O_{10} clusters is realised in the $Tm_5Re_2O_{12}$ structure [18], $Y_5Mo_2O_{12}$ structure type. It comprises distorted ReO_6 octahedra, which form infinite chains along the [010] axis by common edges with alternating rhenium-rhenium distances of 2.455 and 3.219 Å (see Fig. 6). The first one corresponds to the double metal-metal bonding and, therefore, the structure may be considered to belong to the class of structures with edge-sharing Re_2O_{10} groups. These chains are interconnected along the [001] axis by TmO_6 octahedra, linked by the O atoms, which form a common edge between the short rhenium-rhenium bonds. Other Tm atoms are situated in between these layers and have monocapped trigonal prisms oxygen coordination. These TmO_7 prisms are arranged in two nonequivalent zigzag chains.

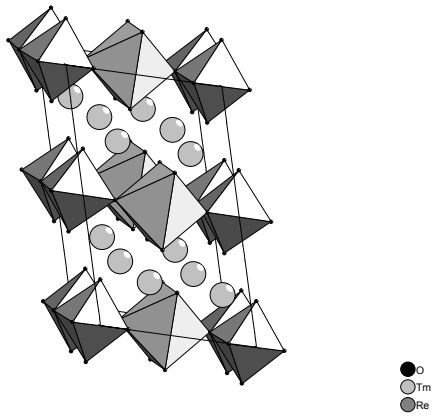

Fig. 6: The structure of the $Tm_5Re_2O_{12}$ compound.

A three-dimensional structure similar to $Tm_5Re_2O_{12}$ described above was found for $CoReO_4$ synthesised under high-pressure (30 kbar) [19]. The connectivity scheme of the coordination octahedra around Co and Re atoms in this compound is identical to that in the rutile structure type. The projection of the $CoReO_4$ structure along [001] is shown in Fig. 7. ReO_6 octahedra are linked by edge-sharing, forming infinite chains with ReO_4 composition. The Re-Re distance in these chains is larger

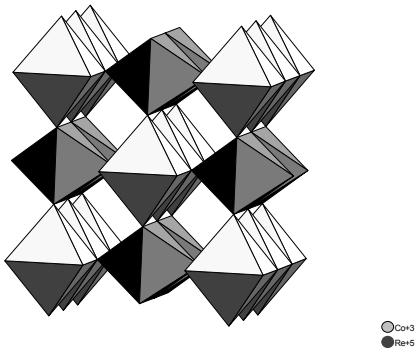

Fig. 7: The structure of the $CoReO_4$ compound.

than in metallic rhenium and equal to 2.8923(3) Å. The infinite chains of rhenium polyhedra are linked via common corners with similar infinite chains of edge-sharing CoO_6 octahedra. This is the only example of a reliably solved structure of an oxide containing rhenium in low oxidation state, +7, and a 3*d* element.

The $BiRe_2O_6$ crystal structure also contains Re_2O_{10} groups [20]. They are linked together by corner-sharing of octahedra, alternating with Bi atoms and form infinite two-dimensional Re_2O_6 layers. The Re_2O_6 layers can be regarded as slices as

in the rutile structure type. There are two different arrangements of oxygen atoms in these layers. One of them can be converted into the other by rotating a ReO_6 octahedron through 90° about its Re-Re axis. This operation is equivalent to a shift of the layer by ½, ½, ½ in the rutile structure. The structure is disordered due to the random stacking of the Re layers. The Re-Re distance of 2.5 Å in the Re_2O_{10} unit is comparable to that in similar compounds. Recently a new compound, $SbRe_2O_6$ with a structure similar to $BiRe_2O_6$ was reported [21]. However, the different stacking sequence of the Re_2O_6 layers in $SbRe_2O_6$ and $BiRe_2O_6$ results in different space groups ($SbRe_2O_6$, *C2/c*; $BiRe_2O_6$, *C2/m*). In contrast to the $BiRe_2O_6$ structure, where each Re_2O_6 layer is disordered in two different arrangements, Re_2O_6 layers in $SbRe_2O_6$ are stacked in the ordered sequence of ABAB….

An orthorhombic modification of rhenium dioxide, β-ReO_2, belongs to the MoO_2 structure type [22] (see Fig. 6). The β-ReO_2 crystal structure contains edge-sharing ReO_6 octahedra, forming infinite chains with Re_nO_{4n+2} composition like in the $Tm_5Re_2O_{12}$ structure described above. Contrary to it, the chains are connected together by corner-sharing, forming a three-dimensional network. Note that the Re-Re distance of 2.61 Å is considerably longer than the same one in other structures containing Re_2O_{10} groups (2.42-2.51 Å). Each Re atom in β-ReO_2 has two short metal-metal distances with its neighbours, for that reason multiplication of metal-metal bonds becomes equal to 1 and leads to its prolongation to 2.61 Å.

Another compound, where Re_2O_{10} clusters are not isolated from each other, is $La_4Re_6O_{19}$. It crystallises with the body-centred cubic cell [23]. The Re_2O_{10} groups are connected by corner-sharing, forming a three-dimensional network with ReO_3 composition, so that two apical oxygen atoms from one cluster are equatorial for the other one. The hexagonal channels in the framework are filled by La atoms, having a 10-fold coordination and forming perfect La_4O tetrahedra (see Fig.7), so the formula of this compound may be written as $(La_4O)\times(Re_6O_{18})$. The formal oxidation state of Re in the $La_4Re_6O_{19}$ structure is $+4^1/_3$, $d_{Re\text{-}Re} = 2.422$ Å.

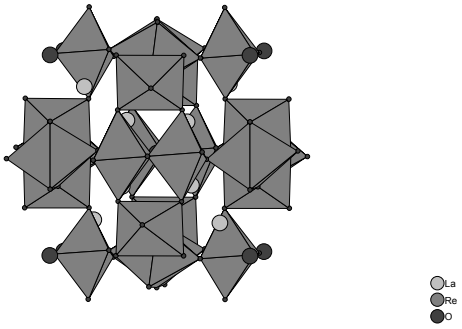

Fig. 8: The structure of the $La_4Re_6O_{19}$ compound.

Re_2O_{10} clusters are connected with each other to form a three-dimensional framework in Sr_xReO_3 ($0.5 \geq x \geq 0.4$) [24] in the same way as in $La_4Re_6O_{19}$. The Sr_xReO_3 compound was synthesised by annealing under high pressure (50 kbar, 900^0C). The Re-Re distance in the Re_2O_{10} group for this structure is 2.429 Å. The only difference between these two structures is filling of the channels in the framework. The Sr atoms are situated in the interstices of the channels statistically (occupation number 0.3) on the 16f position of $Im\bar{3}$ space group and have a 9-fold coordination.

The $Pb_6Re_6O_{19}$ oxide, (S.G. Pn3) [25], was synthesised from the highly reactive ReO_3, which was prepared by decomposition of $Re_2O_7 \times 2THF$. The $Pb_6Re_6O_{19}$ structure comprises the same network of Re_2O_{10} groups as $La_4Re_6O_{19}$ and Sr_xReO_3. There are two crystallographically non-equivalent Pb sites in this structure. The first one forms perfect Pb_4O tetrahedra with oxygen in the centre. The second one belongs to an irregular 12-fold polyhedron, which may be described as two trigonal antiprisms with common three-fold axis, six short equatorial distances of d_{Pb-O} = 2.52-2.62 Å and six long ones of d_{Pb-O} = 3.23-3.53 Å result.

The $Pb_6Re_6O_{19}$, $Sr_{2.4}Re_6O_{18}$ and $La_4Re_6O_{19}$ structures have the same cubic framework formed by Re_2O_{10} groups, but differ by the distribution of A-cations into the hexagonal channels. These formulae can be written as $(Pb_2)(Pb_4O)(Re_6O_{18})$, $(Sr_{2.4})(Re_6O_{18})$ and $(La_4O)(Re_6O_{18})$ to distinguish between atoms belonging to the framework and those located inside the channels. Note that ordering of A-cations occurs with increasing number of filled interstices and leads to a decrease of symmetry. Accordingly, as the Sr atoms fill the interstices statistically, the $Sr_{2.4}Re_6O_{18}$ structure has $Im\bar{3}$ symmetry. Symmetry is reduced to $I23$ by ordering of

the La atoms in the $La_4Re_6O_{19}$ structure. Further addition of A-cations, located in the hexagonal channels, results in the formation of a primitive cubic cell for the $Pb_6Re_6O_{19}$ structure (S.G. Pn3) instead of a body-centred cell as for the other compounds with three-dimensional frameworks of Re_2O_{10} clusters. The $Pb_6Re_6O_{19}$, $Sr_{2.4}Re_6O_{18}$ and $La_4Re_6O_{19}$ structures exhibit three different ways of filling the channels in the cubic framework based on Re_2O_{10} units.

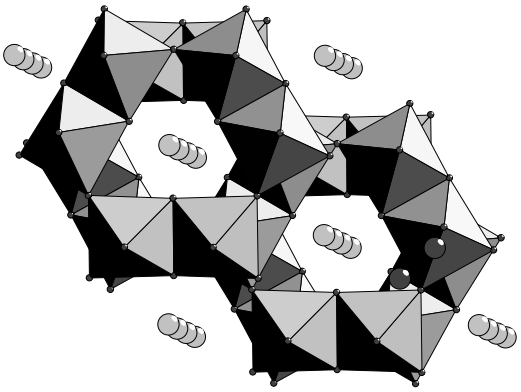

Fig. 9: The structure of the $PbRe_2O_6$ compound.

There is one more compound, $PbRe_2O_6$, with a three-dimensional network of Re_2O_{10} groups in the Pb-Re-O system. This oxide contains Re in its formal oxidation state of +5 and crystallises with a trigonal unit cell (S.G. $R\bar{3}m$) (see Fig. 9). The Re_2O_{10} groups in the $PbRe_2O_6$ structure form a three-dimensional net with channels parallel to the three-fold axis, which are filled by lead atoms [13]. The Re-Re distance within the Re_2O_{10} groups is 3.102 Å and in contrast to all other known structures with this unit, it is considerably longer than in metallic rhenium, and so it cannot be considered as a metal-metal bond. This is a result of the different geometrical arrangements of the Re_2O_{10} groups.

To explain the elongated Re-Re distance in the $PbRe_2O_6$ structure this structure may be compared with the $La_4Re_6O_{19}$ structure described above. Both structures contain Re_2O_{10} units in a three-dimensional network. The packing is, however, different in the two compounds: In $La_4Re_6O_{19}$, the Re_2O_{10} groups are connected by two common corners in such a way that one edge of a second unit links the top oxygen atoms of the first unit. Therefore the distance of the octahedron edge of the first group is the same as the distance of the apical oxygen atoms.

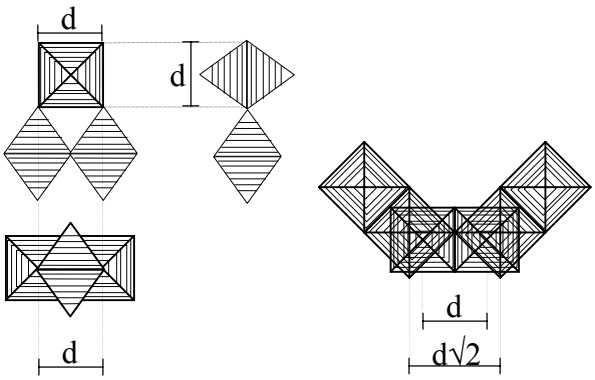

Fig. 10: Description of the connection of two Re_2O_{10} units in $La_4Re_6O_{19}$ (left) and $PbRe_2O_6$ (right).

The $PbRe_2O_6$ structure has a different three-dimensional arrangement: The Re_2O_{10} units are stacked in such a way that the distance between two top oxygen atoms is stretched. Two adjacent Re_2O_{10} groups are connected with each other by only one common corner. Therefore the distance between two apical oxygen atoms is $d\sqrt{2}$, which is the diagonal of the basis of an octahedron of edge length *d*. As the top oxygen atoms of the Re_2O_{10} groups are more distant from each other in $PbRe_2O_6$ than in the other compounds, the Re-Re distance is increased. It seems therefore that the long Re-Re distance of 3.102 Å in $PbRe_2O_6$ is a result of packing effects in the structure. The rhenium-rhenium distance of 3.709 Å for corner-connected ReO_6 octahedra is similar to that observed in ReO_3 (3.747 Å). A schematic description of the connection of two Re_2O_{10} units in $La_4Re_6O_{19}$ and $PbRe_2O_6$ respectively is presented in Fig. 10 for comparison.

Several other compounds with Re in a formal oxidation state less than +7 are known. They are built up from other characteristic structure units and different structure types result as compared to the examples described above. One more compound, $BiReO_4$, has been reported for the $Bi_2O_3/ReO_2/ReO_3$ system. It was defined on the basis of X-ray single-crystal data, that the $BiReO_4$ crystal structure (containing Re (V) with a $5d^2$ electron configuration) consists of sheets of corner-sharing ReO_6 octahedra (S.G. *Cmcm*). These layers are perpendicular to the *b* axis and linked by Bi atoms (alternate sheets being displaced by one-half octahedron) [20].

An oxide with Re in an oxidation state less than +5 and without Re-Re bonding was found in the $PbO\text{-}ReO_2\text{-}ReO_3$ system [26]. This compound, $Pb_2Re_2O_{7-x}$,

has an anion-deficient pyrochlore-type structure. If one considers the pyrochlore structure as built of two interpenetrating networks, the general formula may be written as $A_2O' \times B_2O_6$. The *B* cations are surrounded by oxygen octahedra forming a framework which contains interconnected channels, in which *A* cations and O′ atoms are located. The O′ atoms are bound with *A*-type cations only and do not belong to the framework formed by BO_6 octahedra. The O′ sites may be partially or completely empty, which generates oxygen nonstoichiometry in pyrochlores. It is known that pyrochlores with variable oxygen content, where *A* sites are occupied by cations with a $6s^2$ electron pair (Tl^I, Pb^{II} and Bi^{III}) may exhibit ordering of oxygen atoms and vacancies [27]. One more rhenium-containing compound, $Cd_2Re_2O_7$, with pyrochlore-type structure is known [28].

Two more structure types are reported in the *Ln*-Re-O system (*Ln*: rare-earth elements) with Re in low oxidation states. The first one, Sm_3ReO_7, consists of slightly distorted ReO_6 octahedra, which build up corner-sharing chains along the [001] direction [29]. Rhenium has the formal oxidation state of +5, but no metal-metal bond is observed in this compound. Two crystallographic independent Sm sites, six- and eight-fold coordinated, exist in this structure type. The oxygen arrangements of the first one may be described as a strongly distorted octahedron, which form edge-sharing chains along the [001] direction. The coordination polyhedron for the second Sm site can be described as a rhombic prism. These polyhedra, ReO_6, SmO_6 and SmO_8 are interconnected to each other to form a three-dimensional network.

Another structure type, Ln_6ReO_{12}, (*Ln* = Ho, Er, Tm, Yb, Lu) is the only example of rare-earth rhenium oxides with a formal oxidation state of rhenium +6. The structure comprises isolated ReO_6 octahedra which are connected with LnO_7 units by common oxygen, to six of them by edge-sharing and to six others by corner-sharing [30].

At present, only a few double oxides of alkaline-earth metals and low valence Re have been reported and for only some of them a reliable structural characterisation has been performed. Almost all compounds found in the systems comprising alkaline-earth and rhenium oxides with Re in formal oxidation state between +6 and +7 have perovskite-related structures. Exceptions are the high-

pressure phase, Sr_xReO_3, described above that consists of Re_2O_{10} groups in its structure [24] and the high-pressure phase $Ca_{1+x}Re_2O_6(OH)_{2x}$ (x=0.3) with a pyrochlore-like arrangement [31]. The perovskite structure type exhibits numerous lattice distortions dependent on the type of cations in the *A*- and *B*-sublattices.

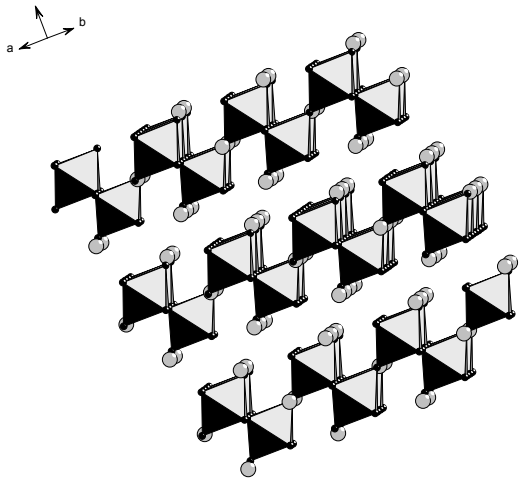

Fig. 11: The structure of the $Ba_3Re_2O_9$ compound.

The $Ba_3Re_2O_9$ [32] oxide has hexagonal perovskite-like structures based on a 9R(*chh*)$_3$ close-packed stacking of the BaO_3 layers where Re atoms are situated in the octahedral interstices. Units of three face-sharing octahedra are linked by corner-sharing and form infinite chains along the [001] direction. The middle octahedron of these units is vacant to overcome the electrostatic repulsion between the highly charged neighbouring Re^{+6} cations.

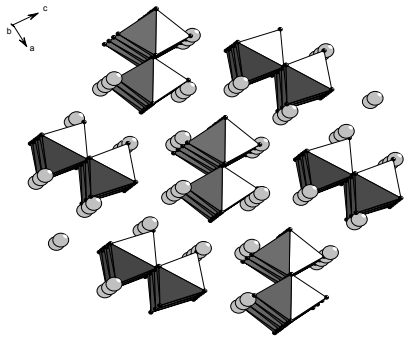

Fig. 12: The structure of the Ba_2ReO_5 compound.

The Ba_2ReO_5 compound [6] is isostructural with Ba_2WO_5 [33] and contains ReO_6 octahedra, which are linked by common corners and form infinite *cis*-bridged

chains, separated by Ba atoms. The $M_5Re_2O_{12}$ (M = Ca, Sr) [34] oxides with Re in the formal oxidation state +7 also crystallises in a hexagonal perovskite-like structure, where Re and M atoms are in a distorted octahedral oxygen coordination, $d_{(Re-O)}$ = 1.80-1.97 Å. The alkaline-earth atoms are situated in the centres of 8- and 9-fold polyhedra. The Ca_3ReO_6 compound [5] belongs to the $A_2BB'O_6$ (Ca_2CaReO_6) perovskites with a "rock-salt" type distribution of Re and Ca atoms over the B-cation sublattice. The tilting and distortion of $Re(Ca)O_6$ octahedra together with B-cation ordering decrease the symmetry from orthorhombic to monoclinic with an angle β close to 90°.

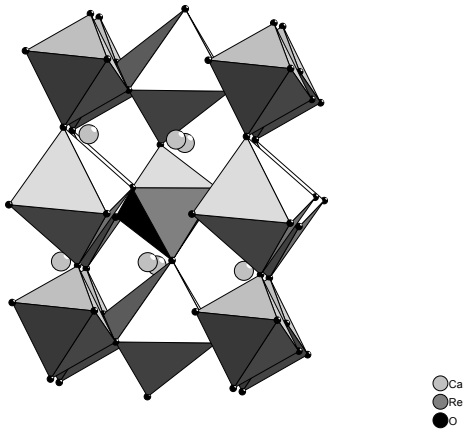

Fig. 13: The structure of the Ca_3ReO_6 compound.

The crystal structure of the recently reported $Ca_{11}Re_4O_{24}$ compound [35] can also be derived from the perovskite structure. The rhenium atoms occupy two crystallographic sites, both with slightly distorted octahedral oxygen coordination. The averaged Re(1)-O distance of 1.931 Å and for Re(2)-O of 1.877 Å clearly reflects the two different oxidation states of rhenium in this compound. The formal oxidation state of Re +6.5 in $Ca_{11}Re_4O_{24}$ is actually a consequence of one half Re^{+6} and the other half Re^{+7}. Four of eleven Ca atoms are distributed with Re atoms in the *B*-sublattice in a rock-salt manner. The *A*-sublattice is not completely occupied and formally the $Ca_{11}Re_4O_{24}$ formula may be written as $Ca_7\square(Ca_4Re_4)O_{24}$, which emphasises the cation-deficient vacancies in the *A*-sublattice.

Since the main point of this work is dealing with the systems containing alkaline-earth elements, it is necessary to describe all known structure types in the *M*-Re-O system (*M* = Ca, Sr, Ba), comprising rhenium in its highest oxidation state, +7.

There are two more structure types with Re^{+7} in addition to the $M_5Re_2O_{12}$ (M = Ca, Sr) oxides described above. The first one is observed for $M(ReO_4)_2 \times 2H_2O$ [36], M = Ca, Sr and Ba. The characteristic structural unit of this type is the isolated ReO_4 tetrahedron. These structures may be described as a scheelite (or for high temperature modifications pseudo-scheelite) structure type.

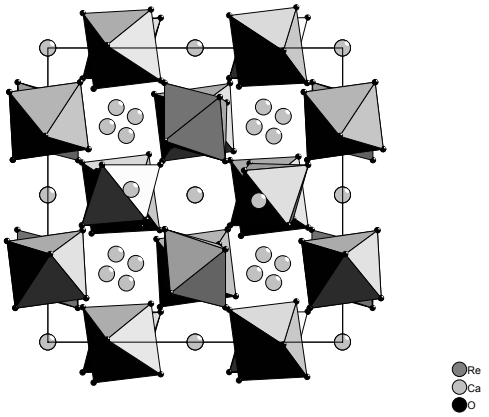

.

Fig. 14: The structure of the $Ca_{11}Re_4O_{24}$ compound.

The $Ba_5(ReO_5)_3O_2$ compound [2] considerably differs from other rhenates with rhenium in its highest oxidation state (see Fig. 15). It crystallises in an apatite type structure with the superoxide anion O_2^-. Re atoms are situated in a square pyramidal oxygen environment. These polyhedra are linked by the O_2Ba_6 octahedron with the O_2^- anion in the centre. The presence of O_2^- anions in this structure was confirmed by Raman studies.

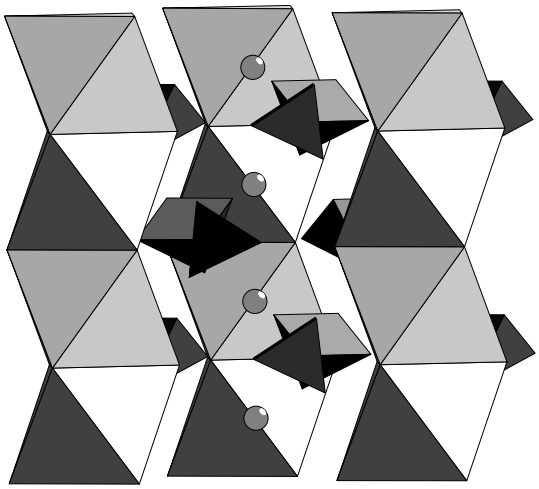

Fig. 15: The structure of the $Ba_5(ReO_5)_3O_2$ compound.

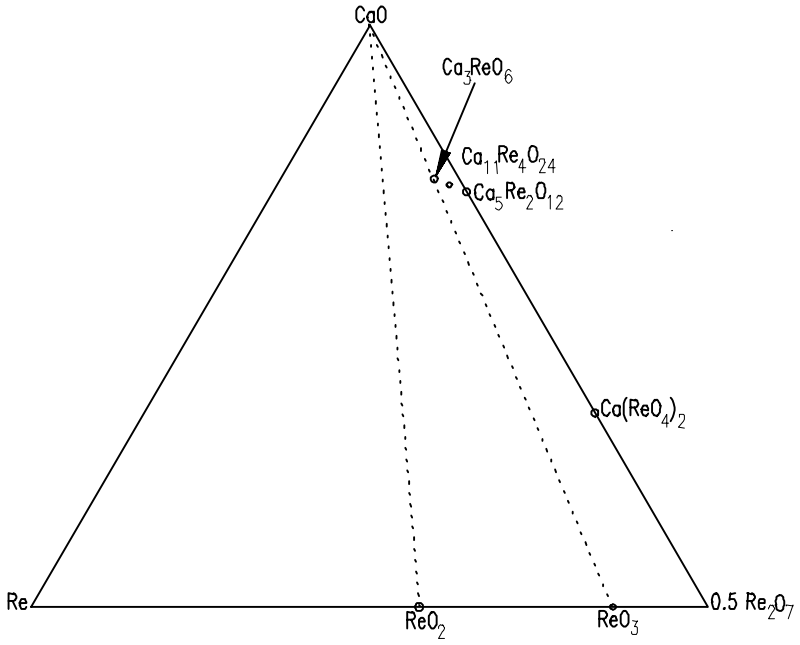

Fig. 16: The state of knowledge in the Ca-Re-O system before this work.

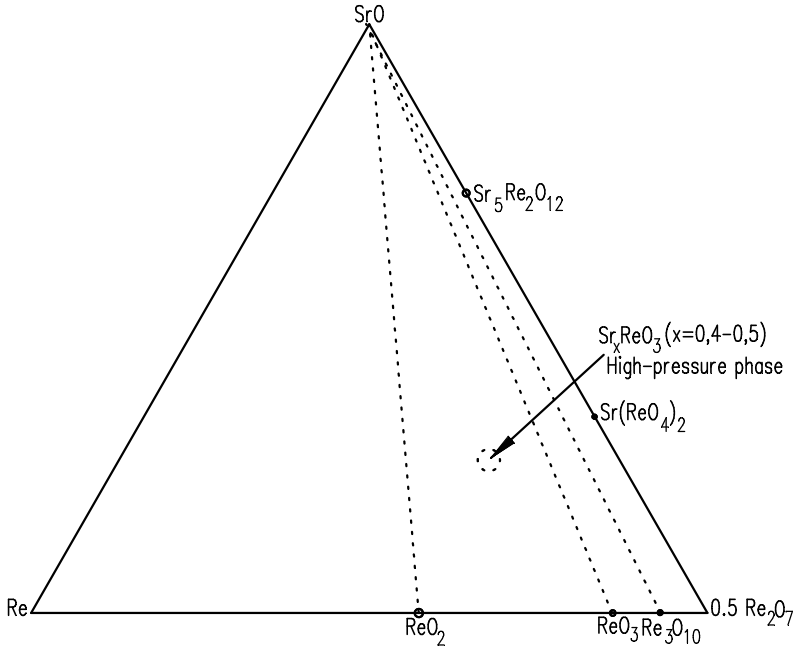

Fig. 17: The state of knowledge in the Sr-Re-O system before this work.

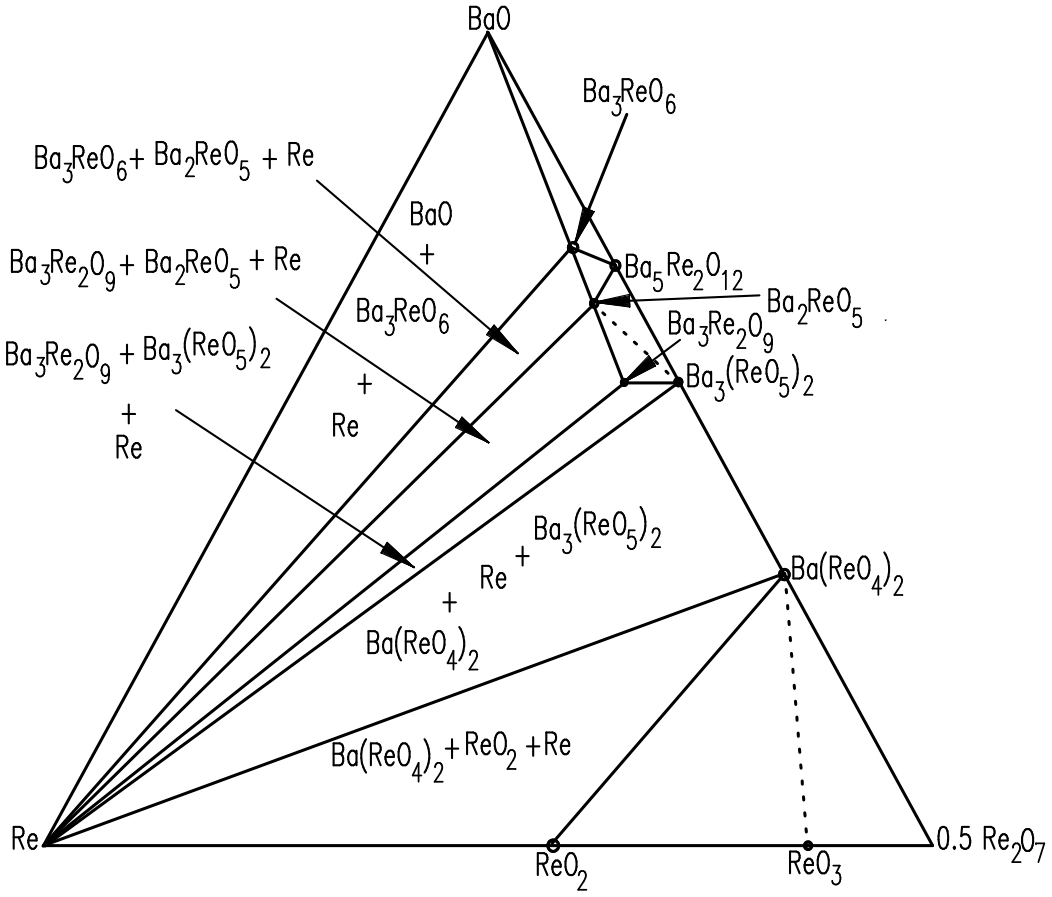

Fig. 18: The proposed BaO-Re-Re_2O_7 phase diagram at 800°C.

The state of knowledge about the *M*-Re-O system (*M* = Ca, Sr and Ba) before this work is schematically summarised in Figs. 16, 17 and 18. The dashed lines in these schemes show the different formal oxidation states for rhenium.

Also numerous examples of more complex oxides with the general formula $A_2B\mathrm{ReO}_6$, where *A* = Ca, Sr, Ba and *B* represent a variety of univalent, divalent and trivalent cations, were reported in the literature [37, 38]. As reported, the structure of many of these compounds is of the ordered perovskite type. But a detailed structure determination or a study of the electrical and magnetic properties of these compounds were not done. Moreover, the suggested cell parameters for some mentioned substances disagree with later theoretical works about different possible perovskite distortions for different *B*-cation arrangements in double perovskites [39, 40]. The structure of only one compound, Ca_3ReO_6 was carefully investigated and redetermined by X-ray powder diffraction and electron microscopy [5]. In the earliest work Sleight [37] indexed a powder pattern of the Ca_3ReO_6 based on an

orthorhombic unit cell with the parameters $a = \sqrt{2}\,a_{per}$, $b = \sqrt{2}\,a_{per}$, $c = 2a_{per}$ (where a_{per} is the perovskite subcell parameter), the same unit cell was suggested for the Ca_2BReO_6 (B = Mg, Cd, Mn, Fe, Co, Ni, Sc, Cr) compounds, but Chamberland [38] reported for Ca_3ReO_6 a doubling of all parameters. However, as shown by Anderson *et. al.* [39], there are no examples of perovskites with the general formula $A_2BB'O_6$, where a chess-board type of B cation's ordering occurs in structures belonging to the orthorhombic crystal system with the superlattice parameters proposed by Chamberland. This type of perovskite structure distortion arises when the A-O distance divided by $\sqrt{2}$ is less than the B-O bond length i.e., when the so called Goldschmidt tolerance factor, $t = (R_A + R_O)/[\sqrt{2}\,(R_B + R_O)]$,is less than 1 ($R_A$, R_B and R_O are the average radii of the ions A, B and oxygen, respectively). Compounds in the perovskite family are found to exist over the range $1.05 > t > 0.78$ [41]. The decrease in coordination number of small A cations requires the distortion of the initial perovskite oxygen framework which may be realised by the rotation of the BO_6 octahedra around $[100]_{per}$ together with a tilt about $[011]_{per}$. However, the possible topological transformations of the perovskite structure do not allow a chess-board ordering of the B cations simultaneously with a rotation and tilting of the BO_6 octahedra in the $a = \sqrt{2}\,a_{per}$, $b = \sqrt{2}\,a_{per}$, $c = 2a_{per}$ orthorhombic unit cell [42]. A detailed structural investigations of such compounds should reveal an expansion of the unit cell or the existence of a monoclinic distortion where the monoclinic angle is close to 90°. As shown in [5] the Ca_3ReO_6 compound adopts monoclinic distorted perovskite type structure.

Another example of the discrepancies between theoretical work and the unit cells proposed for the rhenium-containing compound by Sleight *et al.* [37] is the Sr_2MgReO_6 oxide. A primitive tetragonal cell with $a \approx 2a_{per}$, $c \approx 2a_{per}$ was suggested for this compound. But until now there are no perovskite-related structures known with a rock-salt ordering type of B cations with such kind of distortion [39]. Therefore a detailed study of the Sr_2MgReO_6 structure should be performed to check the correctness of the proposed unit cell.

2.2 Synthetic problems

Despite the variety of crystal structure types observed for phases with rhenium in low oxidation states there is no sufficient information about the stability of these phases and no complete investigation of phase diagrams of ternary systems with Re was done. As mentioned above, the serious synthetic problems hinder the research in oxide systems with rhenium in the low oxidation states. Re oxides with ($V_{Re} < +7$) such as ReO_2 and ReO_3 are easily oxidised to Re^{+7}, moreover, they have strong tendency to disproportionation, and Re_2O_7 can easily escape from the reaction area due to its high volatility. The synthesis techniques for the compounds described above direct to preparation of single crystals, and often special conditions like high temperatures, high pressures, or both together as by the hydrothermal technique are required, but numerous compounds are unstable under these conditions. For that reason the lack of data does not allow to discuss structural regularity and thermodynamic phase diagrams for the reduced Re-based compounds. Criteria for the formation of specific structure types have been considered only for selected compositions. The stability of two different structural types, $La_4Re_6O_{19}$ and $Nd_4Re_2O_{11}$, in the *Ln*-Re-O (*Ln* = rare-earth metal) systems in dependence on the radius of the rare-earth element is discussed in [43]. The similar dependence on the radius of the rare-earth element was shown for some more structure types: Ln_6ReO_{12} [30], Ln_2ReO_5 and $Ln_6Re_4O_{18}$ [44] and $Ln_5Re_2O_{12}$ [45]. There was only one attempt to observe and build a phase diagram for the double rhenium-containing oxides with an alkaline-earth element (BaO-Re-Re_2O_7) [6], see Fig. 18. But even in this case not all phase diagram fields were carefully investigated and not all existing phases were found and correctly described in this system: “The X-ray pattern of Ba_3ReO_6 cannot be satisfactorily indexed” [6]. Sometimes it is not possible to prepare single crystals suitable for a single crystal X-ray experiment, *e.g.* because of the instability of a phase under critical conditions such as high temperature and high pressure. In the cases where only powder material can be obtained, the purity of this phase is of primary importance for structure solution and determination of the physical properties. However, due to the very rich chemistry of rhenium and the resulting serious synthetic problems, it is very difficult to meet this requirement. Only a few

structures could be solved from X-ray or neutron powder diffraction data among, *e.g.* $Pb_6Re_6O_{19}$ [25] Ln_6ReO_{12} [30], Ba_2ReO_5 [6] and Ca_3ReO_6 [5]. Therefore, the most important point for the syntheses of reduced Re-based oxides is a correct choice of appropriate precursors, reagents and synthetic conditions like the partial oxygen pressure and temperature.

2.3 Magnetic and electrical properties of complex rhenium oxides

Although plenty of different complex rhenium oxides have been studied structural investigations in these systems, careful investigations of their magnetic and electrical properties are very rare. Therefore, there is no sufficient information available to draw conclusions about the structure-properties relations. The exception are superconducting rhenium bronzes. As already mentioned, the electrical properties of $La_3Re_2O_{10}$ were measured on single crystals in the temperature range 100 - 298 K [16]. Furthermore, the magnetic and electrical transport properties of $La_4Re_6O_{19}$ have been studied in an early work [23]. As predicted based on its structure, there are only crystallographically equivalent rhenium atoms in $La_4Re_6O_{19}$, and the formal oxidation state of rhenium is $+4^1/_3$. Metallic conductivity was observed for this compound from 4.2 K to room temperature. The formation of metal-metal bonds generally results in localised valence electrons and lower electrical conductivity as illustrated by the metal-semiconductor transitions of VO_2 and V_2O_3, accompanied with the formation of V-V bonds [46]. The electrical measurements on a $SbRe_2O_6$ single crystal have shown metallic conductivity for this compound [21]. These data indicate a wide diversity in the electrical properties of ternary rhenium oxides. Magnetic susceptibility measurements on $La_4Re_6O_{19}$ reveal a Curie-Weiss behaviour in the same temperature range. Further magnetic investigations have been performed on compounds $Ln_4Re_6O_{19}$ with *Ln* = Ce, Pr and Nd and are described in [44]. These compounds are isostructural with $La_4Re_6O_{19}$ and show also paramagnetic behaviour, but with considerably larger values of magnetic moments in comparison to the $La_4Re_6O_{19}$ compound. The magnetic moments for the compounds with *Ln* = Ce, Pr and Nd are in good agreement with the theoretical moments μ_{eff} calculated for the free ions Ce^{3+}, Pr^{3+} and Nd^{3+}. However, for the isotypic compound, $La_4Re_6O_{19}$, where the lanthanum atoms do not carry magnetic moments, a small magnetic moment was also observed. Therefore, in $La_4Re_6O_{19}$ the rhenium atoms seem to have a small paramagnetic contribution to the susceptibility, which just compensates the core diamagnetism. In the same work [44] the magnetic properties of Ln_2ReO_5 (*Ln* = Eu, Gd) were also discussed. They show paramagnetic temperature dependence from

10 K to 300 K, and the observed magnetic moments are in good agreement with the theoretical values for free Eu^{3+} and Gd^{3+}-ions. The magnetic moments were also determined from the Curie constants for $Ln_5Re_2O_{12}$ (*Ln* = Ho, Er), $Pr_3Re_2O_{10}$, $Ln_4Re_2O_{11}$ (*Ln* = Pr, Nd, Sm) [45] and Sm_3ReO_7 [29]. All these compounds show paramagnetic behaviour at least down to 200 K. The first report on magnetic ordering of a compound with rhenium in the oxidation state +4 is about Sm_2ReO_5 [14]. The observed magnetisation in the temperature range $1.8 < T < 100$ K exhibit antiferromagnetic ordering below 2.4(1) K and obey a Curie-Weiss law, modified by a temperature-independent Van Vleck paramagnetism of Sm^{3+}, for $T > 4.5$ K. A similar magnetic behaviour was observed for Yb_6ReO_{12} (oxidation state of Re is +6) with antiferromagnetic ordering below 2.2(1) K in [30]. A magnetic moment of the Re^{6+} ion could be deduced from Lu_6ReO_{12} and its value was determined to $0.74(1)\mu_B$ [30]. Re^{6+} is one of the very rare examples of a $5d^1$ electron configuration. In a crystal field of octahedral symmetry the five $L = 2$ states split into a low lying triplet and a doublet. In the limiting case of infinite crystal field splitting and ideal cubic symmetry, the ground state with effective angular momentum $\tilde{J} = 3/2$ has the Landé factor $g(\tilde{J}) = 0$ [47]. The observed magnetic moment of Re^{6+} in the Lu_6ReO_{12} compound has an anisotropic contribution from further splittings of the triplet due to crystal field effects of lower symmetry and an isotropic contribution due to the finite splitting between doublet and triplet.

Therefore, magnetic investigations of compounds containing rhenium in the oxidation state +6 are very interesting. However, to separate magnetic contributions from lower symmetry effects and finite splitting, ESR experiments on single crystals are essential. In two other studies magnetic properties of such compounds were described: The magnetic susceptibility of $Ca_{11}Re_4O_{24}$ was determined with a Faraday balance in the temperature range between 138 and 296 K [35]. The compound shows Curie-Weiss behaviour with a magnetic moment of $\mu_{exp} = 1.2(1)\mu_B$ per Re(VI) ion. For $Ba_3Re_2O_9$ the magnetic data, also measured with a Faraday balance, suggest a Curie-Weiss behaviour in the temperature region from 80 to 230 K [48], the magnetic moment is $\mu_{exp} = 1.55\mu_B$ per Re(VI) ion. Electrical resistivity measurements on $Ba_3Re_2O_9$ and Ba_2ReO_5 [6] reveal a high room-temperature

resistivity ($\rho \sim 10^7$ Ωcm), which is doubtless a consequence of the orthogonality of the Re t_{2g} orbitals involved in the π–bonding to *cis* oxygen atoms.

ReO_3 is the only example of a rhenium (+6) oxide for which a careful investigation of its magnetic and electrical properties was performed and the structure-properties relations were described in detail. ReO_3 is a very interesting example for a metallic conductor. The mentioned type of conductivity for this compound was explained by Goodenough *et al.* [8] by a comparison of the structures and the physical properties with two other compounds, Sr_2MgReO_6 and Na_xWO_3. Three different models were proposed to explain the origin of the conduction band. The first one was made on the basis of the metallic conductivity of tungsten bronzes: Na - Na bonding via direct overlap of sodium 3*p* orbitals [49]. The second model concerns Re – Re bonding via direct overlap of rhenium t_{2g} orbitals [50]. And the last proposed model was the covalent π bonding via mixing of rhenium t_{2g} and oxygen p_π orbitals [51]. According to the first model, ReO_3, a perovskite structure where *A*-sites are not occupied, should contain localised *d* electrons and behave like a semiconductor (or insulator). Since the radial extension of the 5*d* orbitals of tungsten are similar, metallic conductivity is expected for the second model. Similar, since covalent bonding will be as strong or stronger for the cation of higher formal charge, metallic conductivity is also predicted from the third model. Therefore, if ReO_3 is metallic, an additional experiment is required to distinguish between the second model and the third one. The second proposal is faced with a relatively large rhenium-rhenium separation across a cube face, $d_{Re\text{-}Re} \approx 5.4$ Å. In the perovskite-type compound Sr_2MgReO_6 the Mg^{+2} and Re^{+6} ions order on the B-sites to form two interpenetrating *f.c.c.* sublattices [37]. In such a structure there would be no interference of Re^{+6} – Re^{+6} interactions across the cube faces, and therefore, the second model would predict metallic conductivity. On the other hand, π bonding between oxygen p_π orbitals and transition-metal t_{2g} orbitals can exist only once for each oxygen ion. Therefore, according to the third model, isolated ReO_6 clusters are formed. The outer electron at each rhenium ion is confined to the π bonds of a cluster and does not belong to the crystal as a whole. It follows that Sr_2MgReO_6, according to the third model, is a semiconductor or insulator. The electrical behaviour of ReO_3 and Sr_2MgReO_6 should define which of the proposed models is the most appropriate

for metallic transition-metal oxides with ReO_3 related structures. As shown by Goodenough *et al.* [8], the Sr_2MgReO_6 oxide is a semiconductor and, therefore, the first model is the most appropriate one for the metal conductivity in ReO_3.

This example was described in detail not only to demonstrate the rare case of a carefully performed structure - properties study in the rhenium-containing system. As discussed above, see Chapter 2.1., the structure of Sr_2MgReO_6 was not solved until now and, contradicting unit cells were proposed for this compound. Therefore, even this interesting consideration of the origin of metallic conductivity in ReO_3, is not very reliable, since no detailed structure investigation was carried out for Sr_2MgReO_6.

The recently reported Li_4MgReO_6 compound [52] is the first example of substances containing alkali metals together with rhenium in a low oxidation state, +6. It exhibits unexpected antiferromagnetic spin-glass behaviour. The Re^{+6} sublattice in this compound is best described as a distorted face-sharing tetrahedral framework. Magnetic bulk measurements on this sample show hysteresis behaviour below 12 K, indicating a cooperative magnetism at low temperature. On the basis of low-temperature neutron powder diffraction and μSR experiments magnetic long-range order can be ruled out for Li_4MgReO_6 and a spin-glass ground state was proposed at low temperature, and the spin freezing process is complete at approximately 2.5 K. The spin-glass ground state can be attributed to the high degree of geometric magnetic frustration on the Re+6 sublattice. Furthermore, bonding disorder due to Mg/Li disorder favours the spin-glass ground state as claimed by Bieringer *et al.* [52].

3 Experimental

3.1 Powder diffraction

3.1.1 X-ray powder diffraction

X-ray diffraction data for phase analyses and crystal structure determinations were collected using a STOE STADI/P powder diffractometer ($CuK\alpha_1$ and $CoK\alpha_1$ radiation, curved Ge monochromator, transmission mode, $\Delta 2\theta$ step 0.02^0, PSD counter). For structure solutions extracted integral intensities and a CSD program package [53] were used. The structure refinements were carried out with the RIETAN-97 program [54]. The Rietveld method with a modified pseudo-Voigt profile function was used for the final refinements.

3.1.2 Neutron powder diffraction

Neutron diffraction experiments were performed at different temperatures with the high-resolution Fourier diffractometer (HRFD) at the IBR-2 pulsed reactor in Dubna, Russia.

The IBR-2 is the most intense pulsed source in the world with a peak flux of 10^{16} n/cm^2/s, although its pulse duration is relatively long (~320 μs for thermal neutrons). Due to a special feature, the Fourier method implementation at pulsed neutron sources, HRFD was designed as a very high resolution instrument (in principle, down to $\Delta d/d=5\cdot10^{-4}$) with a good data accumulation rate and good signal to background ratio [55]. The neutron Fourier diffraction technique [56] involves modulations of the neutron beam by a fast Fourier chopper, *i.e.* a rotating disk (rotor) with a pattern of alternating neutron absorbing and neutron transparent slits and a fixed system of identical slits (stator). The transmission of the Fourier chopper does not depend on the number of slits and is equal to 0.25 of the total neutron flux. This

means that the intensity can be much higher than for a Fermi chopper. At the same time, the Fourier chopper provides a short neutron pulse due to the small width of the slits and the high rotation frequency, *i.e.*, it provides good time resolution.

Successful practical realisation of the neutron Fourier method became possible, when the so-called reverse time of flight (RTOF) method of data acquisition was introduced. The basic idea of the RTOF method is an on-line check for each detected neutron, if the registration probability is high or low. The check is realised by a reverse analysis of the neutron source and Fourier chopper states at the time the neutron passed these points. By continuously changing the chopper speed during detection and counting only those neutrons with a high probability of registration in the analyser's memory, one can obtain the TOF distribution of elastically scattered neutrons, *i.e.*, the conventional TOF diffraction pattern.

The expression for the resolution of a time-of-flight powder diffractometer has three terms (in first approximation):

$$R = \Delta d/d = [(\Delta t_0/t)^2 + (\Delta\theta/tg\theta)^2 + (\Delta L/L)^2]^{1/2}, \qquad (1)$$

where Δt_0 is the width of the neutron pulse, $t = 252.778 L\lambda$ with L the total flight path in m, λ the neutron wavelength in Å, θ the Bragg angle in radians and t in μs. The first term is the TOF uncertainty, the second includes all geometrical uncertainties, and the third is the uncertainty in the total flight-path length. It is clear that the time-of-flight contribution can be reduced either shortening the source pulse or by lengthening the flight path.

At IBR-2, which is a so-called “long pulse neutron source”, the flight path would need to be longer than 1 km to reach a resolution close to 0.001. Another and more promising possibility is the utilisation of the correlation technique, either pseudostatistical or Fourier-type. The Fourier method proved to be of advantage for elastic neutron scattering (diffraction), because it allows the use of narrow chopper slits combined with a wide neutron beam. Hereby, high resolution can be achieved without too much loss of intensity.

With the RTOF-method, the gathering of the diffraction spectrum is performed with a continuously changing Fourier chopper frequency from zero to some upper value ω_m. The time-of-flight component of the resolution depends strongly on the Fourier chopper resolution function R_c, which itself depends on the

particular frequency distribution (frequency window) $g(\omega)$. This relationship can be expressed as:

$$R_c(t) \sim \int_0^{\Omega} g(\omega)\cos(\omega t)d\omega, \qquad (2)$$

where $\Omega=N\omega_m$ is the maximum modulation frequency of the incident neutron beam, and N is the chopper slit number. In the first approximation, the full width of $R_c(t)$ is close to Ω^{-1} and is equal to ~7 μs for N=1024 and ω_m=150 Hz (HRFD parameters). It means that even for a flight path between chopper and detector of ~20 m, the time-of-flight term in the resolution function could be as small as $\sim 3.5\cdot 10^{-4}$ at d=2 Å.

For $L \geq 10$ m, the third term in equation (1) can be easily made negligibly small. As for the second term in (1), its value can be optimised by an appropriate choice of incident beam collimation and detector system, depending on the emphasise on either resolution or intensity. For existing neutron Fourier diffractometers, the conventional choice for the detector system is a geometrically time-focusing ^{6}Li-glass detector composed of several photomultipliers, providing an approximately equal contribution into the full peak width.

The important difference of a Fourier diffractometer at a pulsed neutron source is the shape of the correlation background: it looks like a diffraction pattern with wide peaks. At a steady state neutron reactor, the correlation background at any point of the diffraction pattern is equal to the total number of counts, registered during measurement, *i.e.*, it does not depend on the time-of-flight point. As a consequence, the signal to background ratio is much better for a Fourier diffractometer operating at a pulsed neutron source, especially for the low intensity spectrum regions, *i.e.*, at short and long wavelengths. This leads to better quality diffraction patterns and allows for an extended wavelength interval.

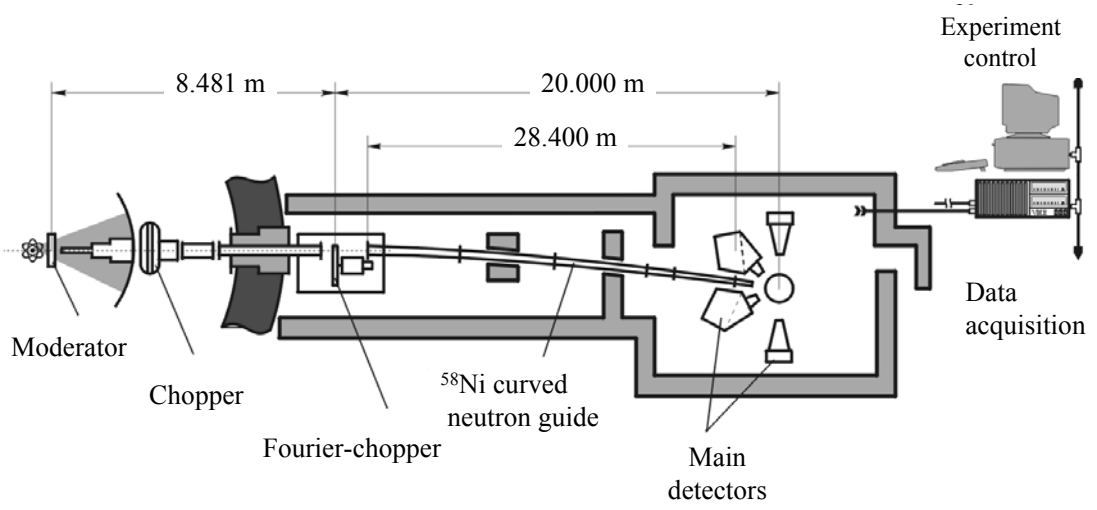

Fig. 19: The layout of the high-resolution Fourier diffractometer (HRFD) at the IBR-2 pulsed reactor.

The experimental set-up of HRFD is shown schematically in Fig. 19. Its main units are: neutron source with moderator, Fourier chopper, detector, and data acquisition system. The latter is a RTOF analyser, used for correlation analysis of source, chopper and detector binary signals. Immediately behind the reactor shielding is a background chopper as a filter for fast neutrons and γ-rays. The distance between the moderator and the Fourier chopper is about 9 m. The neutron beam before the Fourier chopper is formed by a straight neutron guide, coated with ^{58}Ni.

The Fourier chopper, placed behind the second shielding wall, consists of a rotor disk with 540 mm in diameter and a stator plate, both made of Ti-Zr zero matrix alloy. The stator covers the entire 30×200 mm^2 beam cross section at the chopper position. The rotor has a modulation pattern of 1024 radial slits coated with Gd_2O_3 in epoxy resin, 60 mm long and 0.7 mm wide in the middle of its height. The stator has the same pattern and its phase, with respect to the pickup signal indicating the chopper position, can be adjusted by a micrometer screw to put the beam modulation in phase with the pickup signal. The disc is rotated by a 7.5 kW squirrel gauge ac motor equipped with a double incremental encoder. One of the encoder signals is used for the motor speed control and the other for the pickup signal, providing the present chopper disk position for the analyser. The motor is controlled

by a Vector V750 static inverter drive capable of controlling the motor within the rotating speed range of –9000 rpm to +9000 rpm.

The neutron beam at a sample is formed by a horizontally and vertically focusing curved neutron guide 19 m in length, coated with ^{58}Ni. This guide tube acts as both a forming element for the neutron beam and an additional filter of fast neutrons and γ-rays. Its incoming and outgoing window cross-sections are as large as 30×200 and 10×100 mm^2, respectively, and its total length is about 19 m. The flight path between the chopper disc and the sample position is 20000 mm.

3.2 Electron diffraction

The electron diffraction (ED) investigations were performed on a Philips CM200 UT transmission electron microscope, operating at an accelerating voltage of 200 kV and on a JEM 3010 UHR electron microscope, operating at 300 kV. On-line cell parameter determinations were made using the software program package PIEP (Program for Interpreting Electron diffraction Patterns) [57].

3.3 Magnetic measurements

The magnetic properties of the investigated compounds have been studied with a superconducting quantum interference device (SQUID) from Quantum Design in the temperature range from 1.8 to 300 K and field strength up to 6.5 T.

3.4 Thermal analysis

Thermo-analytical data were obtained on a SETARAM Model TGA 92-16.8 thermal analyser with DTA/TG module. The DTA/TG experiments were carried out in a gettered argon atmosphere and in air atmosphere as well.

3.5 Chemicals and sample preparation

*M*O (*M* = Ca, Sr, Ba), MgO (MERCK, 99.999%), Re metallic (Aldrich, 99.995%) and ReO_3 (STREM Chemicals, 99.9%) were chosen as starting materials. *M*O (*M* = Sr, Ba) were obtained by decomposition of MCO_3 (MERCK, GR). Decomposition of $SrCO_3$ was carried out at 900^0C for 24 hours in vacuum, 10^{-4} mbar. $BaCO_3$ was decomposed at 1100^0C for 24 hours in vacuum, 10^{-4} mbar. CaO was obtained by the same decomposition reaction at 950°C for 24 h in air. MgO was calcined at 800°C for 24 hours in air before using for synthesis.

For some syntheses, ReO_3 was obtained, as described in [58]. Metallic Re was solved electrochemically in dry methanol, which was dried by boiling with magnesium methylate. Anode solution of metallic rhenium was carried out in the water-cooled electrochemical cell with non-separated cathode- and anode-space (U = 110 V). Previous dried LiCl (0.025 M) was used as electrolyte admixture. The temperature of the electrochemical cell was kept below 50°C. A rhenium bar of 0.5 × 0.5 cm^2 was used as anode, stainless steel plate, 12 cm^2, as cathode (average anode current density ~ 0.2 A/cm^2). The dissolution reaction was accompanied by a solution colouring. The solution became yellow-orange at the first minutes of the reaction, then green-grey and changed approximately 2 hours later to dark-red. This colour did not change anymore until the end of electrochemical reaction. Crystallisation of the dark-green crystals on the walls of the electrochemical cell began simultaneously with dark-red colouring of the solution. These green crystals of rhenium oxomethylate, $Re_4O_2(OCH_3)_{16}$, were dried and then decomposed at 300°C for 3 hours, resulting in pure ReO_3.

A mixture of monoclinic and orthorhombic forms of ReO_2 was prepared by decomposition of NH_4ReO_4 (STREM Chemicals, 99.999%) at 400°C in a dry nitrogen or argon flow.

The precursors $M_5Re_2O_{12}$ and $M(ReO_4)_2$ (*M* = Ca, Sr, Ba) were synthesised by the following technique: MCO_3 (*M* = Ca, Sr, Ba) was dissolved in diluted nitric acid (~1M), then a stoichiometric amount of NH_4ReO_4 was dissolved in the solution. After slow evaporation (at 100°C), the dry residue was heated at 600°C until gas

elimination stopped, ground in an agate mortar and pressed into pellets. Annealing of the obtained products at 1000°C for 24 hours in air resulted in pure $M_5Re_2O_{12}$ and $M(ReO_4)_2$ samples, respectively.

Samples were synthesised by five different methods:

1) The first one is the standard ceramic technique: a stoichiometric amount of the precursors was intimately mixed, ground in an agate mortar under dry argon atmosphere and placed in alumina crucibles to avoid reaction with the silica tube during annealing. The sample was sealed in a silica tube with 8-10 cm^3 volume at 10^{-3} mbar pressure. Then the sealed silica tubes were placed into a "Nabertherm" furnace and annealed at different temperatures for 40 hours. After annealing all samples were furnace cooled.

2) The second high-temperature synthetic method was used to prepare single crystals. A stoichiometric mixture was intimately mixed, ground in an agate mortar under dry argon atmosphere and filled in a Pt/Rh (90/10%) tube with ca. 0.5 cm^3 volume. The tubes were welded to ensure that they were properly closed. Then the tubes were placed into a "GERO" furnace. The samples were heated to 1400°C at a rate of 200°/h, tempered for 24 hours, cooled to 900°C at a rate of 30°/h and afterwards cooled down to the room temperature at 180°/h.

3) Another high-temperature preparation technique was used to synthesise new compounds in the *M*-Re-O system. The syntheses were carried out in the arc melting furnace. Different precursors, such as $M_5Re_2O_{12}$ and $M(ReO_4)_2$, were intimately mixed in several proportions with alkali-earth oxides, ground in an agate mortar and pressed into 0.5 g pellets. Then the prepared samples were placed into an arc melting furnace MAM 1, Firma Johanna Otto. The syntheses were carried out in argon atmosphere by applying a high voltage between a water-cooled Cu-plate and a tungsten tip. Temperatures between 2800 and 4000°C were achieved in the light arc, and the time for annealing was varied between 3 and 10 seconds. The samples were quenched in a couple of minutes.

4) Syntheses with flux were also carried out. Different substances, such as CaF_2 and BF_6, were used as flux. The attempts to grow single crystals in the Ca-Re-O system followed the method described by Hessen *et al.* with minor modifications. Starting materials were $Ca_5Re_3O_{15}$ powder samples and borate flux of $CaO_{1.79}B_2O_3$

composition. The powder samples were prepared by the same synthetic way as described in 1). The $CaO_{1.79}B_2O_3$ flux (T_M=889°C) was synthesised by heating of a stoichiometric mixture of B_2O_3 (99.999%) and $Ca(NO_3)_2$ (99.999%) in air at 750°C for 48 hours. Initial reagents ($Ca_5Re_3O_{15}$ and $CaO_{1.79}B_2O_3$) were mixed in a 1:3 mass ratio, placed in alumina crucibles and sealed in evacuated silica tubes. The mixture was heated at 1050°C for 3 hours. Then it was cooled with the rate of 6°C/h down to 850°C, halted for a couple of minutes and after that the furnace was cooled to room temperature. The glassy flux was removed by etching with a dilute aqueous HF solution.

5) To control the partial oxygen pressure in the sealed silica tubes during synthesis different mixtures of metal oxides and the same metals (or oxides in a lower oxidation state) were used. The preparation technique in this case is almost the same as described above in 1), but additionally, pressed pellets of partial oxygen pressure controllers were placed into silica tubes before sealing. The temperature of syntheses depended on the required partial oxygen pressure and varied in the range of 600° - 1100°C. For compounds, which are unstable at high temperature, a furnace with two temperature zone was used. One end of the sealed silica tube, where the sample was placed, was put in the “cold” zone, the open furnace end, another one in the zone with temperature, which defined the equilibrium partial oxygen pressure. Temperature of the “cold” zone was controlled by NiCr-Ni digital thermometer GTH 1200 (Greisinger electronics), which was calibrated before use. The samples were quenched after annealing.

4 Results and Discussion

4.1 Sample preparation

As shown in Fig 17 only compounds with rhenium in the highest oxidation state, $Sr_5Re_2O_{12}$ and $Sr(ReO_4)_2$, were known in the case of the Sr-Re-O system and additionally to the isostructural calcium perrhenates only one compound with Re^{+6}, Ca_3ReO_6, was observed and described for the Ca-Re-O system at the beginning of this work. On the contrary, almost all phases in the Ba-Re-O system were carefully investigated. Only in the barium rich range of the phase diagram some questions and uncertainties were not resolved. The standard ceramic synthetic technique, as described in Chapter 3.4., was used to prepare new phases and to investigate their stability in dependence on cation composition of alkali-earth elements and rhenium. Two new compounds, $Sr_{11}Re_4O_{24}$ and $Ba_{11}Re_4O_{24}$, were successfully synthesised with small amounts of impurities (the intensity of the strongest impurity peak is less than 4% of the strongest peak intensity of the main phase) by this synthetic way. Also, all M_2MgReO_6 (M = Ca, Sr, Ba) compounds were successfully prepared as single phase by this technique.

MO (M = Sr, Ba) and ReO_3 oxides were chosen as starting materials for the syntheses of the $M_{11}Re_4O_{24}$ ternary oxides. MO (M = Sr, Ba) were obtained by decomposition of the corresponding carbonates as described above, see Chapter 3.4.. Three moles of MO and one mole of ReO_3 were thoroughly mixed, ground in an agate mortar, pressed into 0.5 g pellets, and placed in alumina boats to avoid reaction of alkali-earth oxide with the silica tube during annealing. The samples were sealed in silica tubes with an 8-10 cm^3 volume at atmospheric pressure in air. The pellets were annealed at 800°C for 48 hours. Finally all samples were cooled in a furnace. Phase composition and the correct choice of unit cell was confirmed by X-ray powder diffraction data and electron microscopy. But the following attempts to prepare single phase samples with other cation compositions by the same synthetic way led to formation of mixtures of several unknown phases, that allowed only for an indexing of the powder diffraction pattern and a refinement of the cell parameters

of these compounds. However, it was impossible to perform an *ab-initio* structure solution or to investigate the magnetic and other properties of these compounds.

Different parameters of synthesis can influence the formation of phases. One of the main parameters of synthesis is the appropriate precursor. This point is of primary importance in the chemistry of rhenium oxides, because of the strong tendency of rhenium oxides in low oxidation states to disproportionate. For example, ReO_3 decomposes to ReO_2 and Re_2O_7 at temperatures above 300°C in vacuum. On the other hand, ReO_2 disproportionates to metallic rhenium and Re_2O_7 above 850°C. Re_2O_7, which is formed in these reactions, can easily escape from the reaction area due to its high volatility as the partial pressure of Re_2O_7 at 604°C is equal to 1 atm. Several precursors were used for sample preparation in the *M*-Re-O systems. Since the synthesised compounds contain rhenium in the formal oxidation state +6.5, ReO_2 or a mixture of metallic Re and ReO_2 were taken as educts instead of ReO_3 in a first try. To replace the highly hygroscopic alkali-earth oxides, the corresponding perrhenates, $M_5Re_2O_{12}$ and different crystallohydrates of $M(ReO_4)_2$ (for Ca – dihydrate, Sr – monohydrate, Ba – dehydrated perrhenate) were used as starting materials instead. However, neither different synthetic routes nor the use of other more stable rhenium oxides (and a substitution of the alkali-earth oxides by perrhenates) resulted in pure, single-phase samples.

Different attempts to grow single crystals of these new phases were performed. The first step, the high-temperature annealing of samples with different cation composition was carried out. This technique is described in Chapter 3.4. topic 2). The idea of this method was to reach the melting point of the required phases and to obtain single crystals, suitable for single crystal X-ray experiments, by very slow cooling. In the Ca-Re-O system high temperature annealing of the samples with cation ratio Ca:Re = 5:3 and 1:1, respectively, gave the same results. The obtained products did not depend on the annealing temperature up to 950°C.

The high temperature treatment led to the formation of the most stable phases in this system, Ca_3ReO_6 and $Ca(ReO_4)_2$, independent on the choice of precursors. The phases of primary interest are therefore unstable at temperatures above 950°C. The same synthetic methods led to similar results for the Sr-Re-O system: only $Sr_{11}Re_4O_{24}$ and $Sr(ReO_4)_2$ phases were formed at temperatures above 950°C. The

melting points of these most stable compounds were apparently not achieved for both systems, since agglomerated powders were obtained.

The same results were achieved by an extra high-temperature treatment of different mixtures of alkali-earth perrhenates and their oxides. Alkali-earth perrhenates were chosen as precursor, because of the high volatility of Re_2O_7, which is one of the products of disproportionation of the rhenium oxides.

Furthermore, syntheses with different flux were carried out. This synthetic technique did not result in the formation of single crystals, probably because of an inappropriate choice of flux (the required phases were not even partially soluble in the selected fluxes, CaF_2, BaF_6, and $CaO_{1.79}B_2O_3$).

All preparation methods applied so far did not result in single phases nor single crystals. Therefore, other synthetic techniques have to be considered. At first, all parameters, which can influence the synthesis, should be observed. The "degrees of freedom" for synthesis are: *i*) choice of precursors (see above) *ii*) temperature *iii*) annealing time *iv*) cation composition *v*) total pressure in the sealed silica tube *vi*) volume of the sealed silica tube and *vii*) partial oxygen pressure. The change of temperature below 950°C and annealing time did not lead to considerable differences of the syntheses results. The partial oxygen pressure can be the most important parameter for the synthesis of ternary rhenium oxides with rhenium in a low oxidation state, since rhenium occurs in intermediate formal oxidation states, for example +6.5 for the $Sr_{11}Re_4O_{24}$ oxide. Different mixtures of metal oxides and the same metals (or oxides in the lower oxidation state), so called getters, were used to control the partial oxygen pressure in a sealed silica tube. The partial oxygen pressure at a specific temperature is well defined in thermodynamic equilibrium, for example for the Ni/NiO system:

$$2Ni + O_2 \leftrightarrow 2NiO. \qquad (1)$$

The Gibbs Free Energy is defined as: G = H – TS, where H is the enthalpy, T the absolute temperature and S the entropy. For a reaction to occur spontaneously at constant temperature and pressure, the change in free energy,

$$\Delta_r G = \Delta_r H - T\Delta_r S, \text{ must be negative, } \Delta_r G < 0. \qquad (2)$$

In equilibrium the Gibbs free energy increment ΔG has a minimum value, then we obtain for our example reaction (1):

$$\Sigma \nu_i \mu_i = 2\mu(\mathrm{Ni}) + \mu(\mathrm{O_2}) - 2\mu(\mathrm{NiO}) = 0 \quad (3)$$

where ν_i are the molar coefficients and μ_i are the chemical potentials. For moderate vapour pressures, the effect of pressure on the thermodynamic potentials of the solids, in our case Ni and NiO, may be neglected, and the chemical potentials depend on temperature only (the composition is constant):

$$\mu(\mathrm{Ni}) = \mu^\circ(\mathrm{Ni})_T \quad (4)$$

$$\mu(\mathrm{NiO}) = \mu^\circ(\mathrm{NiO})_T \quad (5)$$

For the vapour, however,

$$\mu(\mathrm{O_2}) = \mu^\circ(\mathrm{O_2})_T + RT\ln(\mathrm{p(O_2)}) \quad (6)$$

Hence, since ΔH and ΔS do not change significantly with temperature for most reactions, it is possible to use tabulated values for ΔH_f° and ΔS° at room temperature (298 K) to calculate $p(O_2)$ as a function of T:

$$-RT\ln(\mathrm{p(O_2)}) = \Delta_r H^\circ - T\Delta_r S^\circ \equiv \Delta_r G^\circ \quad (7)$$

i.e.

$$\lg(\mathrm{p(O_2)}) = A - B/T \quad (8)$$

with $A = \frac{\Delta H^\circ}{2.303R}$, and $B = \frac{\Delta S^\circ}{2.303R}$, K. Consequently for reaction (1):

$$\lg(\mathrm{p(O_2)}) = 8.861 - 24518.9/T \quad (9)$$

A plot of $RT\ln(\mathrm{p(O_2)}) = -\Delta_r G^\circ$ versus T is a straight line. Plots of this kind have first been proposed by Ellingham [59].

Characteristics of all getters used in the syntheses and their most appropriate temperature and partial oxygen pressure ranges are listed in Table 2. The temperature dependence for these getters versus the logarithm of partial oxygen pressure is shown in Fig. 20.

Table 2. Getters used in syntheses and their characteristics.

Getter	*A*	*B,* K	Temperature range, °C	Partial oxygen pressure range, bar
CoO/Co_3O_4	12.600	15600.0	700-1000	0.001-1
Cu_2O/CuO	10.063	13972.0	700-800	5×10^{-5} -1×10^{-3}
Cu/Cu_2O	7.465	17450.0	650-900	4×10^{-12} -4×10^{-8}
Ni/NiO	8.861	24518.9	700-1050	5×10^{-17} -2×10^{-10}
Co/CoO	8.320	24807.9	800-1000	2×10^{-15} -7×10^{-12}
Fe/FeO	7.206	26045.1	800-1000	9×10^{-18} -6×10^{-14}
Mn/MnO	7.523	40207.6	850-1100	5×10^{-28} -2×10^{-22}

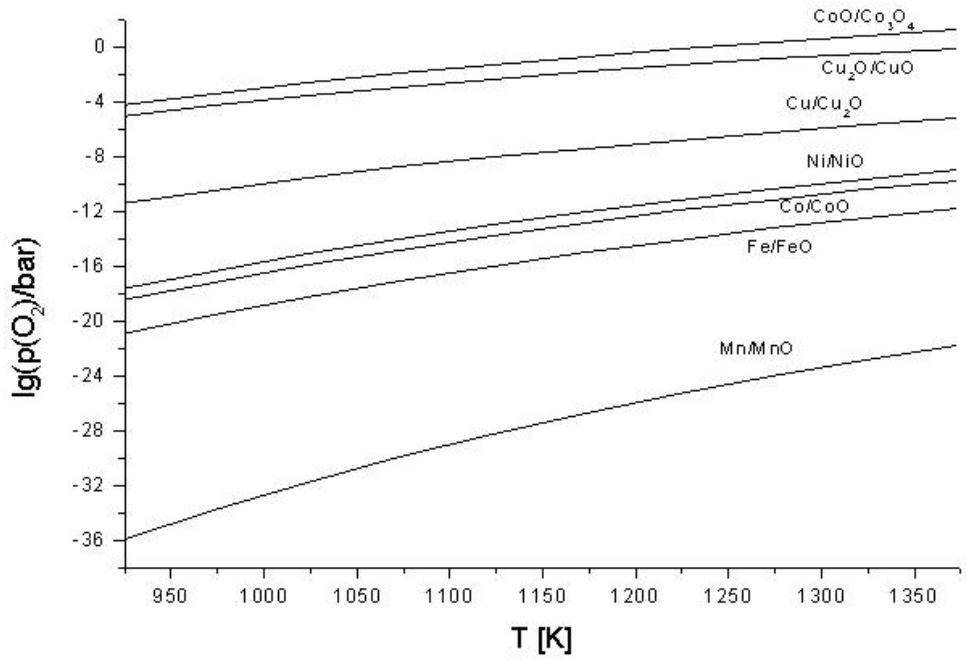

Fig. 20: The modified Ellingham diagram for the getters listed in Table 2.

This synthetic technique allows not only to prepare single-phase ceramics but also to predict phase stability in dependence on partial oxygen pressure and consequently to study the phase diagram of the investigated system.

Numerous syntheses using the preparation technique with controlled partial oxygen pressure were carried out to investigate the *M*-Re-O (*M* = Ca, Sr) systems. The Ba-Re-O system was also reinvestigated. The results of these studies are summarised in the form of a triangular scheme of phase stability. The stability ranges of the different investigated phases in dependence on partial oxygen pressure are listed in Table 3.

The complete phase stability diagram was determined for the Sr-Re-O system. Three new phases were prepared, Sr_3ReO_6, $Sr_{11}Re_4O_{24}$ and $Sr_7Re_4O_{19}$, and their crystal structures were solved and refined. Only one of these phases, $Sr_{11}Re_4O_{24}$, (the most stable in this system) could be prepared as a single phase without explicit control of the partial oxygen pressure in the sealed silica tube. The syntheses of the two other compounds require a careful control of the partial oxygen pressure. A phase analysis of samples with different compositions, synthesised at different partial oxygen pressure, was carried out. The results are summarised in the presented scheme of phase stability for the Sr-Re-O system below, see Fig. 21.

Table 3. Stability ranges with respect to the partial oxygen pressure in the *M*-Re-O (*M* = Ca, Sr, Ba) systems.

Phase name	Products of reduction	Lower $p(O_2)$ limit, bar	Upper $p(O_2)$ limit, bar	Products of oxidation
Sr_3ReO_6	Re + SrO	4.6×10^{-17}	2.3×10^{-15}	$Sr_{11}Re_4O_{24}$ + SrO
$Sr_{11}Re_4O_{24}$	Re + SrO	2.3×10^{-15}	1.1×10^{-3}	$Sr_5Re_2O_{12}$ + SrO
$Sr_7Re_4O_{19}$	Re + SrO	2.3×10^{-15}	1.0×10^{-9}	$Sr_5Re_2O_{12}$ + $Sr(ReO_4)_2$
$Ba_{11}Re_4O_{24}$	Re + BaO	5.0×10^{-16}	1.0×10^{-3}	$Ba_5Re_2O_{12}$ + $Ba_3(ReO_5)_2$
Ca_3ReO_6	Re + CaO	2.0×10^{-18}	1.0×10^{-3}	$Ca_5Re_2O_{12}$ + CaO
$Ca_{11}Re_4O_{24}$	Ca_3ReO_6 + $Ca_5Re_3O_{15}$	5.0×10^{-11}	1.0×10^{-9}	$Ca_5Re_2O_{12}$ + CaO
$Ca_5Re_3O_{15}$	Re + Ca_3ReO_6 + $Ca(ReO_4)_2$	5.0×10^{-11}	1.0×10^{-9}	$Ca_5Re_2O_{12}$ + $Ca(ReO_4)_2$

In the Ba-Re-O system one new phase, $Ba_{11}Re_4O_{24}$, was synthesised and its crystal structure solved. As a consequence some fields in the proposed phase diagram by Cheetham *et al.* [6] were corrected accordingly. For example, in comparison with the phase diagram proposed earlier, neither traces of ReO_2 oxide in its α- nor in its β-modification were found in the rhenium rich samples, annealed at 800°C. Only a mixture of barium perrhenate, $Ba(ReO_4)_2$, and metallic rhenium could be identified by X-ray phase analysis after annealing. The results of this investigation in the Ba-Re-O system are presented below in the scheme of phase stability, see Fig. 22. One more compound with approximated composition Ba_3ReO_6 was observed in this system, but its X-ray powder diffraction pattern could not be indexed, because of unreliable peak position determination due to strong peak overlapping. This compound might be isostructural to the strontium tungsten oxide, Sr_3WO_6 [60],

based on the similarity of their X-ray powder diffraction patterns. A triclinic unit cell was proposed for Sr_3WO_6 with a = 8.361 Å, b = 8.288 Å, c = 8.211 Å, α = 89.78°, β = 89.78°, γ = 89.78°. However, not all reflections observed for Sr_3WO_6 and "Ba_3ReO_6" are indexed on the basis of the proposed cell.

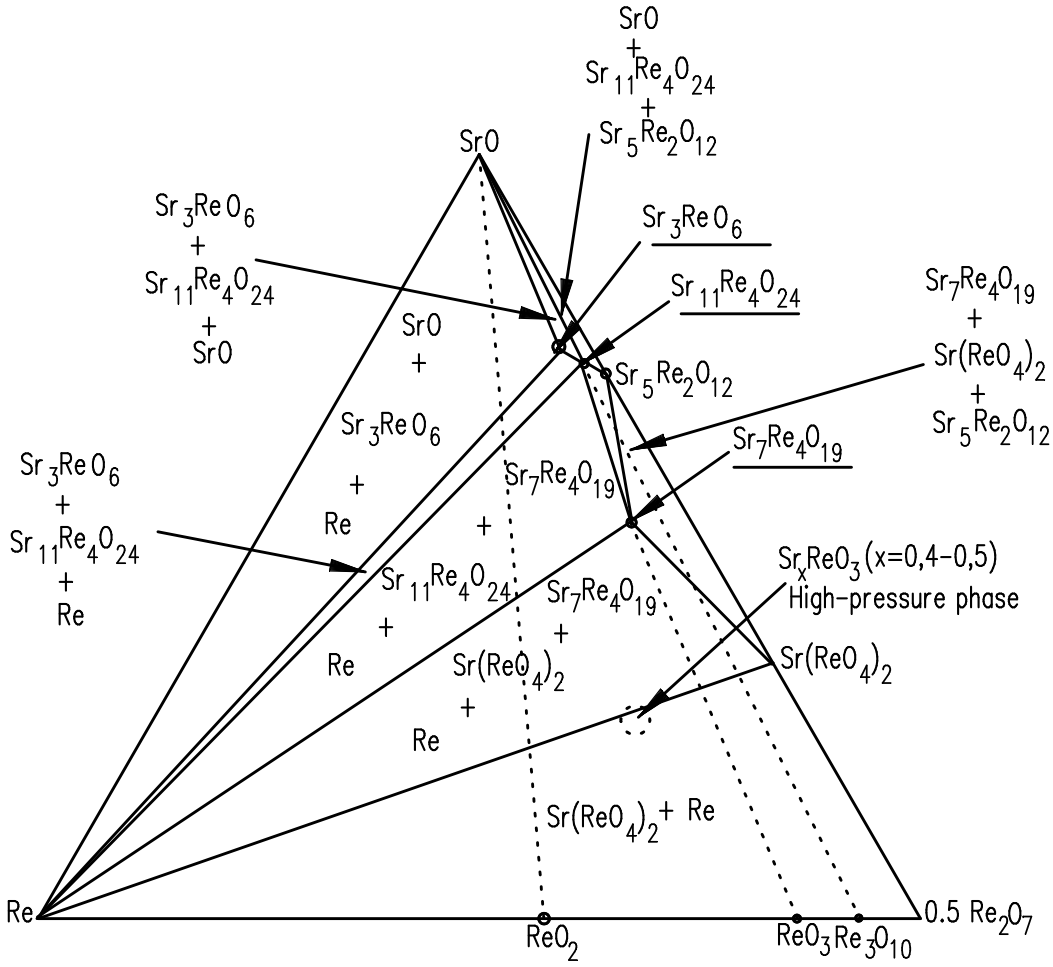

Fig. 21: Scheme of phase stability in the Sr-Re-O system

(the new phases are underlined).

Syntheses of samples with controlled partial oxygen pressure and with barium oxide excess did not lead to a reproducible formation of the early observed compound, "Ba_3ReO_6". It lets conclude that the observed compound may be considered as a complex barium-rhenium oxycarbonate, where carbonate groups substitute BaO_6 octahedra partially in the three-dimensional network of the corner-sharing octahedra BaO_6 like in the well known case of barium-copper oxycarbonate, erroneously denoted as "$BaCuO_2$" [61]. This conclusion is supported by geometrical

considerations for the expected Ba_3ReO_6 complex oxide, which should crystallise in a perovskite-related structure with rock salt ordering of cations in the *B*-subcell, like in the Ca_3ReO_6 [5] and the Sr_3ReO_6 structures (see Chapter 4.2.3). One third of the Ba atoms would occupy the centre of oxygen octahedra, but such an octahedral coordination is very unusual for the big barium atoms, as the ionic radius of Ba^{+2} is 1.36 Å for six-fold coordination [64]. Even in the case of the analogous strontium compound, Sr_3ReO_6, with r_{Sr+2} = 1.16 Å for a 6-fold coordination [64]), the occupancy of octahedral sites by Sr atoms results in a considerable restriction of the stability range in comparison to other observed phases in the Sr-Re-O system as shown in Table 3.

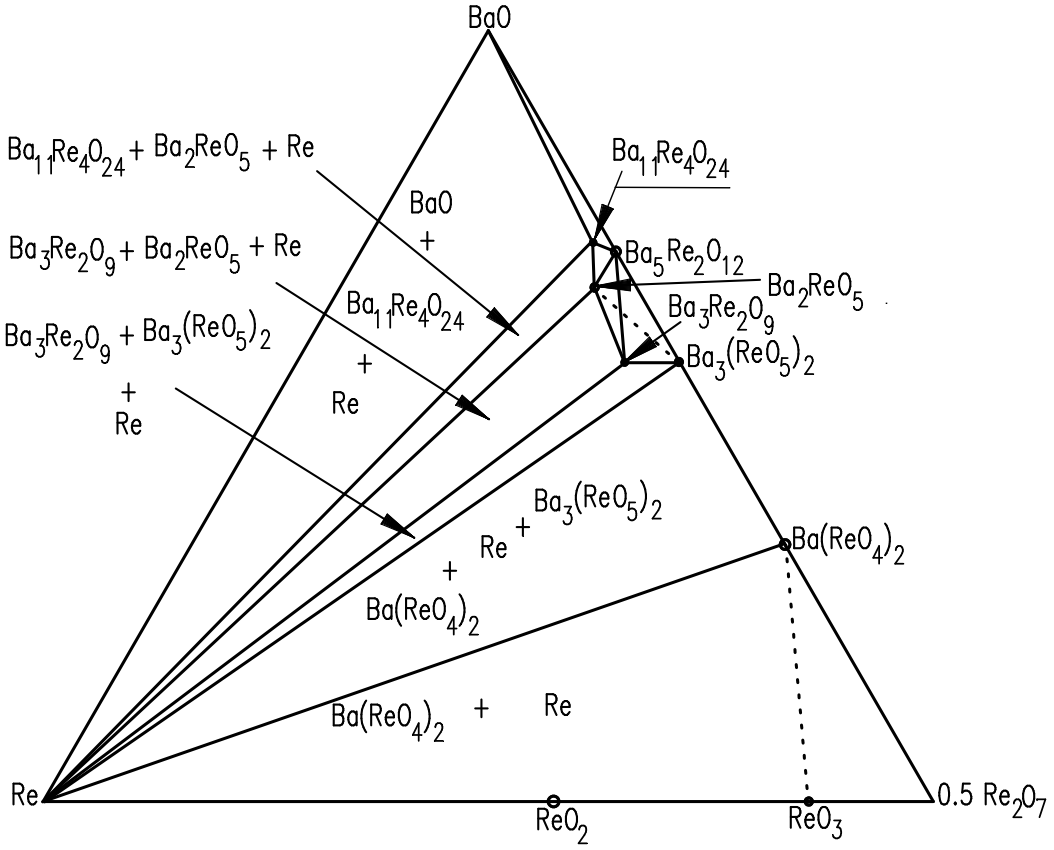

Fig. 22: Scheme of phase stability in the Ba-Re-O system

(the new phase is underlined).

In the Ca-Re-O system the stability of the Ca-rich phases were investigated. Two phases, $Ca_{11}Re_4O_{24}$ and $Ca_5Re_3O_{15}$, could be synthesised as single phase for the

first time. The crystal structures of the complex oxides $Ca_{11}Re_4O_{24}$ and $Ca_5Re_3O_{15}$ were determined recently by X-ray single crystal diffraction [35, 62]. The structure model for $Ca_5Re_3O_{15}$ as proposed in this work based on X-ray powder diffraction data was developed independently from the single crystal study of W. Jeitschko *et al.* [62]. Some discrepancies between the crystal structures revealed from powder diffraction data and single crystal ones were established. These differences are discussed below in Chapter 4.2.4. in detail. The crystal structure investigation of another synthesised compound, $Ca_{11}Re_4O_{24}$, was also carried out by refinement of X-ray powder diffraction data to confirm results, which were published earlier [35]. Two more phases with the approximate cation composition of Ca:Re = 4:3 were found in this system and their cell parameters could be defined on the basis of X-ray powder diffraction pattern indexing and electron diffraction study as well. The unit cell of the first compound has a primitive cubic symmetry with lattice parameter a = 7.8820(3) Å, and the unit cell of the second one is determined as primitive monoclinic with cell parameters a = 5.7190(4) Å, b = 5.6617(4) Å, c = 12.082(1) Å; β = 95.59(1)°. But all attempts to synthesise a single phase sample of these two phases failed. It can be explained due to the following reasons: 1) very close cation compositions of the two phases 2) both phases are unstable at the temperature above 900°C and no getters working at temperatures between 750°C and 900°C and at the same time setting partial oxygen pressure in the tube corresponding the values of 10^{-12}-10^{-15} bar could be found as shown in Fig. 20.

Also attempts to synthesise new compounds with rhenium in low oxidation states, less than +7, in the Mg-Re-O system have been made. But despite different applied preparation methods, which are described above, these efforts failed. A mixture of magnesium perrhenate and metallic rhenium in different proportions in dependence on cation compositions and partial oxygen pressure during the synthesis could be identified only.

4.2 Structure investigations

4.2.1 The crystal structures of the $M_{11}Re_4O_{24}$ double oxides (M = Sr, Ba)

The X-ray powder diffraction patterns of annealed samples with $M_{2.75}ReO_{5.75}$ (M = Sr, Ba) bulk composition were completely indexed based on a body-centred tetragonal cell with a = 11.6779(1) Å and c = 16.1488(2) Å (cell volume V = 2202.26(5) Å^3) for M = Sr; a = 12.2347(5) Å and c = 16.647(1) Å (V = 2496.65(5) Å^3) for M = Ba. The indexing of the X-ray diffraction pattern was confirmed by an electron diffraction study. The preliminary electron diffraction study did not reveal any superstructural spots corresponding to a decrease in symmetry or a unit cell expansion. Since the reflections with hkl: $h+k+l = 2n+1$, $hk0$: h, $k = 2n+1$ and $00l$: $l = 4n+1$ were systematically absent, space group $I4_1/a$ was considered for further crystal structure determination.

The integral intensities of the reflections from the angular range 5°-70° for the diffraction pattern of $Sr_{11}Re_4O_{24}$ were extracted by profile fitting and further used for the calculation of the three-dimensional Patterson distribution. The analysis revealed the positions of Re and for a part of the Sr atoms. The atomic coordinates of the other Sr and oxygen atoms were found by a subsequent Fourier and difference Fourier syntheses. After several iterations good agreement between experimental and calculated patterns was achieved: R_I = 0.011, R_P = 0.056, R_{wP} = 0.079 [63]. The observed, calculated and difference X-ray diffraction patterns are shown in Fig.23.

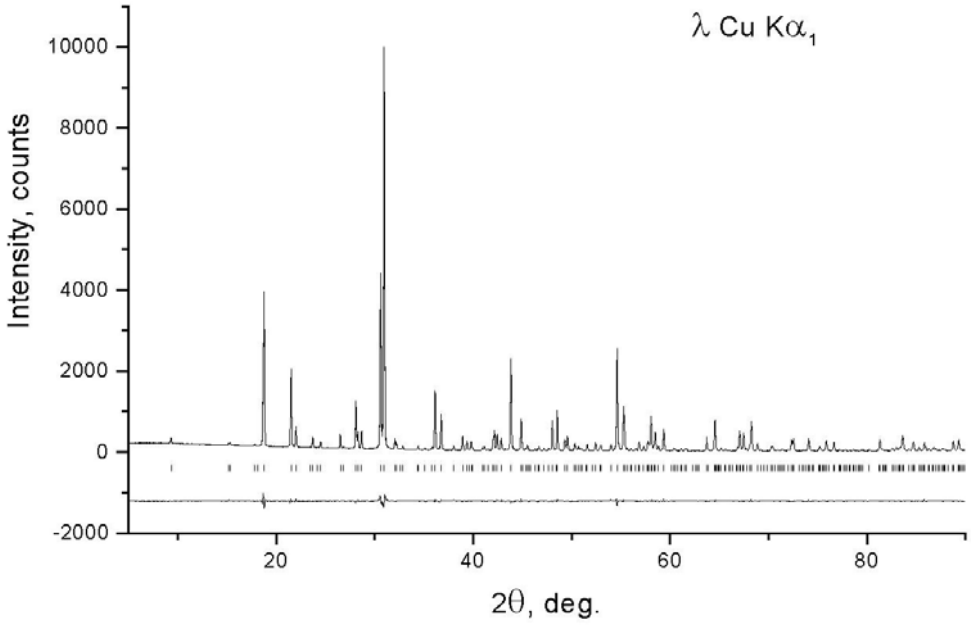

Fig. 23: Experimental, calculated and difference X-ray patterns for $Sr_{11}Re_4O_{24}$.

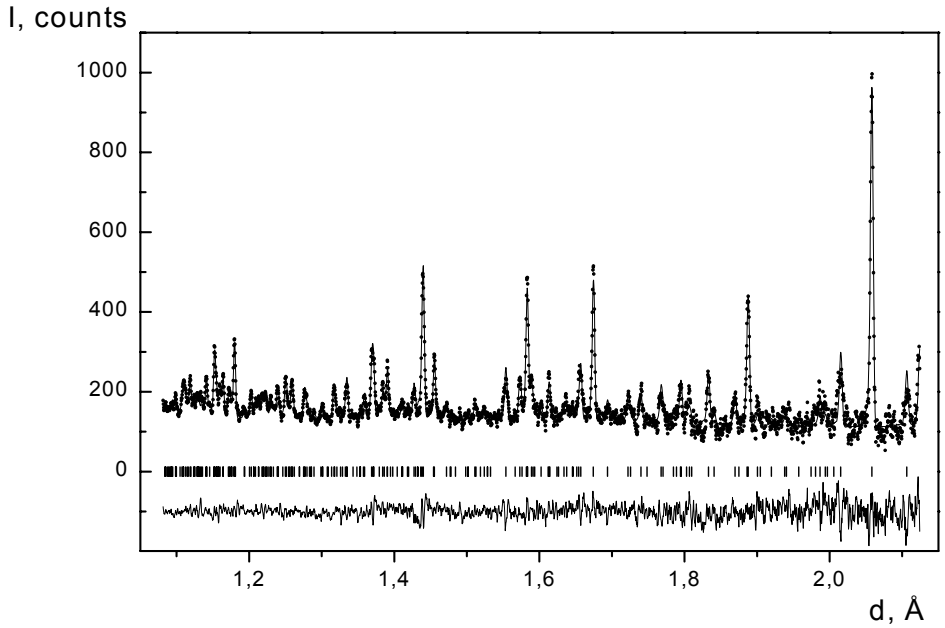

Fig. 24: Experimental, calculated and difference neutron diffraction patterns (TOF) for $Sr_{11}Re_4O_{24}$.

Neutron powder diffraction was performed to check the obtained structure model of $Sr_{11}Re_4O_{24}$. The final refinement was carried out with fixed thermal parameters 0.5 $Å^2$ for the Sr and Re atoms and 1 $Å^2$ for the oxygen ones and is in very good agreement (χ^2 = 1.85) with the refinement based on X-ray powder diffraction data. The composition of this compound, as determined from structure refinement, differs from the bulk composition of the sample and corresponds to the formula $Sr_{2.75}ReO_6$ ($Sr_{11}Re_4O_{24}$). The observed, calculated and difference neutron diffraction patterns are shown in Fig. 24. The crystallographic parameters, positional parameters and the main interatomic distances are listed in Tables 4 - 6 (see Appendix).

The initial atomic positions for a $Ba_{11}Re_4O_{24}$ structure refinement were taken from the $Sr_{11}Re_4O_{24}$ structure, assuming $Ba_{11}Re_4O_{24}$ is isostructural. After sequential iterations a sufficient agreement between experimental and calculated patterns was achieved: R_I = 0.049, R_P = 0.034, R_{wP} = 0.046. The observed, calculated and difference X-ray diffraction patterns are shown in Fig. 25. The parameters of the measurements and refinement, positional parameters and the main interatomic distances for $Ba_{11}Re_4O_{24}$ are listed in Tables 7 - 9 (see Appendix).

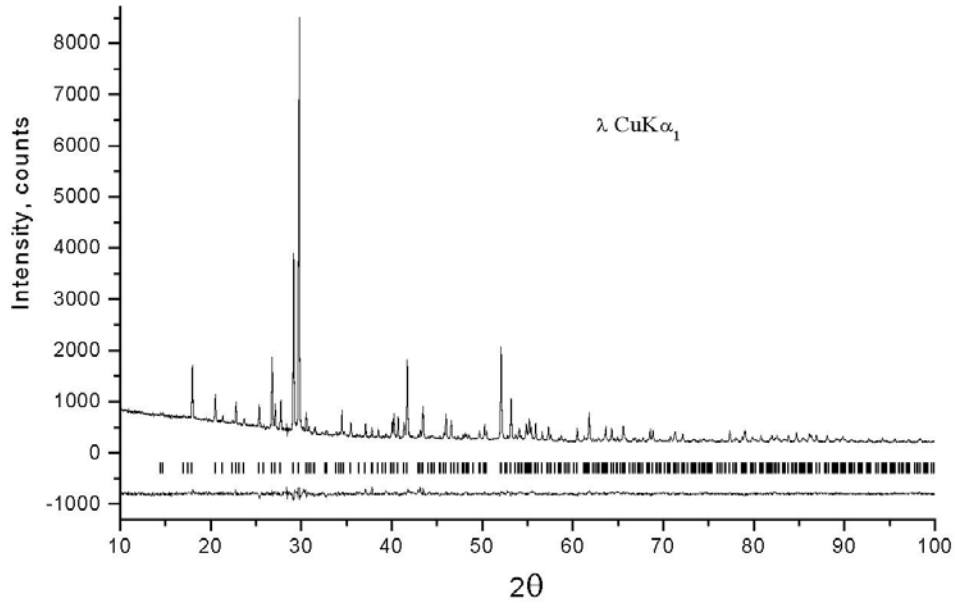

Fig. 25: Experimental calculated and difference X-ray diffraction patterns for $Ba_{11}Re_4O_{24}$.

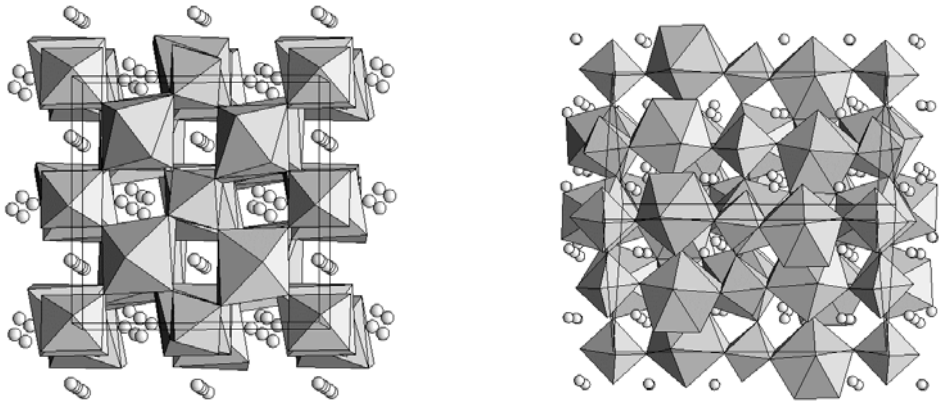

Fig. 26: The projections of the $Sr_{11}Re_4O_{24}$ crystal structure along [001] (left) and [110] (right).

Since the refinement results for $Ba_{11}Re_4O_{24}$ unambiguously confirm the initial assumption that the $Ba_{11}Re_4O_{24}$ compound is isostructural to $Sr_{11}Re_4O_{24}$, their crystal structures will be described further on the example of the latter. The differences in the bond lengths of *M*/O (*M* = Sr, Ba) polyhedra are summarised in Tables 6 and 9. The cell parameters of $M_{11}Re_4O_{24}$ are clearly connected with the

parameters of the perovskite subcell a_{per}: $a = 2\sqrt{2}\,a_{per}$, $c = 4a_{per}$. Formally the $M_{11}Re_4O_{24}$ formula can be written as $M_7\square(M_4Re_4)O_{24}$, which allows us to consider this compound as a cation-deficient perovskite with vacancies in the *A*-sublattice. Two projections of the $Sr_{11}Re_4O_{24}$ crystal structure along the [001] and [110] axes are shown in Fig. 26. Fig. 26 (left) shows that Re and *M*(4) atoms both occupy the *B*-position of the perovskite subcell in an ordered manner forming a "rock salt" type cation sublattice. The remaining *M* atoms are placed in the channels of a three-dimensional framework formed by ReO_6 and $M(4)O_8$ polyhedra, connected by corner sharing and edge sharing. Re(1) and Re(2) atoms are located in distorted octahedra ($d_{Re(1)-O}$ = 1.92-1.97 Å, $d_{Re(2)-O}$ = 1.87-1.88 Å). Since the octahedral coordination is not typical for Sr cations, the perovskite octahedral framework is significantly transformed. So, $Re(1)O_6$ octahedra are only slightly tilted along [110] whereas $Re(2)O_6$ ones are rotated along the same axis by $\approx 45^o$. This changes the *M*(4) oxygen environment from an octahedron to an irregular 8-fold polyhedron where Sr(4)-O distances vary in the range of 2.32-2.87 Å, and Ba(4)-O ones in the range of 2.40-2.85 Å. As a result, the $Re(2)O_6$ octahedron is edge shared by the equatorial oxygen atoms O(4) and O(6) to four $M(4)O_8$ polyhedra and connected with two $M(4)O_8$ ones by corner-sharing via the apical oxygen atoms O(5) (see Fig. 26). $Re(1)O_6$ octahedra are linked with the *M*(4) polyhedra only by corner sharing. The rotation of the ReO_6 octahedra leads to two kinds of nonequivalent channels filled by *A*-cations (see Fig. 26a). In the first one only 3/4 of *A*-positions are occupied by *M*(1) and *M*(2) cations with 12-fold ($d_{Sr(1)-O}$ = 2.59-3.21 Å) and 10-fold ($d_{Sr(2)-O}$ = 2.55-3.26 Å) coordinations, respectively. The second one contains *M*(3) atoms surrounded by eight oxygen atoms ($d_{Sr(3)-O}$ = 2.50-2.97 Å).

The formal oxidation state of Re, calculated from the refined composition, is equal to +6.5. The Re atoms in the $M_{11}Re_4O_{24}$ structure are distributed over two nonequivalent positions and we can expect an ordered placement of Re^{+6} and Re^{+7} cations. The reasonable argument for this ordering is the nonnegligible difference between average Re-O distances for $Re(1)O_6$ ($<d_{Re-O}>$ = 1.95 Å) and $Re(2)O_6$ ($<d_{Re-O}>$ = 1.88 Å) octahedra. These interatomic distances are in very good agreement with the ionic radii of Re^{+6} and Re^{+7} cations for octahedral coordination: $r(Re^{+6})$ = 0.52 Å, $r(Re^{+7})$ = 0.49 Å [34]. Note that we did not use the radius $r(Re^{+7})$ = 0.57 Å as

proposed by Shannon [64] since this value is based on one compound only, $Re_2O_7 \times 2H_2O$, with one highly distorted octahedral site, where the Re-O distances vary between 1.65 Å and 2.16 Å. Certainly, the average value for this radius 0.49 Å, calculated from $Ca_5Re_2O_{12}$ and $Sr_5Re_2O_{12}$ structures [34], is more reliable than the value given by Shannon. Consequently, we can propose that the Re(1) position is preferentially occupied by Re^{+6} cations, whereas Re^{+7} ones situated on the Re(2) site.

The composition $Sr_{11}Re_4O_{24}$ ($Sr_{2.75}ReO_6$) is close to Sr_3ReO_6. An increase of the size of strontium atoms in comparison with the calcium ones in Ca_3ReO_6 results in an essential structural rearrangement of the anion framework and a formation of vacancies in the *A*-sublattice. The type of polyhedra sharing is different for these two structures in spite of the similar *B*-cation "rock-salt" arrangement. In most cases the octahedral tilting distortion of the perovskite structure leads to a change of the first coordination sphere around *A*-cations. At the same time, the coordination environment of *B*-cations remains almost unchanged. The main reason for this distortion is the requirement to optimise the distances between *A*-cations and oxygen atoms. The geometrical relationship between *A*-O and *B*-O distances is determined by the Goldschmidt factor. In contrast the degree of octahedra tilting in the $M_{11}Re_4O_{24}$ structure significantly exceeds the usual tilt angles (which are approximately equal to 10^o) and leads to dramatic changes in the first coordination sphere for half of the *B*-cations. This structural transformation is caused by the large size of *M* cations (*M* = Sr, Ba), which have to be surrounded by more than six oxygen atoms.

The crystal structure type of $M_{11}Re_4O_{24}$ (*M* = Sr, Ba) is closely related to two other structures of the already known compounds with the same stoichiometry, $Ca_{11}Re_4O_{24}$ [35] and $Sr_{11}Os_4O_{24}$ [65]. The structure of $Sr_{11}Os_4O_{24}$ has been refined in the centrosymmetric, monoclinic space group $I2/a$, while for $Ca_{11}Re_4O_{24}$ non-centrosymmetric, the tetragonal space group $I4_1$ was unambiguously established. Both structures may be considered to be derived from the common tetragonal, higher symmetry space group $I4_1/a$ of $M_{11}Re_4O_{24}$ (*M* = Sr, Ba) through a translationengleiche (*t*) transformation. The attempts to refine the data for $Sr_{11}Re_4O_{24}$ in the other space groups were carried out with moderate success. Both refinements resulted in residuals of $R_I = 0.09$, as compared to $R_I = 0.011$ in the refinement with

the correct space group $I4_1/a$. These minor differences in the $M_{11}Re_4O_{24}$ structures for M = Ca and M = Sr, Ba can be traced to the different space requirements of the calcium and strontium atoms. In $Ca_{11}Re_4O_{24}$ the calcium atoms have coordination numbers of 8 and 9. In contrast, the strontium atoms, occupying the A-sublattice, have clearly coordination numbers of 10 and 12.

4.2.2 The crystal structure of $Sr_7Re_4O_{19}$

The X-ray powder diffraction pattern of an annealed sample with bulk composition $Sr_7Re_4O_{19}$ was completely indexed based on a *C*-centred monoclinic cell with a = 13.6379(3) Å, b = 5.6035(2) Å, c = 10.3700(3) Å and β = 98.348(2)°. The symmetry was confirmed by electron diffraction. As no additional extinction rules are observed, three space groups, *C*2, *Cm* and *C*2/*m*, have to be considered for crystal structure solution only.

Due to the similarity between the cell parameters of this compound and the already known compound $Ba_7Ir_6O_{19}$ (S.G. C 2/m) [66], the crystal structure of $Ba_7Ir_6O_{19}$ was used as an initial structure model for refinement based on the X-ray powder diffraction data. The Sr and Re atoms occupy the Ba and Ir atoms positions of the $Ba_7Ir_6O_{19}$ crystal structure, while the Ir(3) position remains unoccupied. After sequential iterations, good agreement between experimental and calculated patterns was achieved: R_I = 0.032, R_P = 0.058, R_{wP} = 0.079. However, some reflections with indices 0*k*0 were not fitted well enough. The March-Dollase function was used to take the preferred orientation along the [010] direction into account. The following values of reliability factors were obtained: R_I = 0.018, R_P = 0.050, R_{wP} = 0.068 [67] and a preferred orientation parameter, r, of 0.94(1) [68]. The observed, calculated and difference X-ray diffraction patterns are shown in Fig. 27. The final refinement was carried out with one common thermal parameter for all oxygen atoms. The crystallographic parameters, positional parameters and characteristic interatomic distances for $Sr_7Re_4O_{19}$ are listed in Tables 10, 11 and 12, respectively (see Appendix).

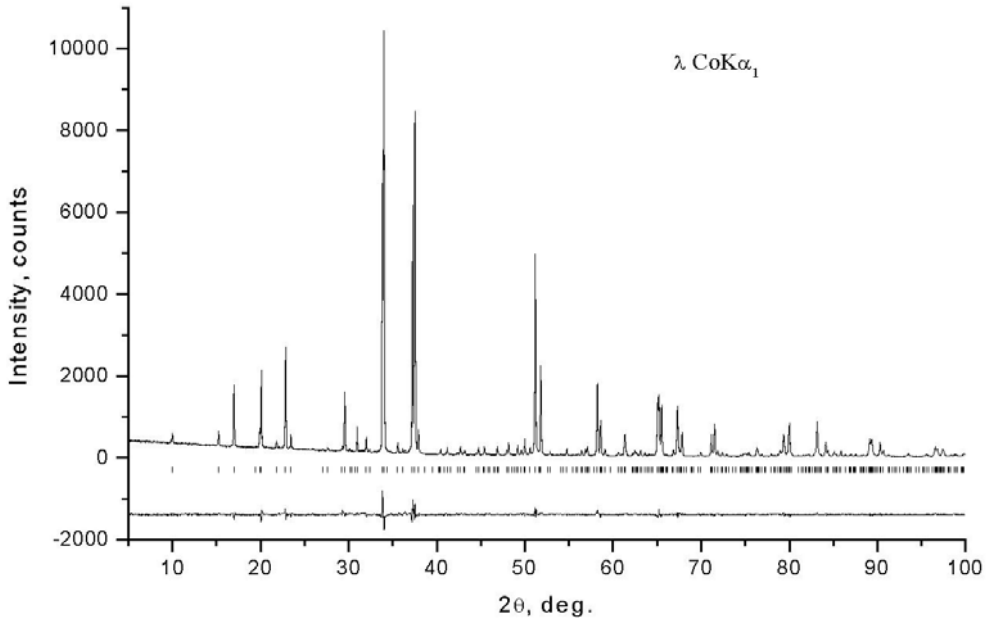

Fig. 27: Experimental, calculated and difference X-ray patterns for $Sr_7Re_4O_{19}$.

As mentioned above, the $Sr_7Re_4O_{19}$ crystal structure can be derived from the $Ba_7Ir_6O_{19}$ structure [66]. The $Ba_7Ir_6O_{19}$ structure consists of units of three face-shared, slightly distorted IrO_6 octahedra . These units are linked together by corner-sharing and form a two-dimensional network in the *a/b*-plane. Ba atoms have a 10- and 12- coordination of oxygen atoms. Note that the $Ba_7Ir_6O_{19}$ structure is closely related to the hexagonal nine-layer $BaRuO_3$ structure [69], which consists of similar units of three face-shared RuO_6 octahedra. These units build up the three-dimensional network in contrast to the $Ba_7Ir_6O_{19}$ structure. The complex oxide with the proposed composition $Sr_3Re_2O_9$ reported in the literature [48] was suggested to be isostructural with the $Ba_3Re_2O_9$ [32] oxide. Its structure can be derived from the $BaRuO_3$ crystal structure by removing Ru atoms from the middle octahedron of the three face-sharing octahedra units to overcome the electrostatic repulsion between highly charged neighbouring Re^{+6} cations. The crystal structure of $Sr_7Re_4O_{19}$ can be derived from the $Ba_7Ir_6O_{19}$ structure in the same way. This results in infinite *cis*-bridged chains of the ReO_6 octahedra linked by common corners. Each chain is connected with another one by corner-sharing of each second ReO_6 octahedron.

These infinite structure fragments are held together by 10- and 12-fold coordinated Sr atoms.

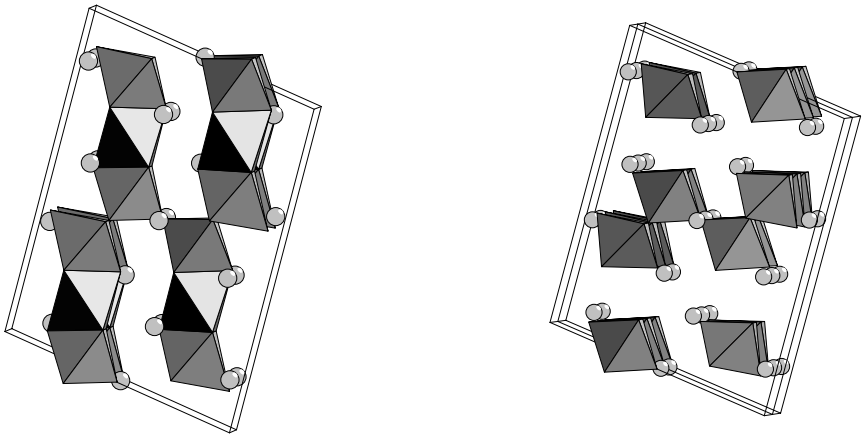

Fig. 28: The projections along the [010] axis of the $Ba_7Ir_6O_{19}$ (left) and the $Sr_7Re_4O_{19}$ (right) crystal structures.

The projections along the [010] axis of the $Ba_7Ir_6O_{19}$ (left) and the $Sr_7Re_4O_{19}$ (right) crystal structures are shown in Fig. 28. There are two nonequivalent Re positions in the $Sr_7Re_4O_{19}$ crystal structure. As mentioned above Re atoms are situated in the distorted octahedra. The average Re-O distance is 1.95 Å and 1.94 Å for Re(1) and Re(2) atoms, respectively, in good agreement with the ionic radius of Re^{6+} (0.52 Å) for CN = 6. Sr atoms have two different coordinations. Sr(1) and Sr(4) are twelve-fold coordinated, Sr(2) and Sr(3) have 10 neighbouring oxygen atoms each. The Sr(4) environment is regular in contrast to other Sr/O-polyhedra and can be described as a four capped cube . Other Sr atoms have irregular oxygen coordination. The $Sr_7Re_4O_{19}$ structure may be considered as an intermediate structure between Ba_2ReO_5 [6] and $Ba_3Re_2O_9$ [32] structures. The Ba_2ReO_5 compound contains ReO_6 octahedra linked by common corners and form infinite *cis*-bridged chains. In contrast, corner-sharing ReO_6 octahedra build infinite layers in the $Ba_3Re_2O_9$ structure. The $Sr_7Re_4O_{19}$ structure consists of two isolated, infinite chains of corner-sharing ReO_6 octahedra connected with each other. These three different structure motives are shown in Fig. 29. So, a new $Sr_7Re_4O_{19}$ double oxide can be considered as the fourth member of the $A_{4+n}Re_4O_{16+n}$ structure family (n = 0, 1, 2,...), where *A* is an alkali-earth metal.

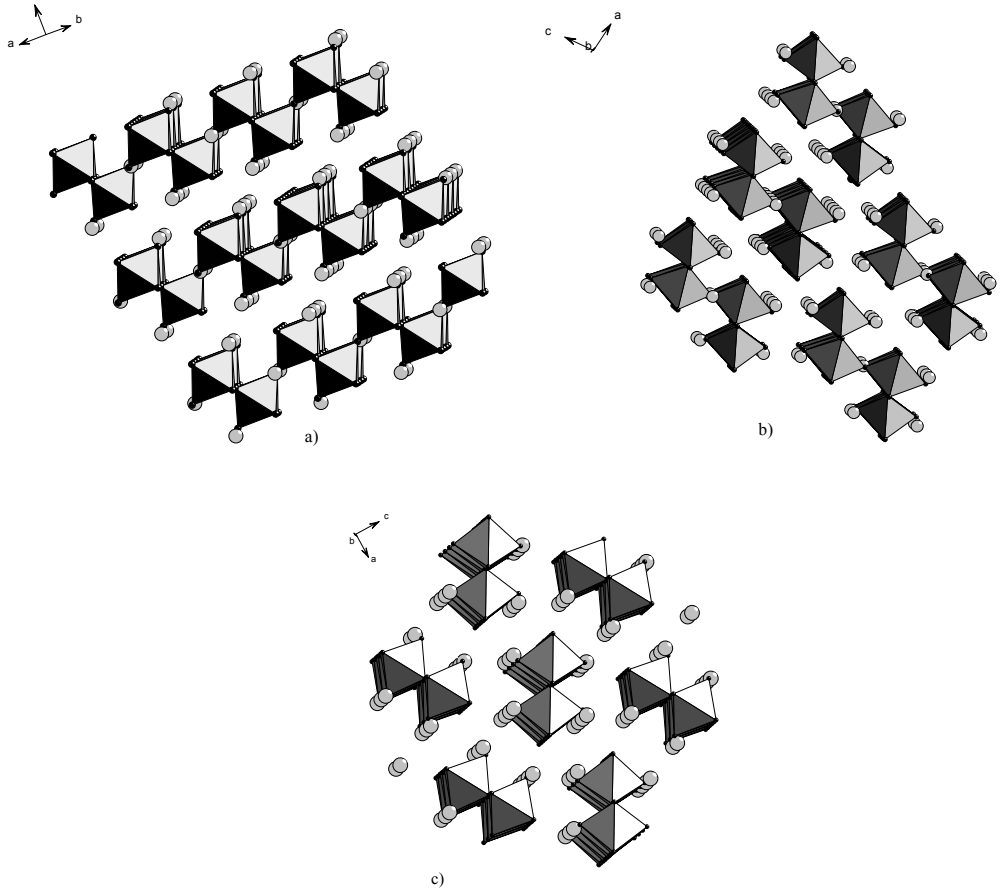

Fig. 29 The main structure motives of

$Ba_3Re_2O_9$ (a), $Sr_7Re_4O_{19}$ (b) and Ba_2ReO_5 (c).

4.2.3 The crystal structure of the Sr_3ReO_6 double perovskite

A new ternary oxide, Sr_3ReO_6, has been synthesised by annealing in an evacuated silica tube under controlled partial oxygen pressure $p(O_2) = 4.6\times10^{-15}$ bar at 740°C for 24 hours. To control partial oxygen pressure a mixture of Ni and NiO was used. The structure investigation of the Sr_3ReO_6 complex oxide was carried out using X-ray powder diffraction. Its cation composition was determined by EDX analysis, Sr : Re = 3.00(4) : 1.00(4). The powder diffraction pattern of the Sr_3ReO_6 oxide was indexed, based on an *I*-centred monoclinic cell with a = 8.1177(8) Å, b = 5.9103(6) Å, c = 5.9422(6) Å, β = 90.47(1)°. The symmetry of the crystal structure and unit cell parameters were confirmed by an additional electron diffraction study. The crystal structure of the Ba_2SbBiO_6 oxide (S.G. *I*2/*m*) was chosen as an initial model for the refinement of the Sr_3ReO_6 structure, because of the similarity of the X-ray powder diffraction patterns, cell volumes and indexing. After several refinement sequences the following reliability factors were achieved: R_I = 0.077, R_P = 0.135. These high reliability factors may be explained by strong overlapping of the peaks of the main phase with impurity peaks. Because of the very narrow stability range of Sr_3ReO_6 all attempts to prepare pure phases of this compound failed. Despite the maximum intensity of an impurity peak is less than 5% of the intensity of the strongest peak of Sr_3ReO_6 we could neither exclude regions with impurity peaks nor carry out a multiphase refinement, because of the large number of different admixture phases, such as $Sr(OH)_2$, $SrCO_3$, and strontium hydroxide hydrates with different water content. But on the basis of the electron microscope study, the X-ray powder data of this compound and EDX analysis one can conclude that the proposed structure model is quite reliable.

The Sr_3ReO_6 complex oxide adopts a distorted perovskite structure with Sr and Re ordered on the *B*-sites in “rock-salt” manner. Formally the Sr_3ReO_6 formula can be written as Sr_2SrReO_6. The Sr_3ReO_6 complex oxide could be considered as a Ba_2SbBiO_6 type of perovskite structure distortion [70]. The ReO_6 and SrO_6 octahedra are cooperatively rotated about the [011] axis of the perovskite subcell and $a^0b^-b^-$ tilted with respect to Glazer's notation [42]. The *A*-sites in a perovskite cell are occupied by the remaining Sr atoms. This compound is stable in the narrow range of

partial oxygen pressure from 4.6×10^{-17} to 2.3×10^{-15} bar only. At a higher partial oxygen pressure the Sr_3ReO_6 oxide decomposes to a mixture of SrO and $Sr_{11}Re_4O_{24}$. The formal Re valence in Sr_3ReO_6 increases from +6 to +6.5 due to a formation of cation vacancies in the *A*-sublattice, that leads to a change in the coordination number of the Sr atoms in the *B*-sublattice from 6 to 8. A further increase of the partial oxygen pressure to 1.1×10^{-3} bar leads to decomposition of $Sr_{11}Re_4O_{24}$ to $Sr_5Re_2O_{12}$ [34] and SrO. In this case all Re atoms with the oxidation state +6 in $Sr_{11}Re_4O_{24}$ are oxidised to Re^{+7}, and vacancies in the *B*-sublattice are formed. This oxidation sequence can be considered as a stepwise increase of the amount of cation vacancies in the *A*- and *B*-sublattices from $Sr_6Re_2O_{12}$ through $Sr_{5.5}Re_2O_{12}$ to $Sr_5Re_2O_{12}$, as shown in Eq.11:

$$Sr_6Re_2O_{12} \rightarrow Sr_{5.5}Re_2O_{12}+½SrO \rightarrow Sr_5Re_2O_{12}+½SrO. \quad (11)$$

The thermal analysis results of the Sr_3ReO_6 oxide are given in Fig. 30.

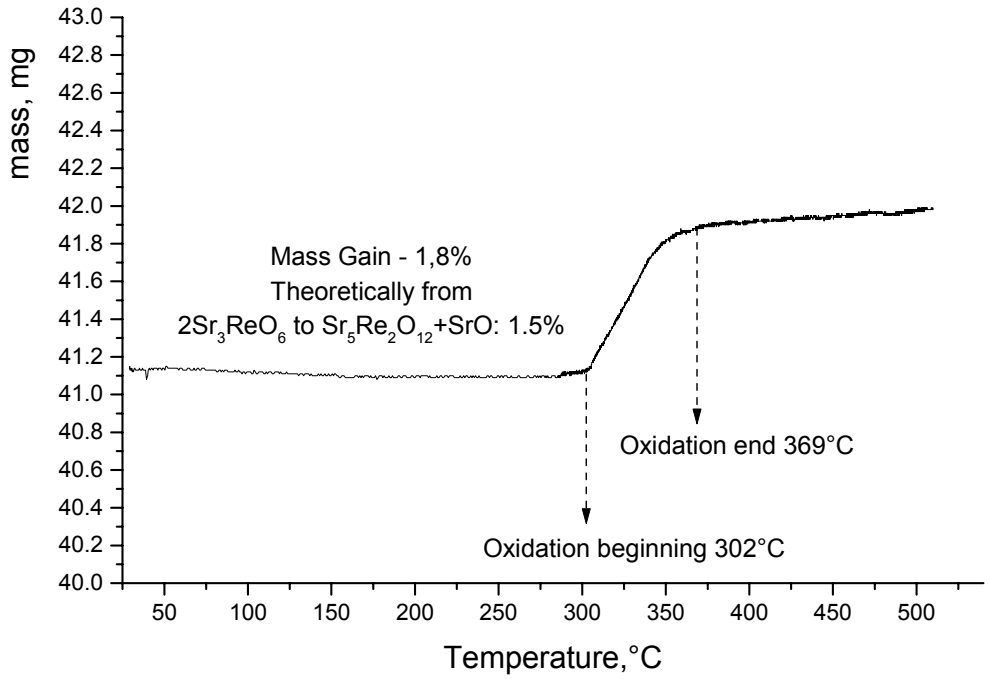

Fig. 30: TG-oxidation curve of Sr_3ReO_6.

The projections along the [001] axis of Sr_3ReO_6 (a) and the structural relations between Sr_3ReO_6 (a) [A_2ABO_6], $Sr_{11}Re_4O_{24}$ (b) [$A_{1.75}ABO_6$] and $Sr_5Re_2O_{12}$ (c) [$A_{1.75}A_{0.75}BO_6$] are shown in Fig. 31.

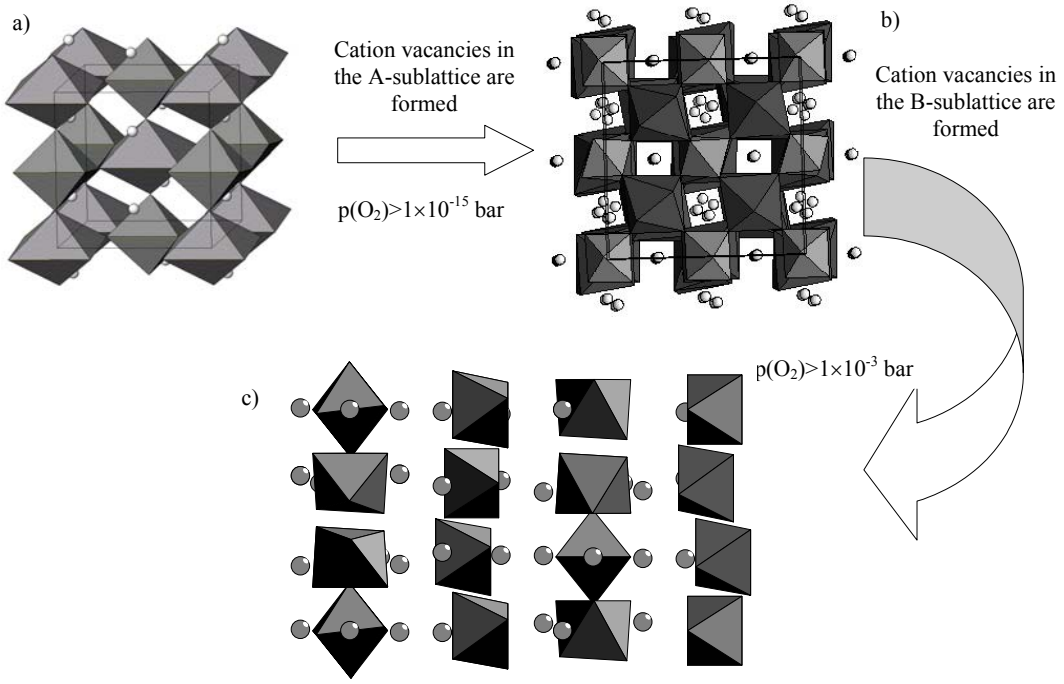

Fig. 31: Structural relationships between Sr_3ReO_6 (a) [A_2ABO_6], $Sr_{11}Re_4O_{24}$ (b) [$A_{1.75}ABO_6$] and $Sr_5Re_2O_{12}$ (c) [$A_{1.75}A_{0.75}BO_6$].

The structure relationships between double perovskites of complex alkali-earth rhenium oxides and the way of their structure changing in dependence on the alkali-earth elements radii are shown in Fig. 32.

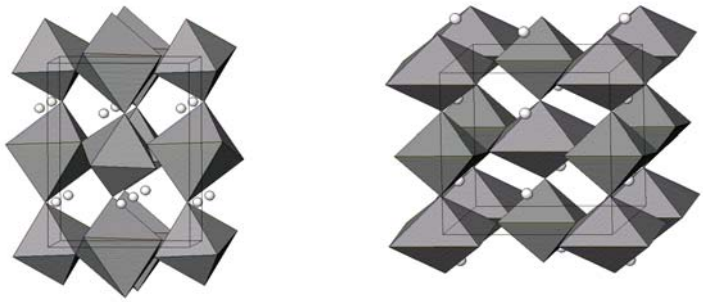

Ca_3ReO_6, S.G. P $2_1/n$
cooperatively octahedra tilt $a^+b^-b^-$

Sr_3ReO_6, S.G. I 2/m
$a^0b^-b^-$ isostructural to Ba_2SbBiO_6

Ba_3ReO_6 ???
oxycarbonate isostructural to Sr_3WO_6 ???

Fig. 32: Structure relationships between double perovskites of complex alkali-earth rhenium oxides.

4.2.4 The crystal structure of the $Ca_5Re_3O_{15}$ mixed valence compound

A single phase of the complex oxide $Ca_5Re_3O_{15}$ has been synthesised by solid state reaction of five moles of CaO and three moles of ReO_3 in an evacuated (10^{-5} mbar) sealed silica tube under a partial oxygen pressure, controlled by a mixture of Cu_2O/CuO at 700°C for 35 hours ($p(O_2) = 3.4\times10^{-11}$ bar). Its crystal structure was determined by X-ray powder analysis (space group *Amm*2; a = 5.6107(1) Å, b = 15.6913(5) Å, c = 7.2224(2) Å; Z=2). The crystal structure refinement for $Ca_5Re_3O_{15}$ was carried out using X-ray powder diffraction data using the RIETAN-97 program (R_I = 0.0135, R_P = 0.0413, R_{wP} = 0.0564). The atomic coordinates for the starting refinement were taken from a structure model as proposed by Jeitschko for a $Ca_5Re_3O_{15-x}$ single crystal [62] (see Table 15, see Appendix), but with the O(5) position fully occupied. The final refinement was carried out with common thermal parameters for the oxygen atoms. The results show some disagreements with the structure obtained from single crystal data (Jeitschko *et al.* [62]). A first attempt to refine the structure with a splitting of the Re2 position did not result in satisfying reliability factor, such as R_I = 0.028. The refinement of the occupancy parameters of Re2a and Re2b gave the following results: the Re2a position is fully occupied g=1.02(5) and the Re2b position vacant, g=0.01(6). The refinement of the $Ca_5Re_3O_{15}$ structure with only two rhenium sites, Re1 and Re2a, gave reliable results. The observed, calculated and difference X-ray diffraction patterns for the mixed valence oxide $Ca_5Re_3O_{15}$ are shown in Fig. 33. The positional parameters and characteristic interatomic distances are listed in Tables 17 and 18, respectively (see Appendix).

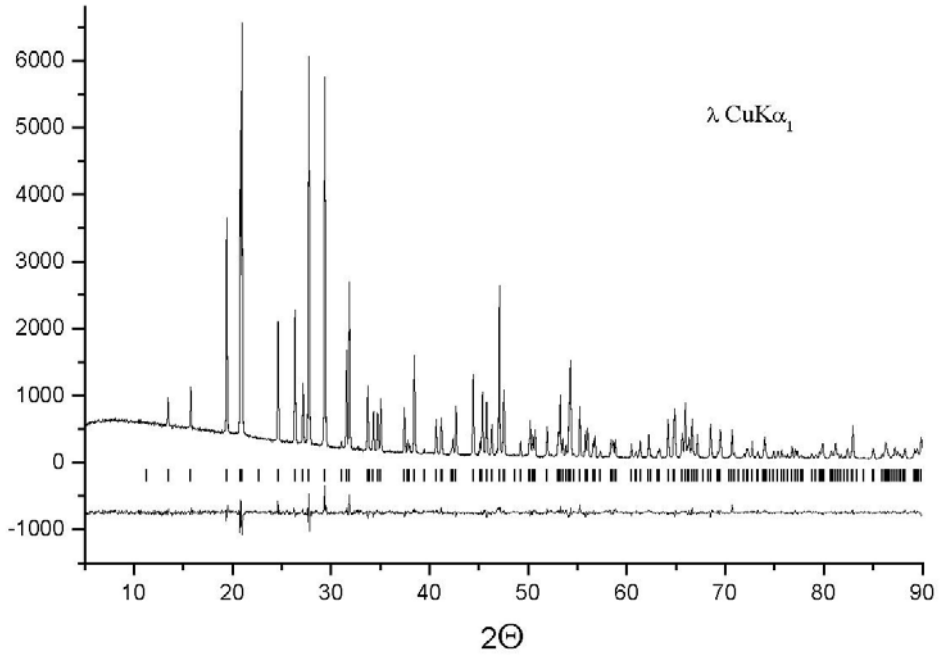

Fig. 33: Observed, calculated and difference X-ray diffraction patterns for the $Ca_5Re_3O_{15}$ sample.

Of the two different rhenium atoms one has square-pyramidal oxygen coordination, and Re(1)-O distances varying between 1.64 and 1.95 Å. The other rhenium site has trigonal-bipyramidal oxygen coordination (coordination number, CN 5). These two different coordination polyhedra are connected together by Ca atoms. The projection along the [100] axis of $Ca_5Re_3O_{15}$ is shown in Fig. 34.

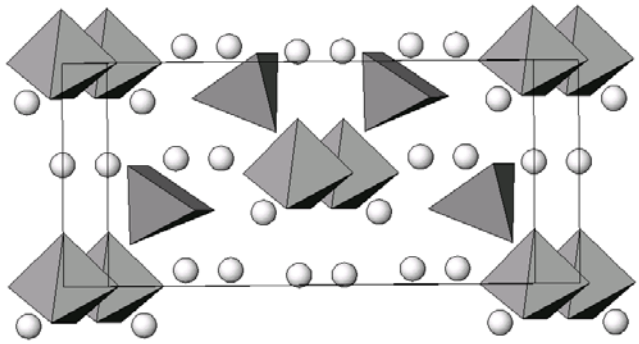

Fig. 34: Projection of the proposed $Ca_5Re_3O_{15}$ crystal structure along the [100] axis.

The formal oxidation state of rhenium in this compound, calculated with the assumption that the O(5) site is fully occupied, is equal to 6⅔. The average Re(1)-O distance of 1.86 Å is considerably longer than the average Re-O distance of 1.80 Å for the square-pyramidal rhenium sites in $Ba_5(ReO_5)_3Cl$ [71], where the rhenium atoms are in the formal oxidation state +7. Therefore, a structure corresponding to the formula $Ca_5Re^{+7}{}_2Re^{+6}O_{15}$ can definitely be ruled out, even though it is attractive, because neither one of the two rhenium atoms has a mixed oxidation number. The average Re(1)-O distance mentioned above and the average Re(2)-O distance in the trigonal-bipyramidal rhenium polyhedra of 1.845 Å suggest that the Re atoms in the $Ca_5Re_3O_{15}$ structure have a formal oxidation state of less than +7, and one additional electron per formula unit is not delocalized in the structure. All three different calcium sites in $Ca_5Re_3O_{15}$ have seven oxygen neighbours in monocapped trigonal prismatic coordination and with Ca-O distances between 2.231 and 2.59 Å.

4.2.5 The crystal structures of double perovskites with M_2MgReO_6 composition (M = Ca, Sr, Ba)

The X-ray diffraction patterns of the annealed samples with M_2MgReO_6 (M = Ca, Sr, Ba) bulk composition were completely indexed based on a primitive orthorhombic unit cell with parameters a = 5.4141(3) Å, b = 5.5455(2) Å, c = 7.7052(3) Å for M = Ca, an I-centred tetragonal cell with parameters a = 5.5698(2) Å, c = 7.9265(4) Å for M = Sr,. and based on an F-centred cubic cell with a = 8.0850(2) Å for M = Ba. This indexation is only in slight disagreement with the cell parameters reported by Sleight *et al.* [38] for the calcium and barium containing compound, while the indexing for Sr_2MgReO_6 performed by Sleight *et al.* is completely different from the cell parameters found in this work.

The Ba_2MgReO_6 structure model for refinement was taken as from Woodward [40] for the F-centred cubic cell and a BO_6 octahedra tilt system, where $a = b = c = 2a_{per}$, $a°a°a°$ tilt system corresponding to Glazer's notation [42]. After sequential iterations good agreement between experimental and calculated patterns was achieved: R_I = 0.022, R_P = 0.045, R_{wP} = 0.059. The observed, calculated and difference X-ray diffraction patterns are shown in Fig. 35. The crystallographic parameters, positional parameters and characteristic interatomic distances for Ba_2MgReO_6 are listed in Tables 19, 20 and 21, respectively (see Appendix).

For the refinement of the structure of Sr_2MgReO_6 an initial structure model was again taken from Woodward [40]. There is only one possible model for an I-centred tetragonal cell with the cell parameters $a \approx \sqrt{2}\, a_{per}$, $b \approx \sqrt{2}\, a_{per}$, $c \approx 2a_{per}$, and an $a°a°c$ tilt system corresponding to Glazer's notation [42]. The following reliability factors were achieved: R_I = 0.023, R_P = 0.059, R_{wP} = 0.078. The observed, calculated and difference X-ray diffraction patterns are shown in Fig. 36. The final refinement was carried out with one common thermal parameter for all oxygen atoms. The crystallographic parameters, positional parameters and characteristic interatomic distances for Sr_2MgReO_6 are summarised in Tables 22, 23 and 24 (see Appendix).

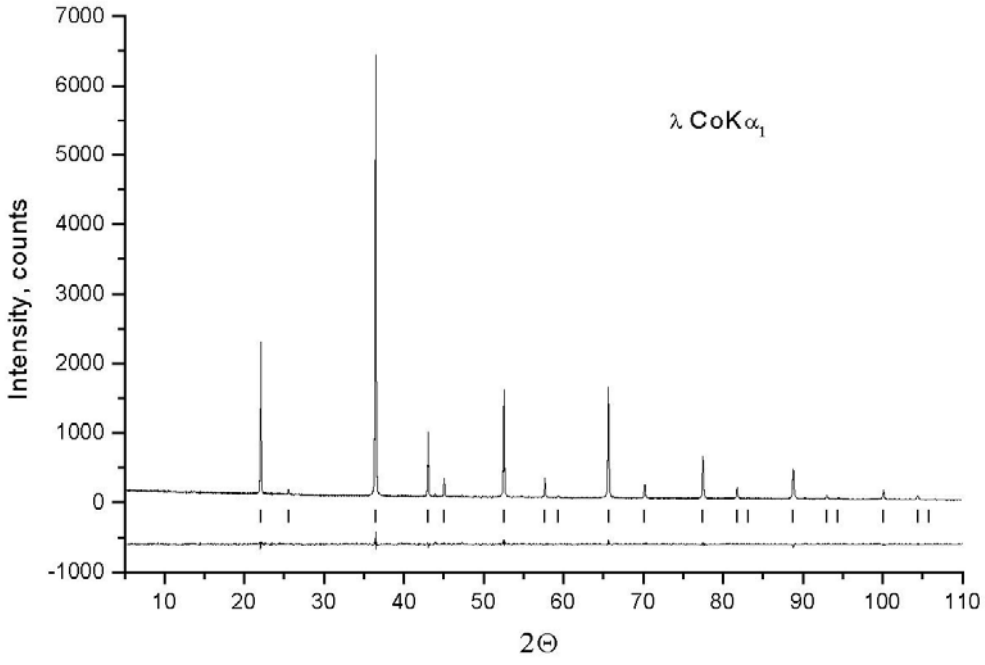

Fig. 35: Observed, calculated and difference X-ray diffraction patterns for Ba_2MgReO_6.

As noted above, the X-ray powder diffraction pattern of an annealed sample with Ca_2MgReO_6 bulk composition was completely indexed on the basis of a primitive orthorhombic cell. This type of distortion of the perovskite subcell is consistent with the value of the Goldschmidt factor $t = 0.9$, calculated from the ionic radii given by Shannon *et al.* [64]. The only *h*0*l*: $h + l = 2n$ systematic extinction was unambiguously detected. It allowed to propose as possible space groups *Pmmn* or $Pmn2_1$. The presence of 0*kl*: $k = 2n + 1$ reflections provides the evidence that this structure does not belong to the $GdFeO_3$ type [72], and the distribution of *B* cations is ordered and not random. The initial model for the refinement was based on the perovskite structure where *B* positions are occupied by Mg and Re atoms in a chess-board manner, and the Ca atoms situated on the *A* positions.

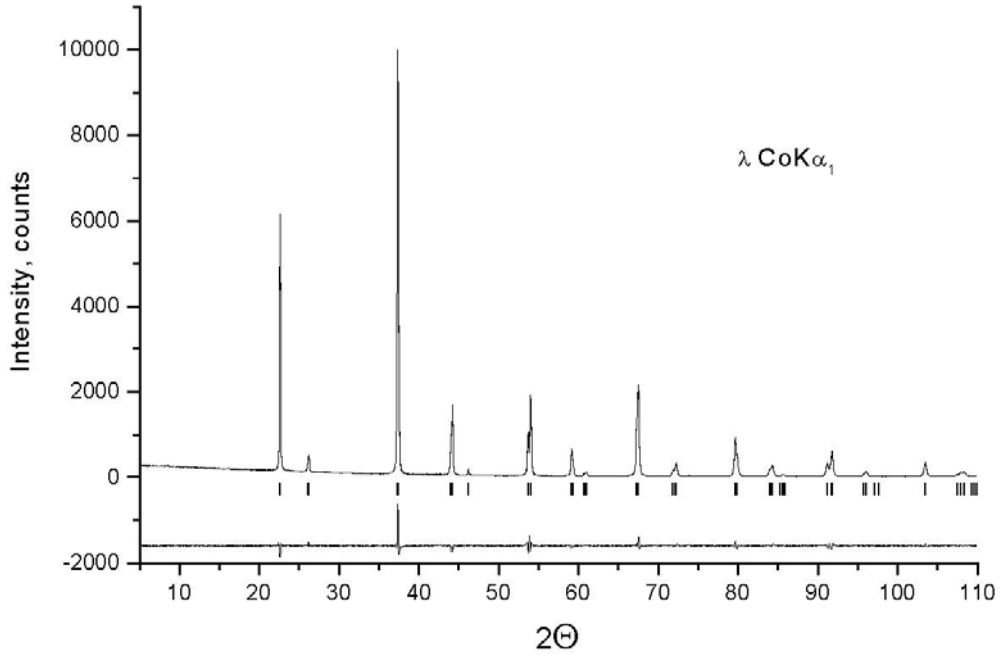

Fig. 36: Observed, calculated and difference X-ray diffraction patterns for Sr_2MgReO_6.

However, the subsequent refinement of this model led to too high values of reliability factors (R_I > 0.09) and unreasonable values for both the thermal parameters for the oxygen atoms and for the metal-oxygen distances. This indicates that the real symmetry might be lower than orthorhombic or an increase in unit cell dimensions is needed. Nevertheless, the structural refinement confirmed a chess-board ordered distribution of *B* cations and indicated that an anion sublattice distortion could not be determined perfectly within the orthorhombic cell described above.

As shown by Anderson *et al.* [39], and later supported by the example of the Ca_3ReO_6 structure [5], compounds with this kind of perovskite distortion can adopt structures with an expanded unit cell or crystallise in a monoclinic structure with a monoclinic angle close to 90°. We failed to detect reflections on the X-ray pattern which could arise from an increase in cell parameters. The electron diffraction study of this sample confirmed the conclusion that no cell expansion occurs. Further

refinements were therefore made using a monoclinic unit cell, despite the fact that the X-ray diffraction pattern was successfully indexed in terms of the orthorhombic one. According to the extinction rules, the space groups $P2_1/n$ and $P2/n$ have been considered. The space group symmetry $P2_1/n$ and initial atomic coordinates were taken from the crystal structure of Ca_3ReO_6. Hereby, a decrease of the reliability factor, R_I, down to 6.2 % was achieved with the thermal parameter for Mg atom fixed to the value 0.5 $Å^2$. A refinement of the thermal parameter of Mg atoms gives even better agreement, but the thermal parameter becomes negative. This is an indication that a *B* cation position might be partly occupied by Ca atoms. To check this assumption samples with different Ca and Mg content, $Ca_{3-x}Mg_xReO_6$ (x = 0.5, 0.75, 1.0, 1.5), were synthesised, but only for x = 1.0 a pure sample of Ca_2MgReO_6 could be prepared. All samples with x < 1 showed an admixture of Ca_3ReO_6, and in the case of Mg excess, x > 1, magnesium oxide, MgO, as impurity. The cell parameters of Ca_2MgReO_6 and Ca_3ReO_6 do not depend on the bulk compositions of the samples. It means that there is no solid solution of these two phases and one can assume that the cation composition of Ca_2MgReO_6 is exactly the x =1 case. Electron diffraction study does not only confirm the chosen unit cell for Ca_2MgReO_6, it also indicates that Ca and Mg atoms are statistically distributed on all *A* positions and on half of the *B* positions. Re atoms occupy the remaining *B*-sites in a rock salt manner. The best refinement of this structure model results in reliability factors R_I = 0.032, R_P = 0.052, R_{wP} = 0.071 with Ca and Mg atoms occupying one quarter of all *B* positions each. Consequently, ¾ of all *A* positions are occupied by Ca atoms and the remaining ¼ by Mg . The final refinement was carried out with one common thermal parameter for all oxygen atoms. The observed, calculated and difference X-ray diffraction patterns are shown in Fig. 37. The crystallographic parameters, positional parameters and characteristic interatomic distances for Ca_2MgReO_6 are listed in Tables 25, 26 and 27, respectively (see Appendix).

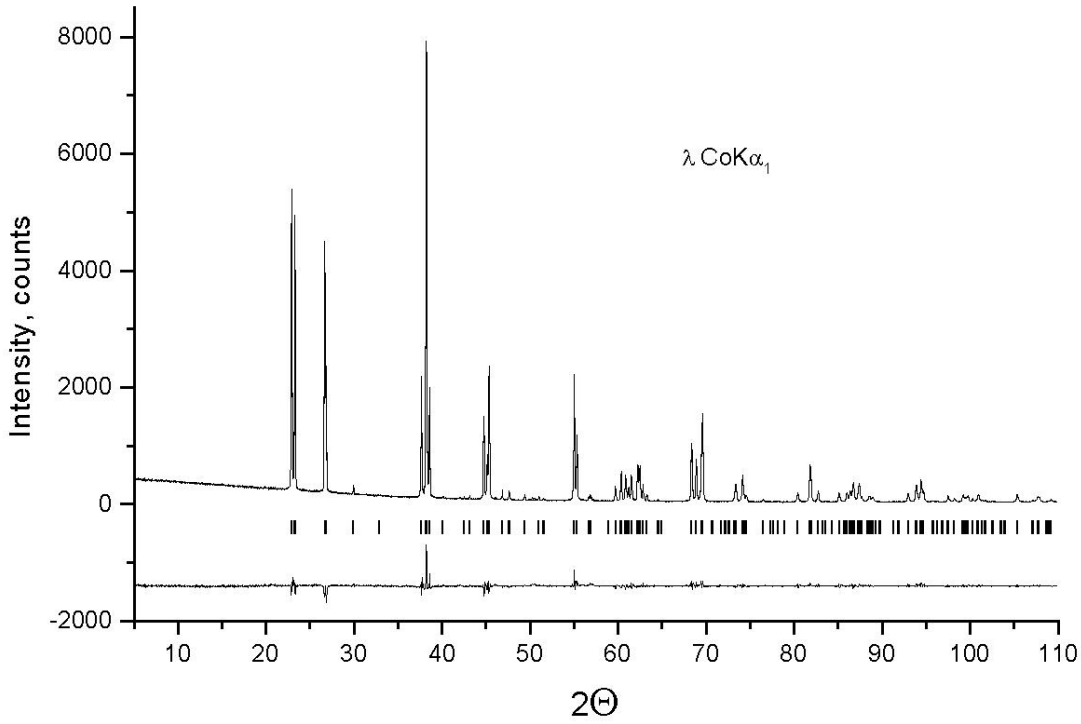

Fig. 37: Observed, calculated and difference X-ray diffraction patterns for Ca_2MgReO_6.

The Ca_2MgReO_6 crystal structure is shown in Fig. 38*c*). Re cations have an almost regular octahedral oxygen environment while Ca(2) and Mg(2) atoms are situated in slightly distorted octahedra. Since Ca and Mg atoms are too small to fit into the 12-fold coordinated *A* position, ReO_6 and (Ca, Mg)O_6 octahedra are cooperatively tilted along $[011]_{per}$ and rotated along $[100]_{per}$ to reduce to eight equal (Ca, Mg)(1) - O distances as compared to 12 in the high-symmetric, undistorted structure.

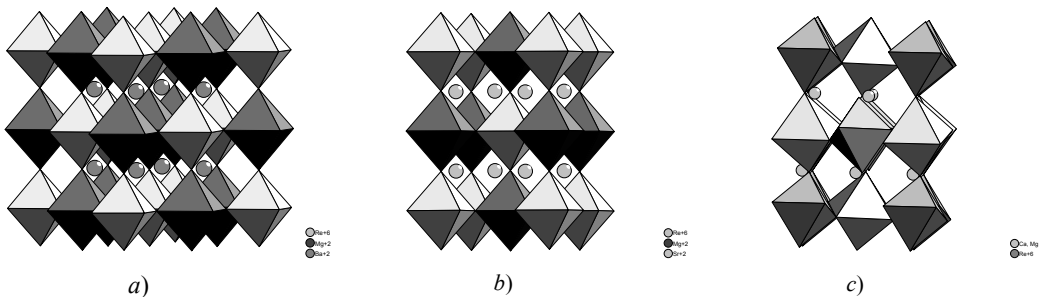

a) *b*) *c*)

Fig. 38: The crystal structures of MMg$_2$ReO$_6$ for *M* = Ba *a*), Sr *b*) and Ca *c*)

4.3 Magnetic properties

4.3.1 Magnetic properties of $Sr_{11}Re_4O_{24}$

$Sr_{11}Re_4O_{24}$ orders with a weak ferromagnetic component below the Curie temperature of T_C = 12(1) K as deduced from the temperature dependence of magnetisation at constant field strength of 0.25 T (see Fig. 39).

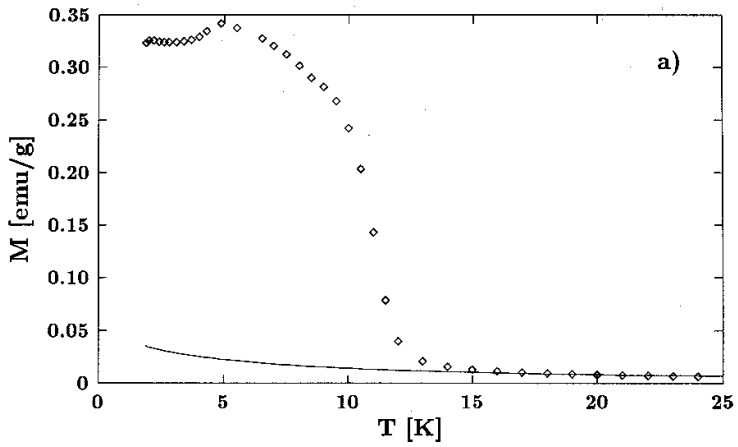

a)

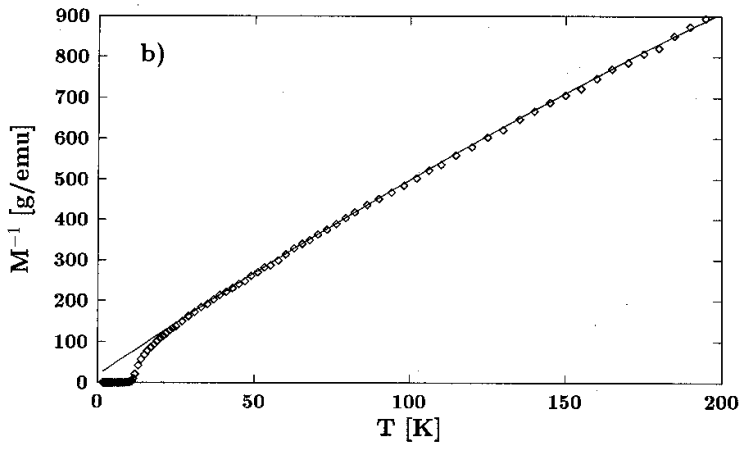

b)

Fig. 39: Temperature dependence of magnetization (a) and its inverse (b) for $Sr_{11}Re_4O_{24}$ at a constant field strength of 0.25 T.

A Curie-Weiss law, modified by an additional temperature independent contribution M_0,

$$M(T) = \frac{C}{T - \Theta} + M_0, \tag{11}$$

was fitted to the data from 30 to 200 K, revealing $M_0 = 1.65 \cdot 10^{-4}$ emu/g, Θ = -3.5 K and a paramagnetic moment of $0.80 \mu_B$ per Re^{+6} ion. Re^{+6} belongs to the very rare case of a $5d^1$ electron configuration. In a crystal field of octahedral symmetry the orbital levels split into a doublet and a low-lying triplet. The Landé factor *g* for the latter is zero, and a non-vanishing value for the magnetic moment is due only to a crystal field of lower symmetry and contributions from the doublet for a finite value of crystal field splitting [47]. A quantitative analysis of these effects must be based on the anisotropy of the *g* tensor and requires a single crystal.

The field dependence of magnetisation was measured at different temperatures below T_C (see Fig. 40 for T = 5 and 10 K). Starting from saturation the magnetisation decreases linearly with field, followed by a pronounced kink and smoothly joining into linear behaviour for saturation in opposite field direction. The field dependence can be described by

$$M(H) = M_1(H) + M_2(H), \tag{12}$$

with

$$\mathrm{M_1(H)} = \begin{cases} \alpha\ (H + H_0), & H \text{ decreasing} \\ \alpha\ (H - H_0), & H \text{ increasing} \end{cases} \tag{13}$$

and

$$\mathrm{M_2(H)} = \begin{cases} 2\alpha H_0 \tanh\left[(H + H_C)/\sigma\right], & H \text{ decreasing and } H < -H_C, \\ 2\alpha H_0 \tanh\left[(H - H_C)/\sigma\right], & H \text{ increasing and } H > H_C, \\ 0, & \text{else.} \end{cases} \tag{14},$$

$$2\alpha H_0 = \mathrm{M_{H \to 0}} \tag{15},$$

where $\mathrm{M_{H \to 0}}$ is the linear extrapolation of the saturation part of the hysteresis loop to zero field, $H \to 0$. Four parameters, α, H_0, σ, and H_C, have to be fitted to the observed data points. The results are given in Table 13 (see Appendix), and the calculated hysteresis loops are shown in Fig. 40 as drawn lines. The agreement is excellent for T = 5 to 8.4 K, but at 9.3 K slight deviations can be seen in the field

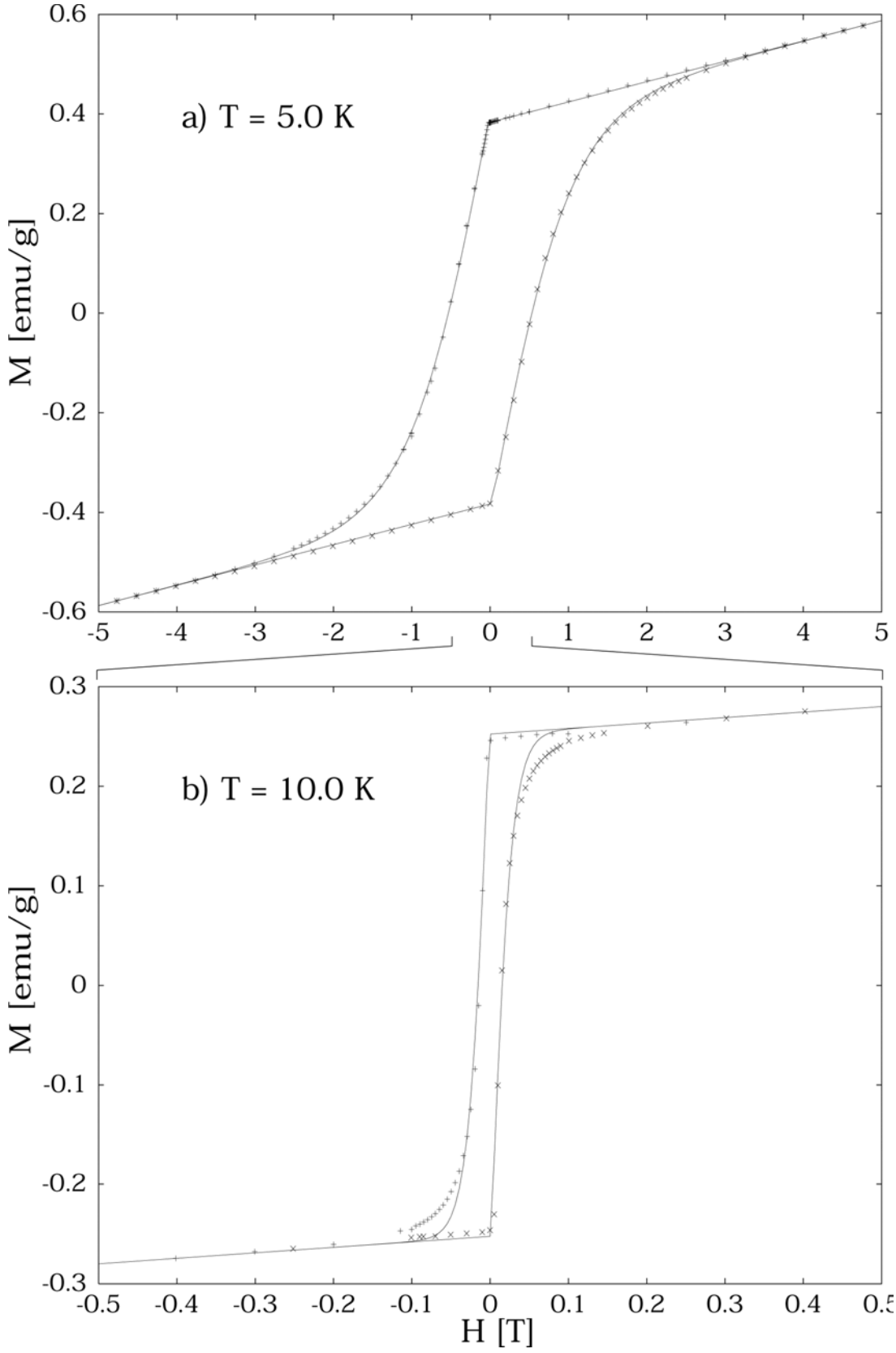

Fig. 40: Hysteresis loops of $Sr_{11}Re_4O_{24}$ at 5.0 K (a) and 10.0 K (b).

range approaching saturation, more pronounced at 10 K. The areas within one complete loop are calculated according to

$$\int_{loop} MdH = 4\alpha H_0(H_C + \sigma \ln 2) \tag{16}$$

and given in Table 13, too. The remanent magnetisation provides precise values for the temperature dependence of the resulting ferromagnetic component. Following an implicit function, notified by the same function obtained in molecular field approximation for a ferromagnetic spin-half system,

$$\frac{\mu(T)}{\mu_0} = \tanh \frac{\mu(T)/\mu_0}{T/T_C}, \tag{17}$$

yields $\mu_0 = 0.0734\mu_B$ per Re^{+6}-ion and T_C =11.94 K (see Fig. 41). This small value of μ_0 as compared to the paramagnetic moment of $0.8\mu_B$ indicates very weak ferromagnetism in $Sr_{11}Re_4O_{24}$ at low temperature.

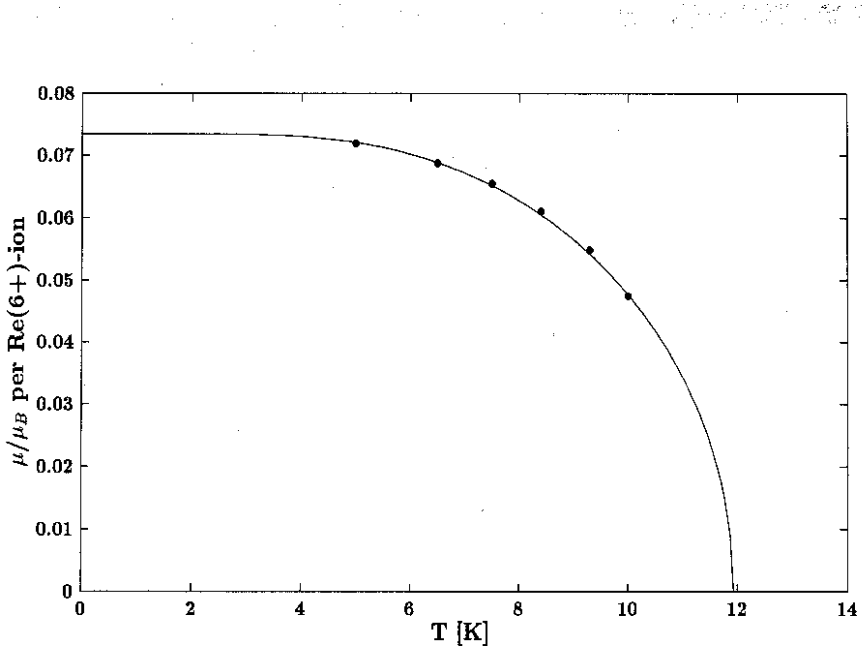

Fig. 41: Observed and calculated temperature dependence of spontaneous magnetisation.

4.3.2 Magnetic properties of $Sr_7Re_4O_{19}$

$Sr_7Re_4O_{19}$ shows unexpected magnetic behaviour also. The temperature dependence of magnetisation at a constant field strength of 0.01 T is shown in Fig. 42. These results are in good agreement with previous investigations of magnetic properties of the reported compound with the proposed composition "$Sr_3Re_2O_9$" [48].

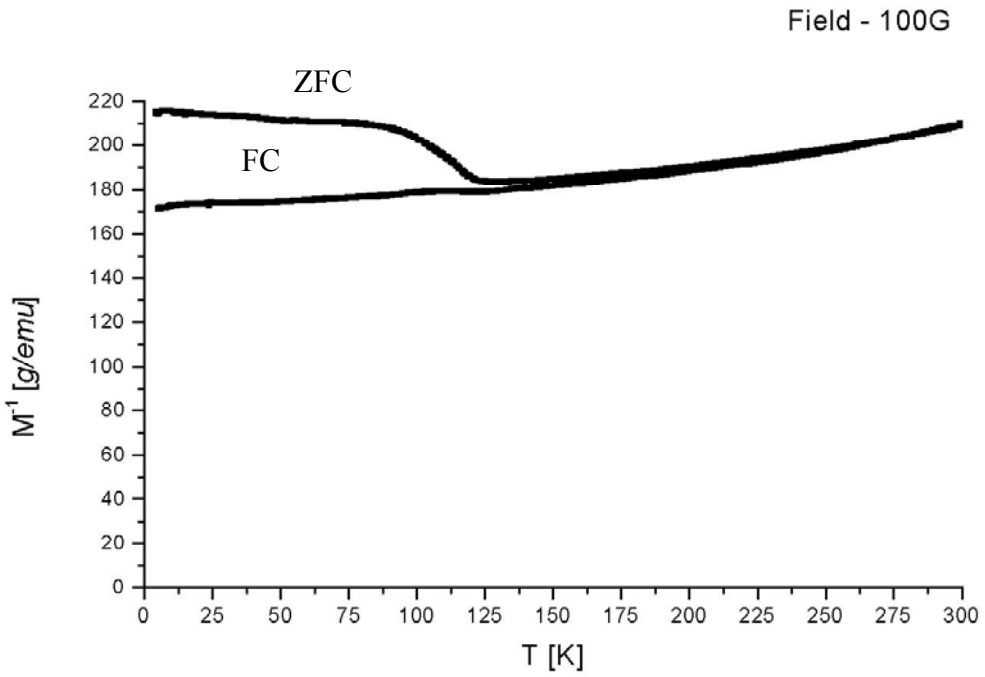

Fig. 42: Temperature dependence of inverse magnetisation of $Sr_7Re_4O_{19}$ at the constant field strength of 0.01 T.

As shown in Chapter 4.1 this composition corresponds to a mixture of $Sr_7Re_4O_{19}$ and strontium perrhenate, $Sr(ReO_4)_2$, or its hydrates. Because of a diamagnetic contribution from compounds containing rhenium in its highest oxidation state, +7, the observed temperature-independent paramagnetism between 80 and 300 K can be completely assigned to the $Sr_7Re_4O_{19}$ oxide. This is a very unusual magnetic behaviour of a rhenium oxide with Re in a low oxidation state, +6. Together with the reported semiconducting behaviour of "$Sr_3Re_2O_9$" it was explained by the delocalization of the $5d^1$ electron in rhenium (VI), since the two-dimensional interactions of vertex-connected octahedra in the structure might be consistent with

the electrical properties of "$Sr_3Re_2O_9$" [48]. The new knowledge about the $Sr_7Re_4O_{19}$ structure (see Chapter 4.2.2) requires a reconsideration of the magnetic properties of this compound.

The field dependence of magnetisation was measured at different temperatures below T_C (see Fig. 43 for T = 110 and 300 K).

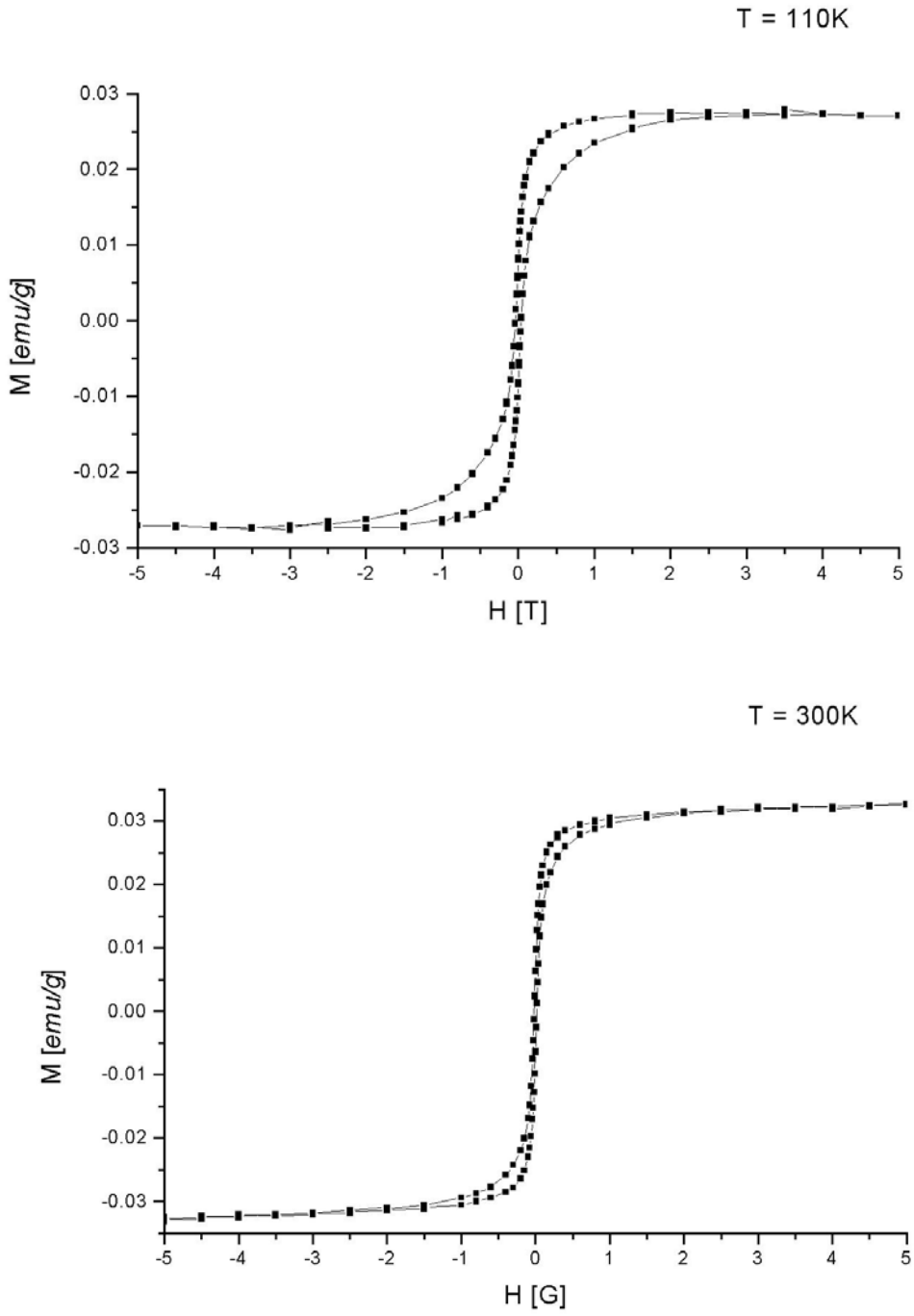

Fig. 43: Hysteresis loops of $Sr_7Re_4O_{19}$ at 110.0 K (a) and 300.0 K (b).

The field dependence can be described by Equations 12-15. Four parameters, α, H_0, σ, and H_C, have to be fitted to the observed data points. The results are given in Table 14 (see Appendix). The areas within one complete loop are calculated according to equation (15) with the parameters given in Table 14 also. A linear extrapolation of the hysteresis-loops areas to zero gives a very rough estimation of T_C of 380 K. $Sr_7Re_4O_{19}$ is probably the first example of a Re^{+6} oxide with a magnetically ordered structure at room temperature. To understand the origin of such an unusual magnetic behaviour neutron diffraction investigations have to be performed.

4.3.3 Magnetic properties of Sr_3ReO_6

Sr_3ReO_6 orders with a weak ferromagnetic component below the Curie temperature of $T_C \approx 10$ K as deduced from the temperature dependence of magnetisation at the constant field strength of 0.25 T (see Fig. 44). The hysteresis loops, measured at T = 5.0, 7.0 and 9.0 K, confirm this assumption (see Fig. 45).

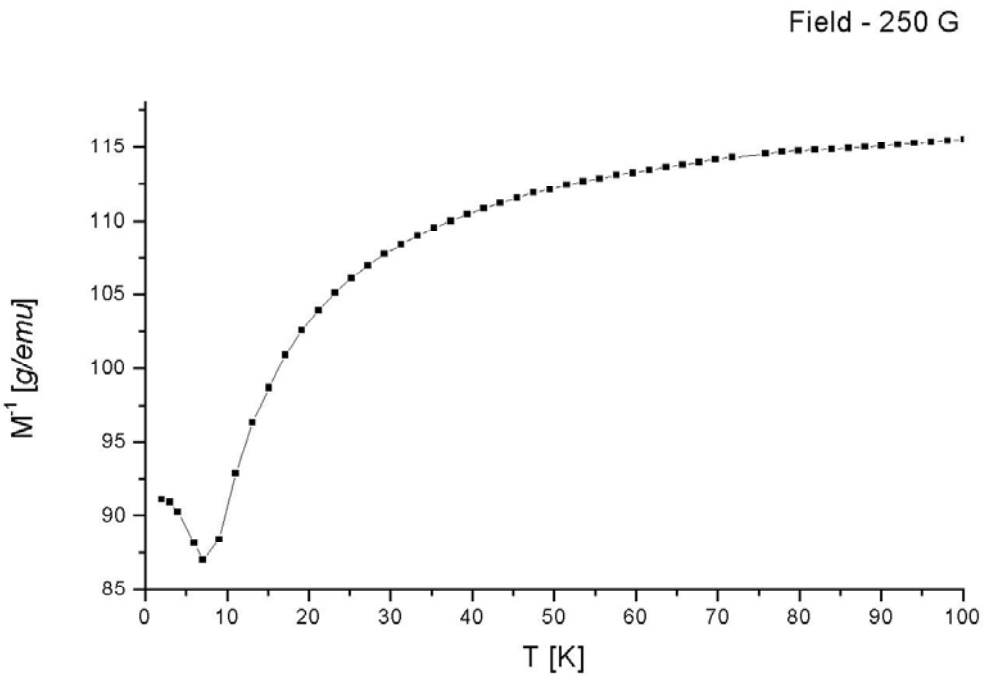

Fig. 44: Temperature dependence of inverse magnetisation of Sr_3ReO_6 at the constant field strength of 0.025 T.

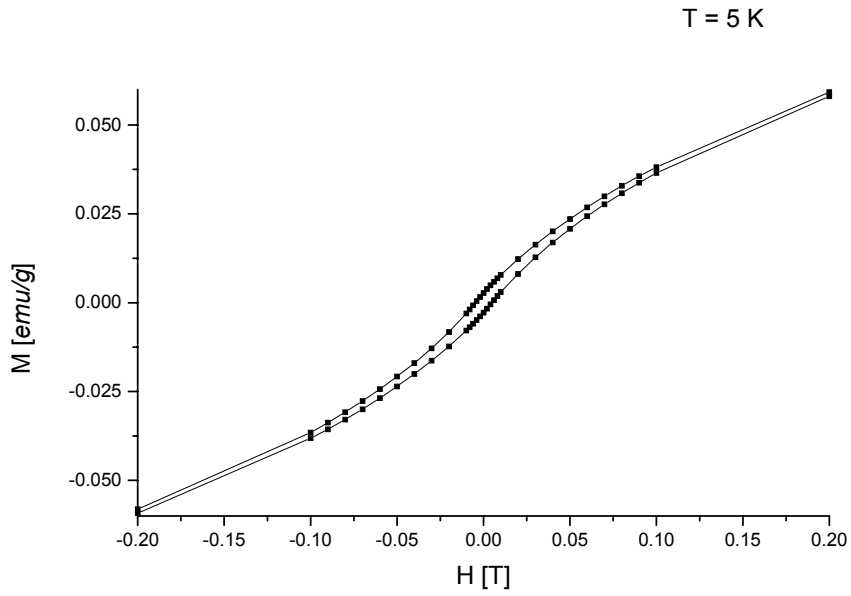
T = 5 K
M [emu/g]
H [T]
0.050
0.025
0.000
-0.025
-0.050
-0.20
-0.15
-0.10
-0.05
0.00
0.05
0.10
0.15
0.20

a)

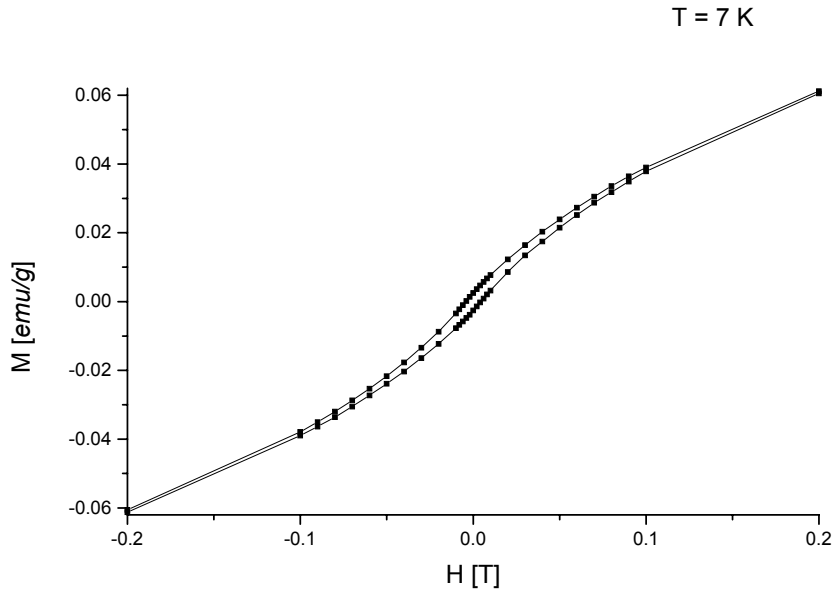
T = 7 K
M [emu/g]
H [T]
0.06
0.04
0.02
0.00
-0.02
-0.04
-0.06
-0.2
-0.1
0.0
0.1
0.2

b)

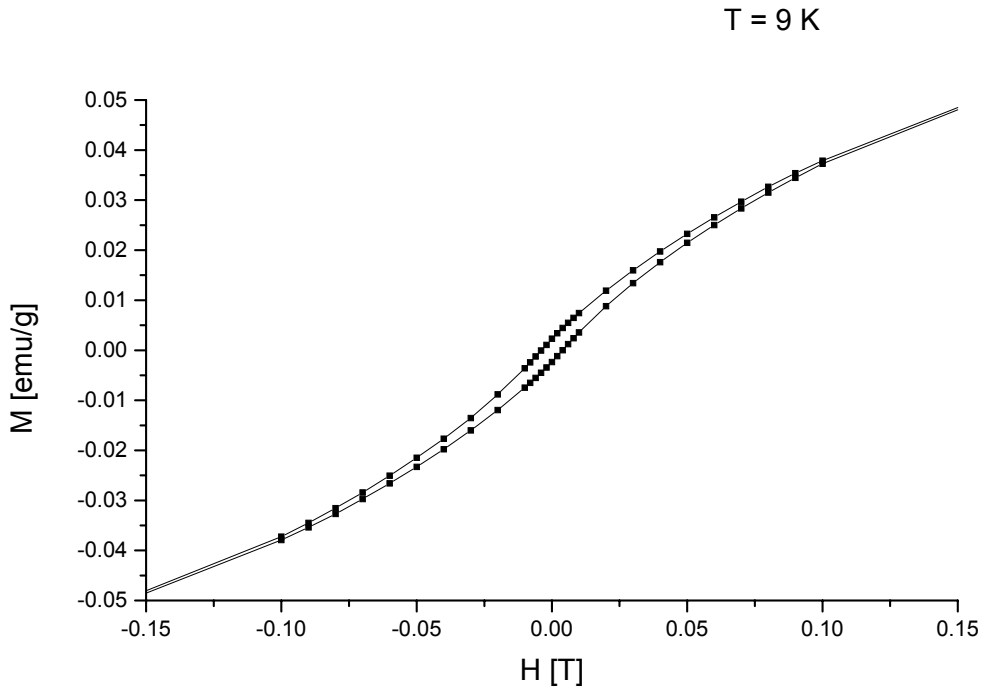

c)

Fig. 45: Hysteresis loops of Sr_3ReO_6 at 5.0 K (*a*), 7.0 K (*b*) and 9.0 K (*c*).

4.3.4 Magnetic properties of $Ca_5Re_3O_{15}$

In the case of $Ca_5Re_3O_{15}$ unusual magnetic behaviour below 25 K was observed also. Fig. 46 shows its temperature dependence of magnetisation. One can see that this dependence may be described by a Curie-Weiss law for temperatures from 30 to 300 K. It consequently corresponds to paramagnetic behaviour of $Ca_5Re_3O_{15}$ at this temperature. Then on the base of temperature dependence and field dependence of magnetisation at different temperatures below 25 K (5, 15 and 23 K) as well we can assume that the $Ca_5Re_3O_{15}$ compound orders ferrimagnetically also (see Fig. 47).

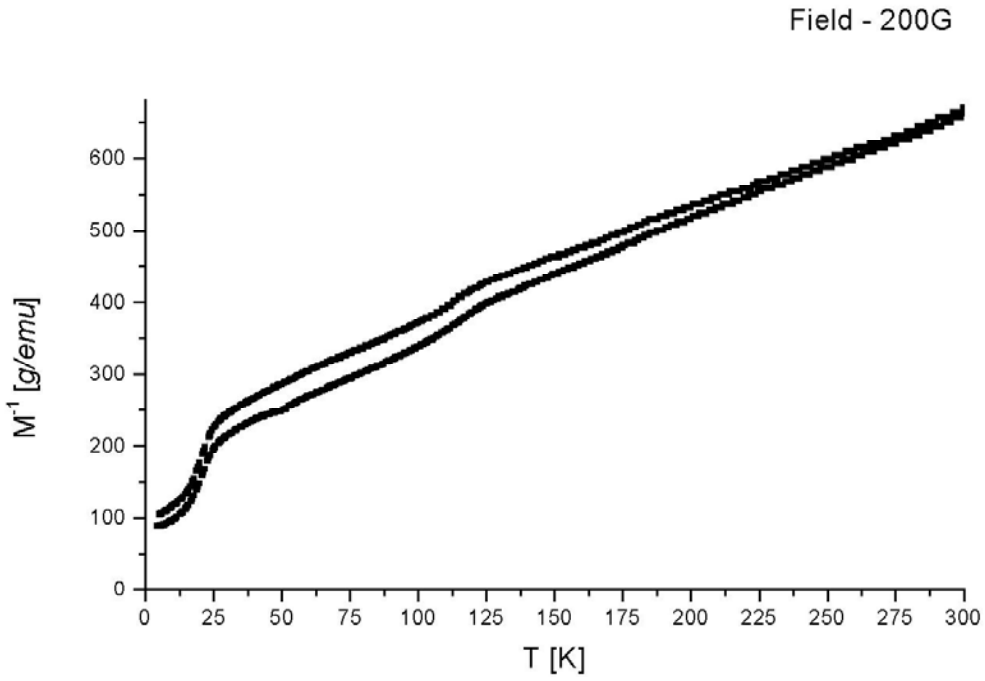

a)

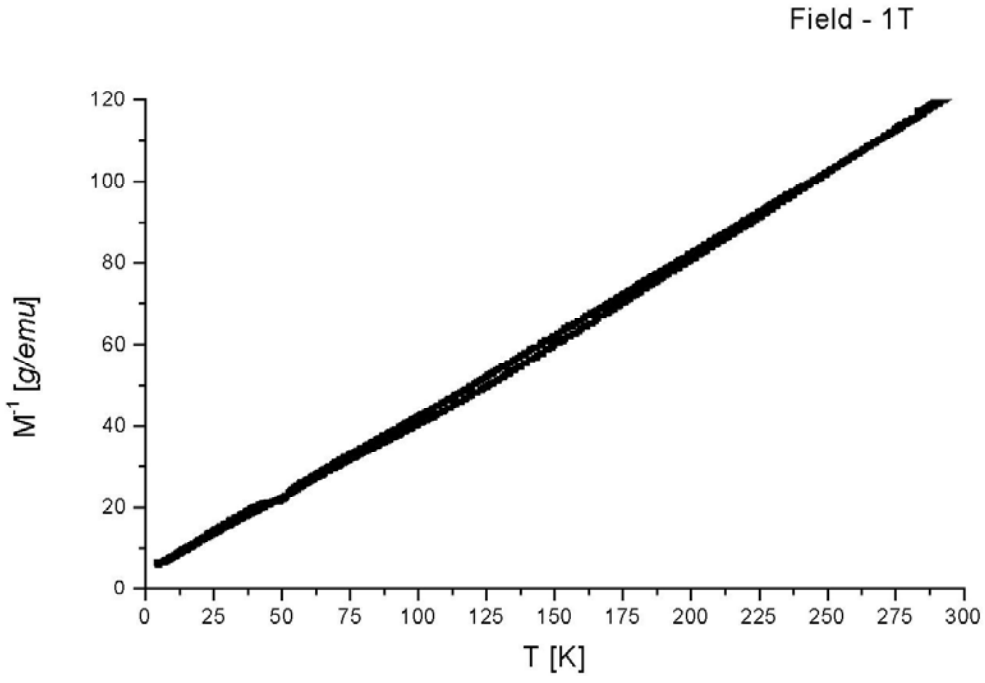

b)

Fig. 46: Temperature dependence of inverse magnetisation of $Ca_5Re_3O_{15}$ at the constant field strength of *a*) 0.02 T and *b*) 1.00 T.

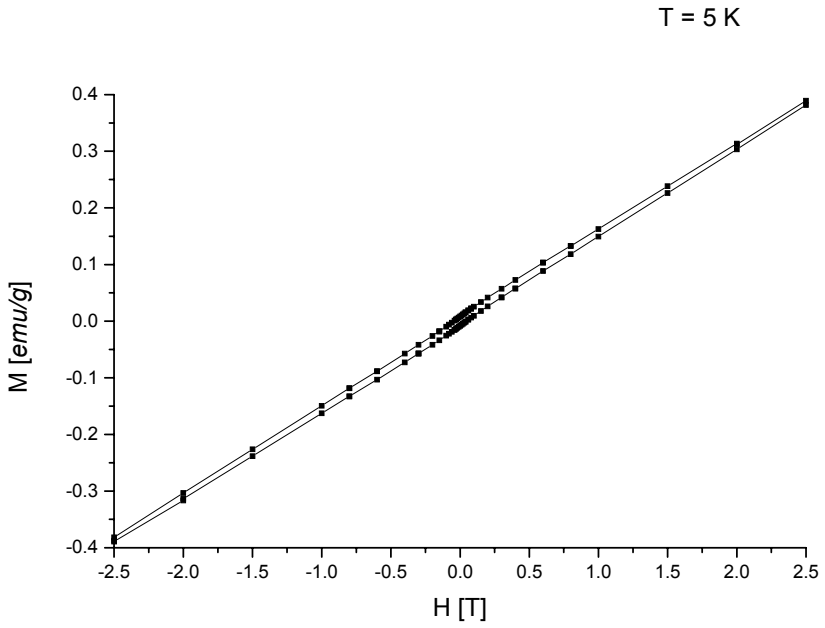
T = 5 K
M [emu/g]
H [T]
0.4
0.3
0.2
0.1
0.0
-0.1
-0.2
-0.3
-0.4
-2.5
-2.0
-1.5
-1.0
-0.5
0.0
0.5
1.0
1.5
2.0
2.5

a)

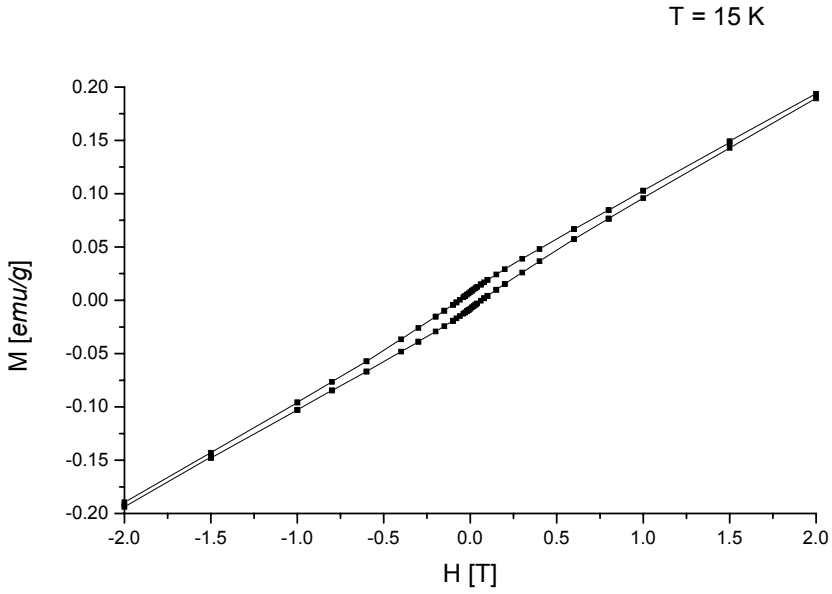
T = 15 K
M [emu/g]
H [T]
0.20
0.15
0.10
0.05
0.00
-0.05
-0.10
-0.15
-0.20
-2.0
-1.5
-1.0
-0.5
0.0
0.5
1.0
1.5
2.0

b)

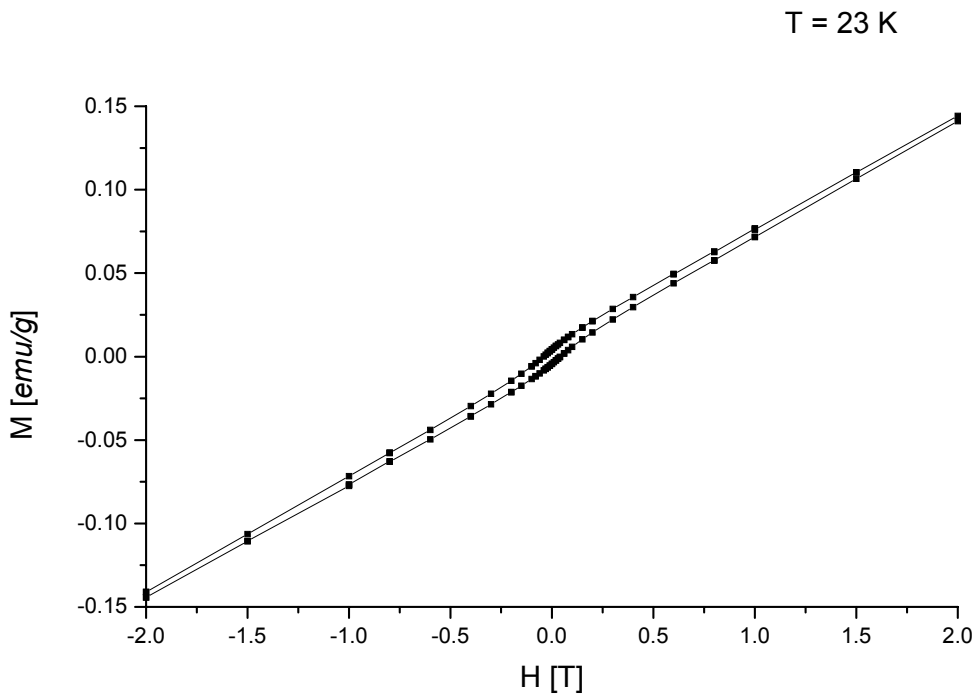

c)

Fig. 47: Hysteresis loops of $Ca_5Re_3O_{15}$ at 5.0 K (*a*), 15.0 K (*b*) and 23.0 K (*c*).

4.3.5 Magnetic properties of M_2MgReO_6 (M = Ca, Sr, Ba)

The magnetic properties of M_2MgReO_6 (M = Ca, Sr, Ba) were also studied. A similar unexpected behaviour as in the case of the $Sr_7Re_4O_{19}$ oxide was observed. The temperature dependence of magnetisation shows an anomalous course in the case of Ca and Ba containing samples. The results of the zero-field cooled measurements drastically differ from the field cooled ones, and their observed values are negative till 18 K at the field strength of 100 Gauss for Ca_2MgReO_6 (see Fig. 48) and till 19 K at the same field strength for the Ba- containing substance (see Fig. 50). Then Ca_2MgReO_6 and Ba_2MgReO_6 demonstrate temperature independent curve course of magnetisation to 300 K from 30 K and 25 K respectively. Despite this observation hysteresis loops were observed for both of them and for the Sr-containing compound inclusive at 300 K also (see Figures 51, 52 and 53). The temperature dependence of magnetisation for Sr_2MgReO_6 looks similar to the $Sr_7Re_4O_{19}$ ones (see Fig. 49).

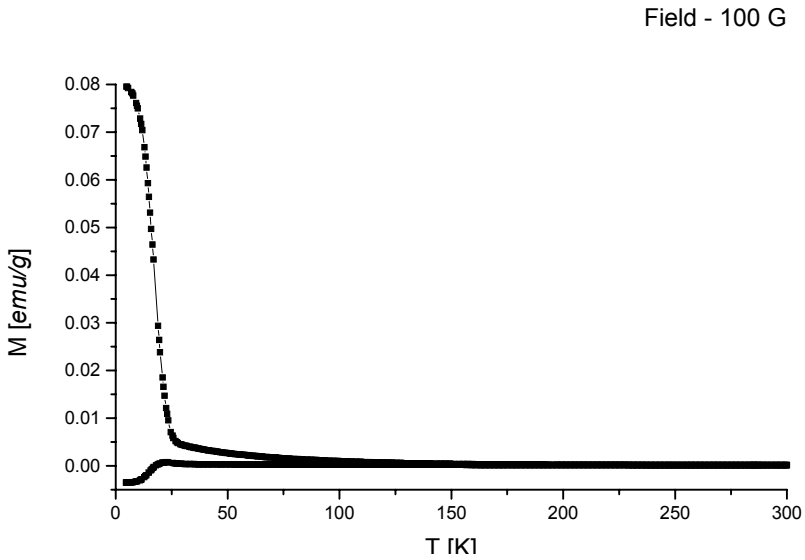

a)

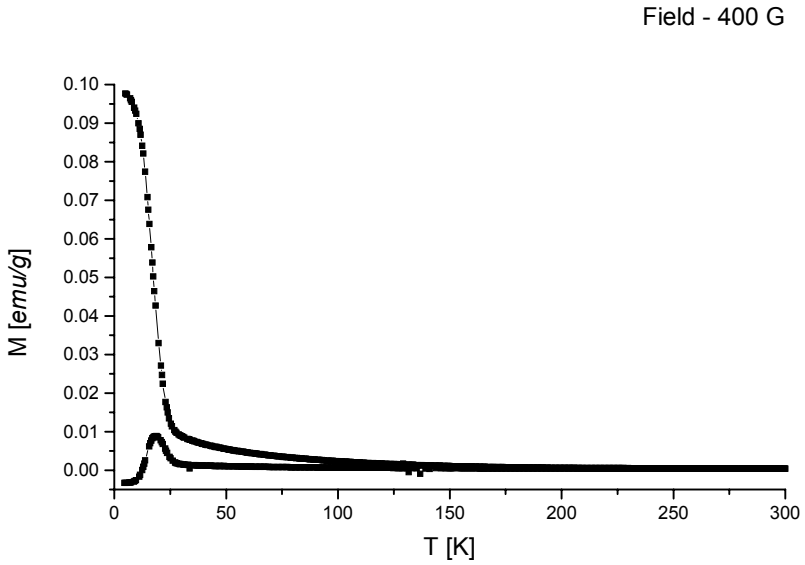

b)

Fig. 48: Temperature dependence of magnetisation of Ca_2MgReO_6 at the constant field strength of *a*) 0.01 T and *b*) 0.04 T.

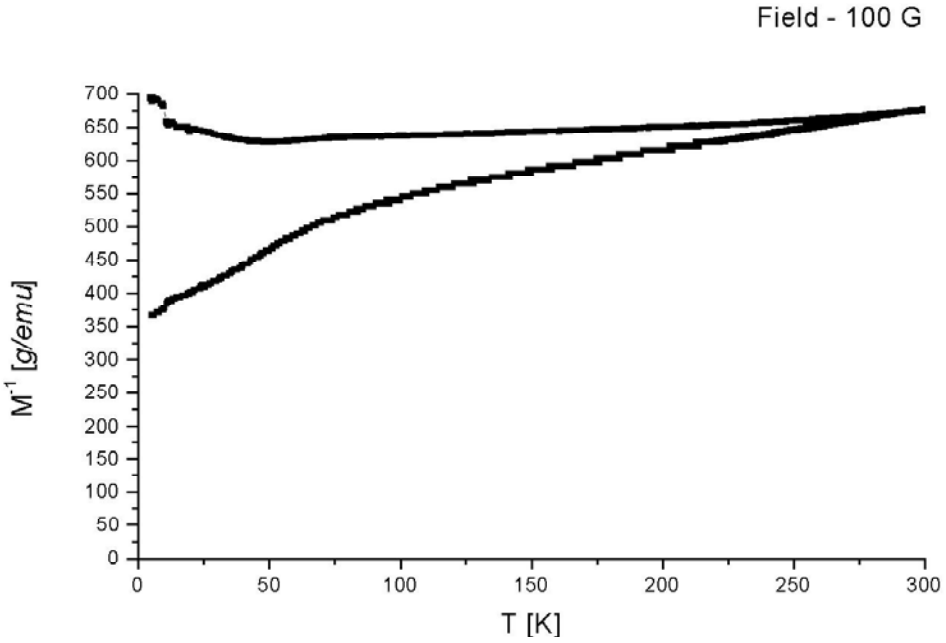

a)

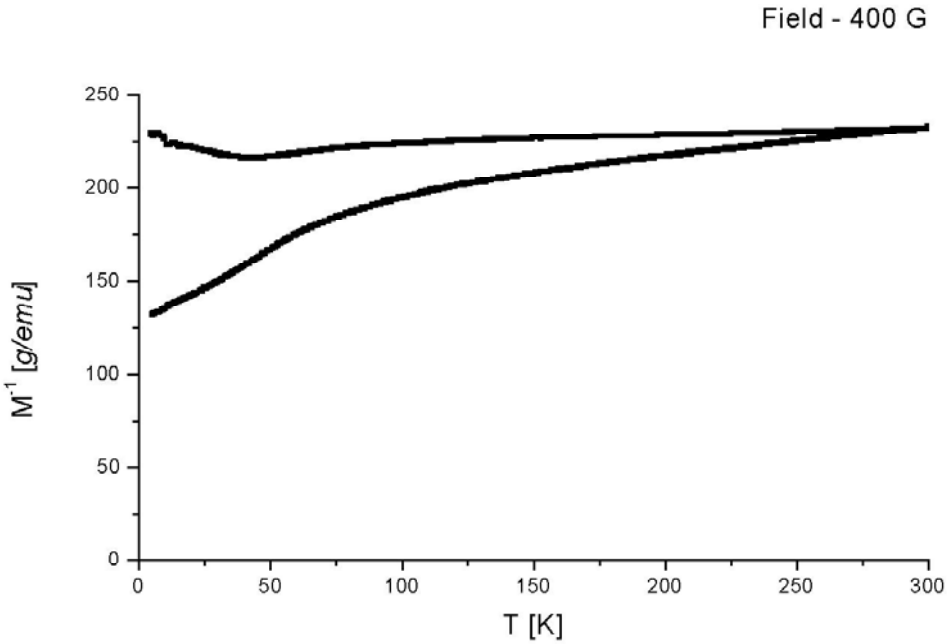

b)

Fig. 49: Temperature dependence of inverse magnetisation of Sr_2MgReO_6 at the constant field strength of *a*) 0.01 T and *b*) 0.04 T.

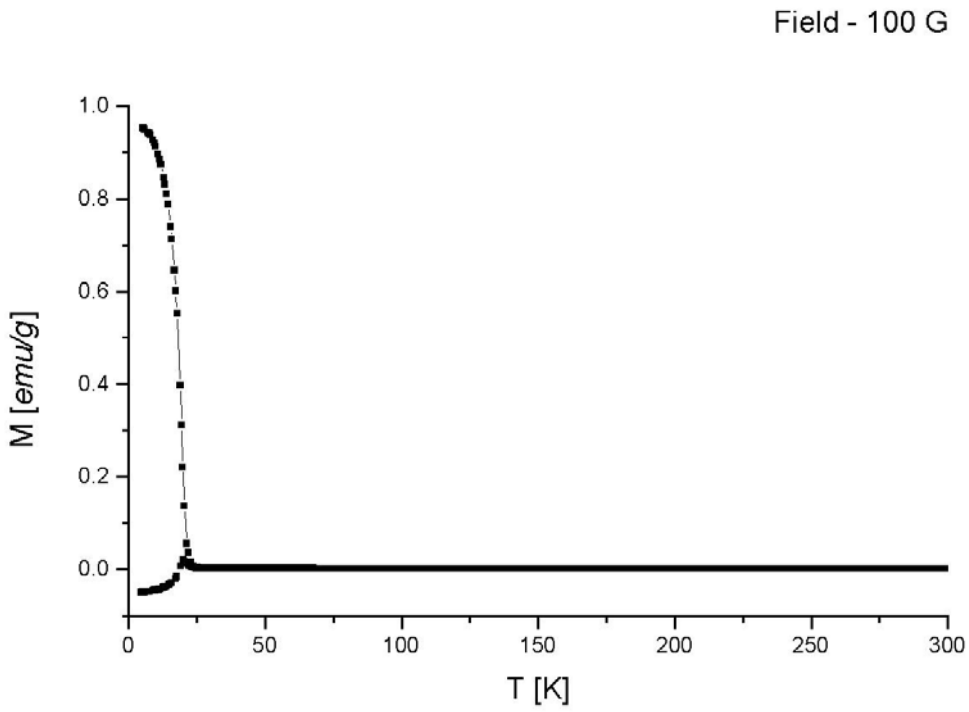

a)

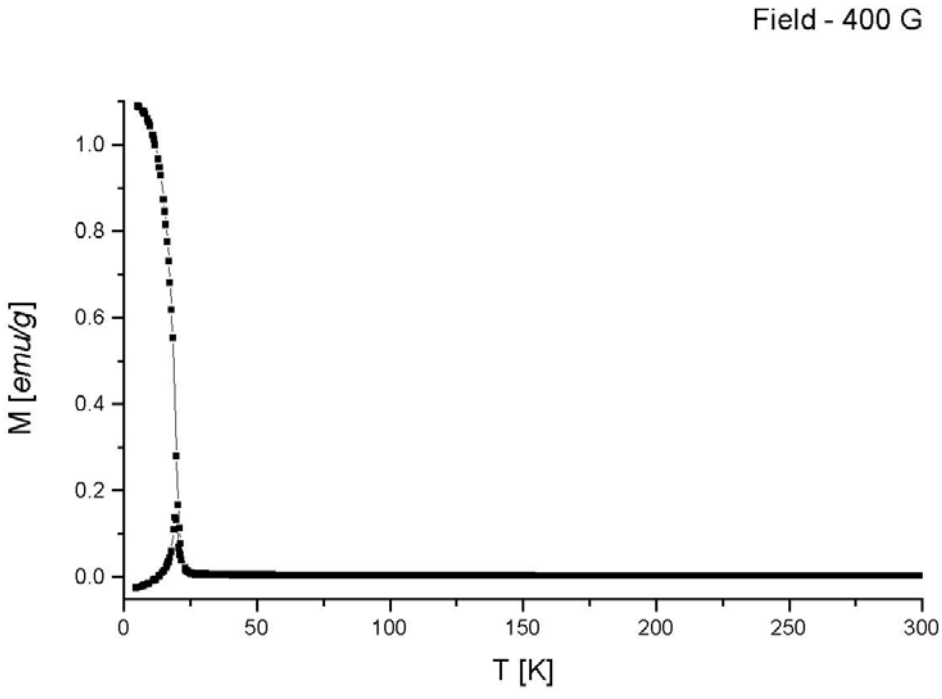

b)

Fig. 50: Temperature dependence of magnetisation of Ba_2MgReO_6 at the constant field strength of *a*) 0.01 T and *b*) 0.04 T.

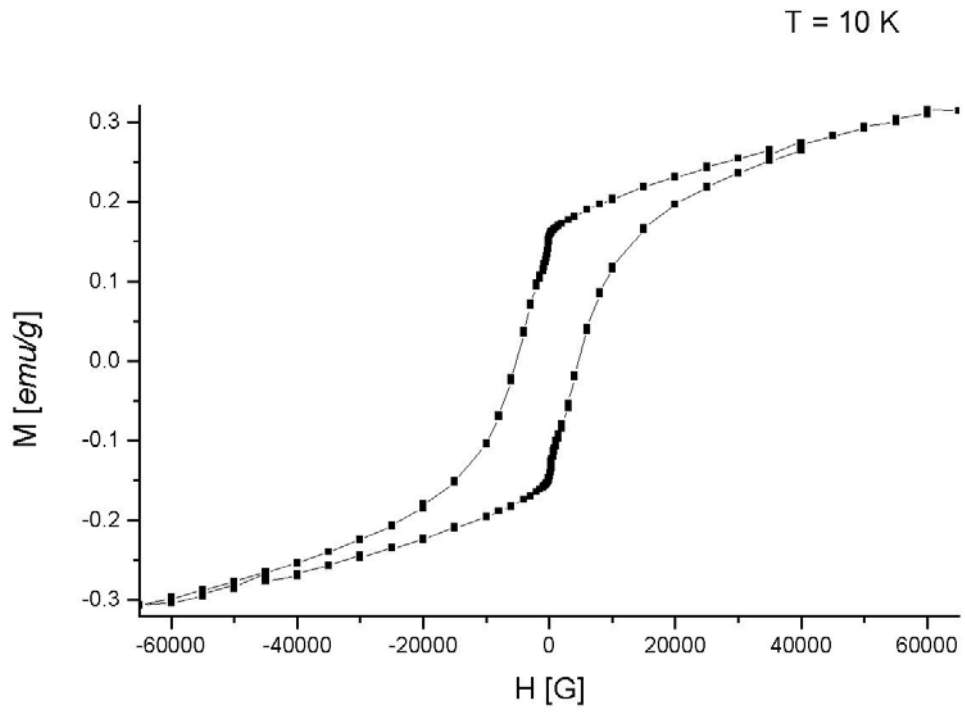
T = 10 K
M [emu/g]
H [G]
0.3
0.2
0.1
0.0
-0.1
-0.2
-0.3
-60000
-40000
-20000
0
20000
40000
60000

a)

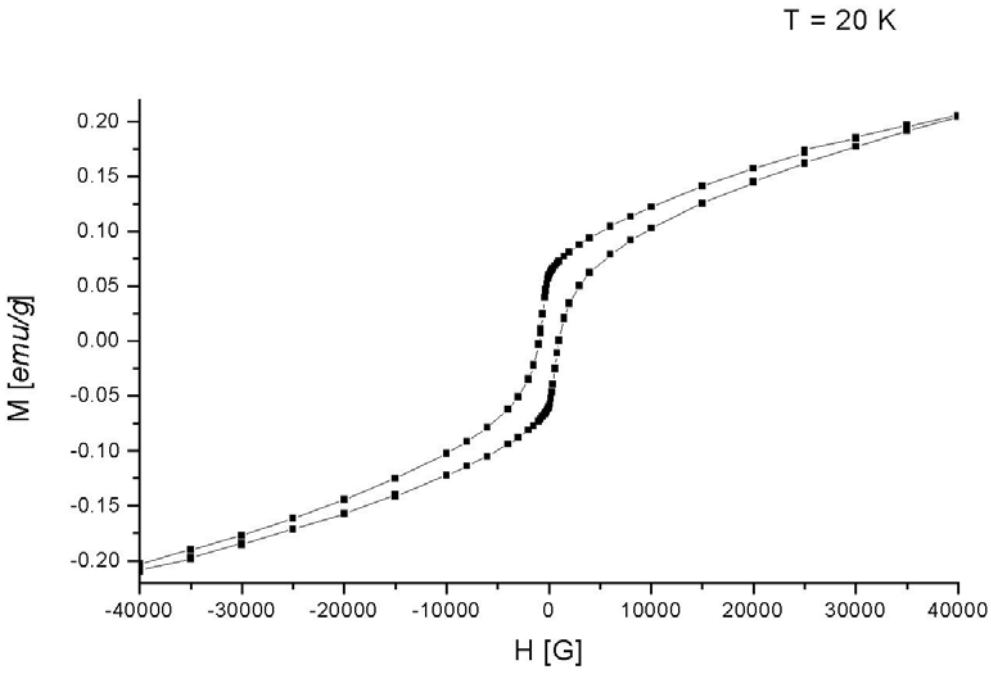
T = 20 K
M [emu/g]
H [G]
0.20
0.15
0.10
0.05
0.00
-0.05
-0.10
-0.15
-0.20
-40000
-30000
-20000
-10000
0
10000
20000
30000
40000

b)

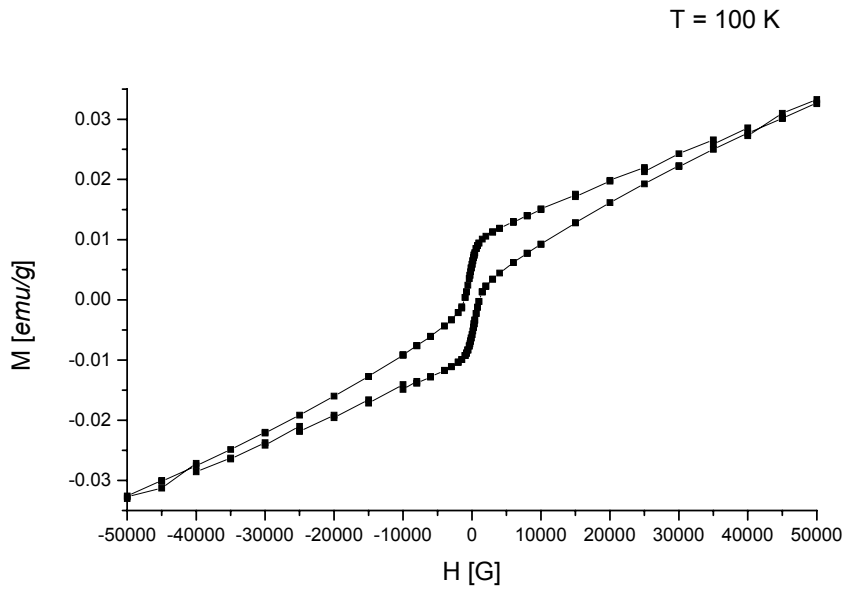

c)

Fig. 51: Hysteresis loops of Ca_2MgReO_6 at 10.0 K (*a*), 20.0 K (*b*) and 100.0 K (*c*).

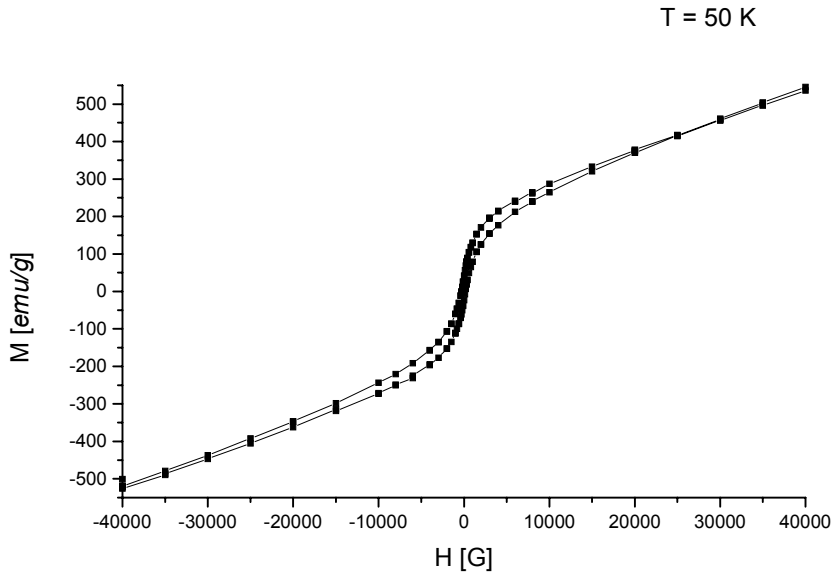
T = 50 K
M [emu/g]
H [G]
500
400
300
200
100
0
-100
-200
-300
-400
-500
-40000
-30000
-20000
-10000
0
10000
20000
30000
40000

a)

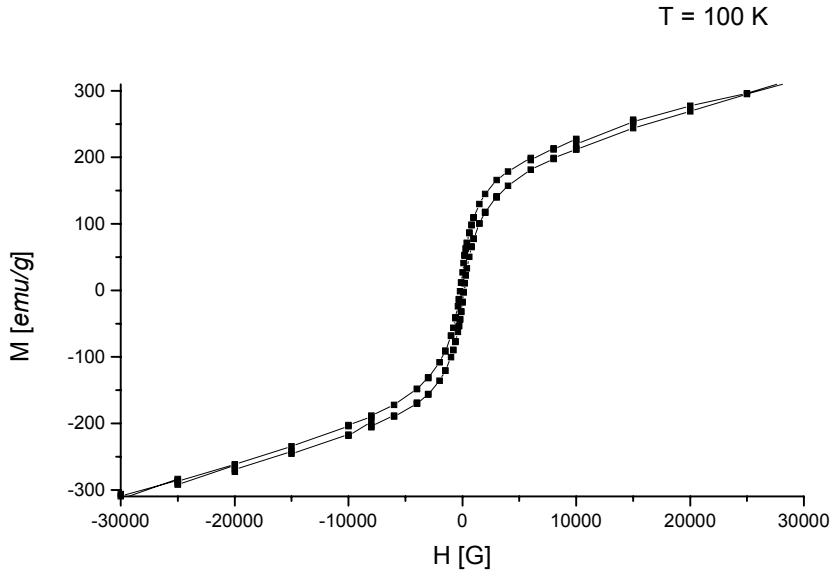
T = 100 K
M [emu/g]
H [G]
300
200
100
0
-100
-200
-300
-30000
-20000
-10000
0
10000
20000
30000

b)

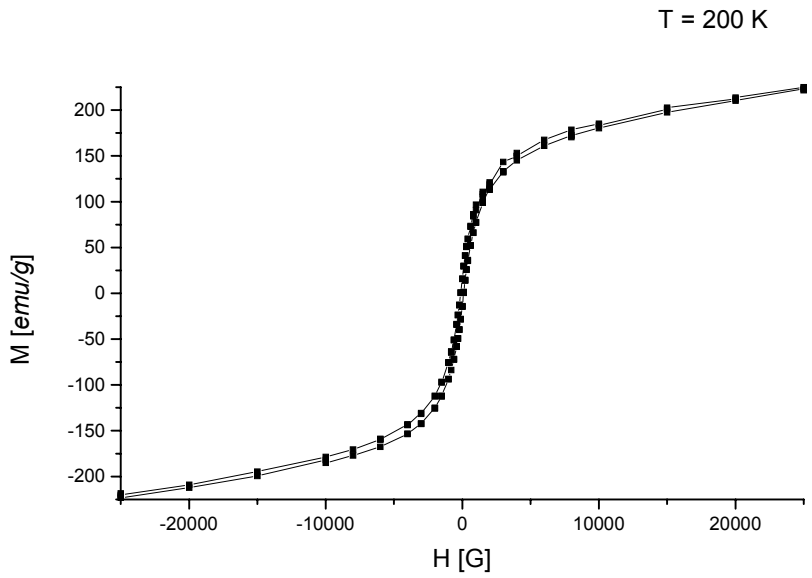

c)

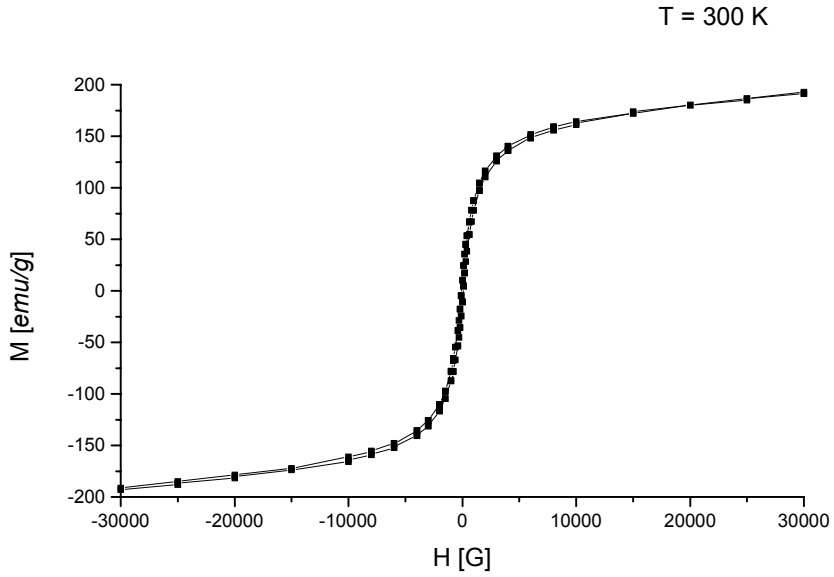

d)

Fig. 52: Hysteresis loops of Sr_2MgReO_6 at 50.0 K (*a*), 100.0 K (*b*), 200.0 K (*c*) and 300.0 K (*d*).

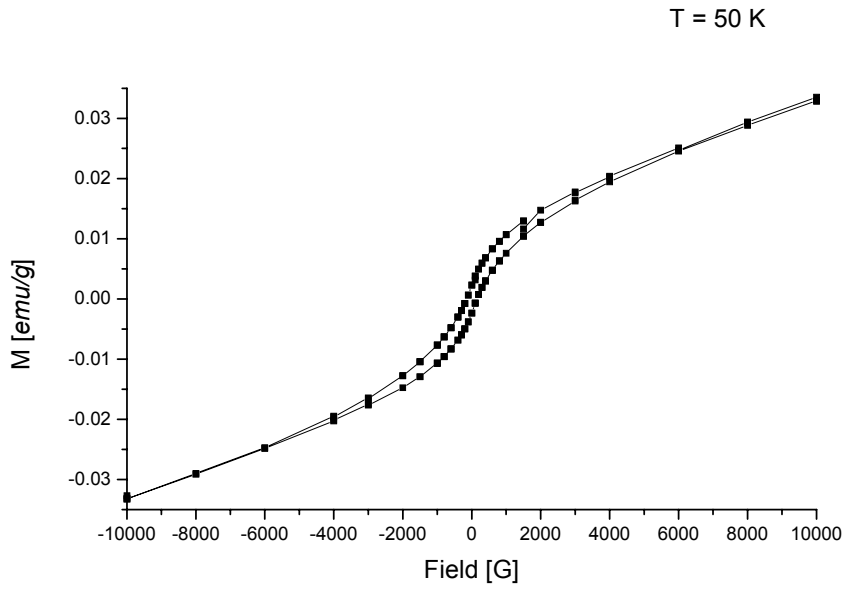

a)

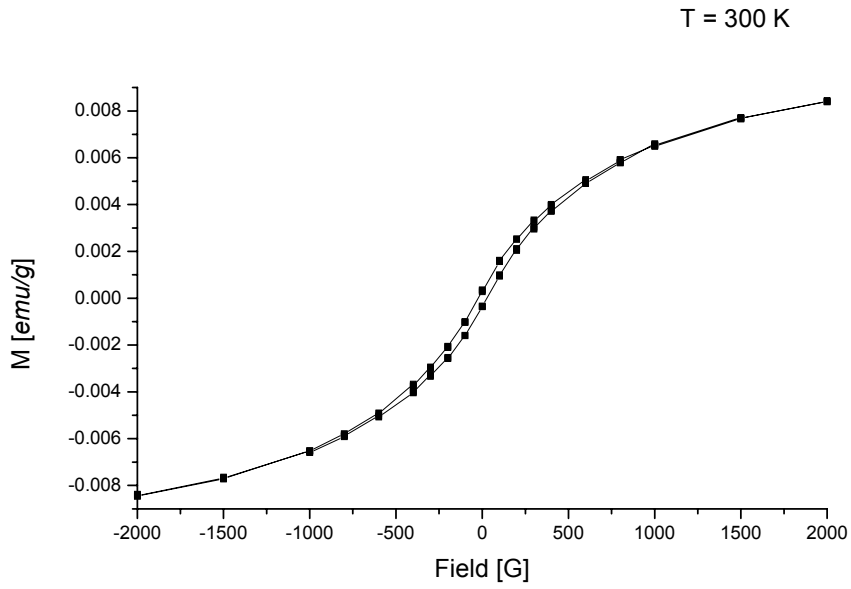

b)

Fig. 53: Hysteresis loops of Ba_2MgReO_6 at 50.0 K (*a*) and 300.0 K (*b*).

These results point at a ferromagnetic contribution in all M_2MgReO_6 magnetic structures at room temperature. The lack of data concerning possible magnetic order in these oxides do not allow us to explain these unusual magnetic properties.

5 Summary

In this work crystalline phases in the system of alkali-earth elements, rhenium and oxygen have been prepared and characterised with respect to their crystal structures and magnetic properties. The results are summarised in schemes of phase stability for Ca-Re-O, Sr-Re-O and Ba-Re-O.

Hereby new compounds could be established like Sr_3ReO_6, $M_{11}Re_4O_{24}$ (M = Sr, Ba) and $Sr_7Re_4O_{19}$ and their crystal structures were solved and refined. In the Ca-Re-O system two new compounds were synthesised and their cell parameters were defined. Two more substances in this system, $Ca_{11}Re_4O_{24}$ and $Ca_5Re_3O_{15}$, were synthesised in a pure phase polycrystalline form for the first time. Furthermore, the crystal structures of the already reported compounds could be solved, $Ca_{11}Re_4O_{24}$, or had to be reconsidered, $Ca_5Re_3O_{15}$. These results are discussed in the light of the conditions of synthesis (related to the phase stability, especially with respect to the partial oxygen pressure) and the relationships between the different crystal structures. For example, a very close relation holds with respect to the basic perovskite structure. Most observed structures are derived from the perovskite-type by ordered cation distributions, resulting in superstructure cells, or by rotations and tilting of octahedra, resulting in a symmetry breaking in order to allow for more appropriate coordination polyhedra of the alkali-earth ions than in the ideal perovskite structure.

Investigations in the Mg-Re-O system were carried out additionally. Despite of the different synthetic techniques applied no new compounds with rhenium in the low oxidation states could be prepared in this system. It can be explained by common tendency of alkali-earth elements to form compounds with perovskite-related structures (almost all investigated compounds in the M-Re-O (M = Ca, Sr, Ba) system belong to the perovskite structure type with different distortions of this structure), but in comparison to the other alkali-earth elements magnesium has not an appropriate radius to occupy A-sites in the perovskite structure. Therefore, high pressure techniques are required to obtain new reduced complex oxides in the Mg-Re-O system.

Furthermore, the crystal structures of the already reported M_2MgReO_6 (M = Ca, Sr, Ba) compounds were determined, and the cell parameters of the Ca- and Sr-containing compounds were redefined.

On the base of the performed investigations on alkali-earth rhenium oxides and the literature data concerning other complex rhenium oxides, one may conclude that the formal oxidation state of rhenium, in which it occurs in ternary oxides, depends on the basic properties of other cations. So, rare-earth rhenium oxides are known in the wide range of rhenium oxidation state, from +4 to +7. At the same time, alkali-earth rhenium oxides, synthesised without applying high-pressure techniques, are known only with rhenium in the formal oxidation state between +6 and +7 as shown in this work. Furthermore, ternary rhenium oxides with alkali elements were found only for the rhenium formal oxidation state of +7.

Magnetic properties of all new compounds were investigated. In all cases an unusual temperature dependence of magnetisation was observed. The general feature of magnetic properties of all oxides studied is a weak ferromagnetism. At the same time the ordering temperature depends unambiguously on contents of the Re^{+6} ions in the structures. This dependence is so strong that in the case of $Sr_{11}Re_4O_{24}$, where only half of the rhenium atoms have the oxidation state of +6, the ordering temperature is 12(1) K, since in the case of $Sr_7Re_4O_{19}$, where all rhenium atoms are in +6 oxidation state, hysteresis loops were observed at 300 K and the estimated ordering temperature is about 380 K. The nature and origin of these curious properties are unclear and require further studies of the corresponding magnetic structures by neutron diffraction.

6 Appendix

Space group	$I4_1/a$
a (Å)	11.6779(1)
c (Å)	16.1488(2)
Cell volume (Å ^{3})	2202.26(5)
Z	4
Calculated density (g/cm^3)	6.312
Radiation	Cu Kα_1
2θ range, time/step	5-100^o, 60 s
No. of reflections	564
Refined parameters	54
Reliability factors	R_I=0.011, R_P=0.056, R_{wP}=0.079

Table 4: Measurements and refinements parameters for $Sr_{11}Re_4O_{24}$.

Atom	x/a	y/b	z/c	B, Å ^{2}
Sr(1)	0	1/4	1/8	1
Sr(2)	1/2	1/4	0.6175(8)	1
Sr(3)	0.2068(2)	-0.0131(8)	-0.1399(6)	1
Sr(4)	0.2126(7)	0.2324(8)	0.5311(5)	1
Re(1)	0	0	0	1
Re(2)	0	0	1/2	1
O(1)	0.8607(9)	0.126(1)	0.2712(5)	0.5
O(2)	0.628(1)	0.1363(8)	0.2479(6)	0.5
O(3)	0.2790(8)	0.235(1)	0.3667(5)	0.5
O(4)	0.829(1)	0.171(1)	0.6657(6)	0.5
O(5)	0.9045(8)	0.125(1)	0.4774(6)	0.5
O(6)	0.3148(9)	0.1435(9)	0.6759(7)	0.5

Table 5: Positional and thermal displacements parameters for $Sr_{11}Re_4O_{24}$ from neutron diffraction data.

Sr(1) - O(1)	3.21(2)×4	Sr(4) - O(1)	2.65(2)×1
Sr(1) - O(2)	2.86(2)×4	Sr(4) - O(2)	2.45(2)×1
Sr(1) - O(3)	2.59(1)×4	Sr(4) - O(3)	2.76(1)×1
Sr(2) - O(1)	2.67(2)×2	Sr(4) - O(4)	2.50(1)×1
Sr(2) - O(2)	2.73(2)×2		2.52(1)×1
Sr(2) - O(3)	3.26(1)×2	Sr(4) - O(5)	2.32(1)×1
Sr(2) - O(5)	2.55(1)×2	Sr(4) - O(6)	2.82(2)×1
Sr(2) - O(6)	2.67(1)×2		2.87(1)×1
Sr(3) - O(1)	2.62(2)×1	Re(1) - O(1)	1.97(2)×2
	2.59(2)×1	Re(1) - O(2)	1.95(2)×2
Sr(3) - O(2)	2.84(2)×1	Re(1) - O(3)	1.92(1)×2
	2.97(2)×1	Re(2) - O(4)	1.88(1)×2
Sr(3) - O(3)	2.62(1)×1	Re(2) - O(5)	1.87(1)×2
	2.60(1)×1	Re(2) - O(6)	1.88(1)×2
Sr(3) - O(4)	2.61(1)×1		
Sr(3) - O(5)	2.59(1)×1		
Sr(3) - O(6)	2.50(1)×1		

Table 6: Characteristic interatomic distances (Å) for $Sr_{11}Re_4O_{24}$ as obtained from neutron diffraction data.

Space group	$I4_1/a$
a (Å)	12.2416(1)
c (Å)	16.6602(2)
Cell volume (Å ^{3})	2496.65(5)
Z	4
Calculated density (g/cm^3)	7.022
Radiation	Cu Kα_1
2θ range, time/step	5-100^o, 60 s
No. of reflections	564
Refined parameters	54
Reliability factors	R_I=0.049, R_P=0.034, R_{wP}=0.046

Table 7: Measurements and refinements parameters for $Ba_{11}Re_4O_{24}$.

Atom	x/a	y/b	z/c	B, Å ^{2}
Ba(1)	0	1/4	1/8	1.14(8)
Ba(2)	1/2	1/4	0.6080(1)	0.75(5)
Ba(3)	0.2092(1)	0.0095(1)	0.1349(1)	1.07(4)
Ba(4)	0.2095(1)	0.2755(1)	0.52895(7)	1.07(4)
Re(1)	0	0	0	0.44(3)
Re(2)	0	0	1/2	0.77(3)
O(1)	0.851(1)	0.114(1)	0.2341(9)	1.6(1)
O(2)	0.625(1)	0.171(1)	0.2344(9)	1.6
O(3)	0.252(1)	0.242(1)	0.3558(5)	1.6
O(4)	0.871(1)	0.152(1)	0.6549(8)	1.6
O(5)	0.924(1)	0.094(1)	0.5262(8)	1.6
O(6)	0.314(1)	0.158(1)	0.6739(9)	1.6

Table 8: Positional and thermal displacements parameters for $Ba_{11}Re_4O_{24}$.

Ba(1) - O(1)	3.25(2)×4	Ba(4) - O(1)	2.68(2)×1
Ba(1) - O(2)	2.89(2)×4	Ba(4) - O(2)	2.50(2)×1
Ba(1) - O(3)	2.65(1)×4	Ba(4) - O(3)	2.78(1)×1
Ba(2) - O(1)	2.70(2)×2	Ba(4) - O(4)	2.55(1)×1
Ba(2) - O(2)	2.76(2)×2		2.56(1)×1
Ba(2) - O(3)	3.29(1)×2	Ba(4) - O(5)	2.40(1)×1
Ba(2) - O(5)	2.58(1)×2	Ba(4) - O(6)	2.80(2)×1
Ba(2) - O(6)	2.70(1)×2		2.85(1)×1
Ba(3) - O(1)	2.65(2)×1	Re(1) - O(1)	1.98(3)×2
	2.63(2)×1	Re(1) - O(2)	1.95(2)×2
Ba(3) - O(2)	2.88(2)×1	Re(1) - O(3)	1.91(2)×2
	2.99(2)×1	Re(2) - O(4)	1.87(2)×2
Ba(3) - O(3)	2.61(1)×1	Re(2) - O(5)	1.87(2)×2
	2.63(1)×1	Re(2) - O(6)	1.89(2)×2
Ba(3) - O(4)	2.65(1)×1		
Ba(3) - O(5)	2.65(1)×1		
Ba(3) - O(6)	2.55(1)×1		

Table 9: Characteristic interatomic distances (Å) for $Ba_{11}Re_4O_{24}$.

Space group	*C*2/*m*
a (Å)	13.6432(1)
b (Å)	5.60509(5)
c (Å)	10.37483(9)
β	93.3504(5)°
Cell volume (Å ^{3})	784.97(1)
Z	2
Calculated density (g/cm^3)	7.032
Radiation	Co Kα_1
2θ range, time/step	5-100^o, 90 s
March-Dollase parameter, r*	0.94(1)
No. of reflections	340
Refined parameters	52
Reliability factors	R_I=0.018, R_P=0.050, R_{wP}=0.068

Table 10: Measurements and refinements parameters for $Sr_7Re_4O_{19}$.

* - see Ref. [68]

Atom	x/a	y/b	z/c	B, Å ^{2}
Sr(1)	0.7923(3)	0	0.4061(4)	0.5(1)
Sr(2)	0.5839(3)	0	0.1588(4)	0.8(1)
Sr(3)	0.8593(3)	0	0.0470(4)	1.1(1)
Sr(4)	0	1/2	1/2	0.9(2)
Re(1)	0.0354(2)	0	0.3190(2)	0.99(7)
Re(2)	0.3280(2)	0	0.2164(2)	0.63(6)
O(1)	0.624(1)	0.752(2)	0.376(2)	1.2(1)
O(2)	0.240(1)	0.748(3)	0.157(2)	1.2(1)
O(3)	0.426(1)	0.260(3)	0.287(2)	1.2(1)
O(4)	0.392(1)	0	0.071(2)	1.2(1)
O(5)	0.048(2)	0	0.145(2)	1.2(1)
O(6)	0.690(1)	0	0.610(2)	1.2(1)
O(7)	0	0	1/2	1.2(1)

Table 11: Positional and thermal displacements parameters for $Sr_7Re_4O_{19}$.

Sr(1) - O(1)	2.65(1)×2	Sr(4) - O(1)	2.69(2)×4
	2.78(2)×2	Sr(4) - O(3)	2.72(2)×4
Sr(1) – O(2)	2.98(2)×2	Sr(4) - O(6)	2.70(3)×2
Sr(1) - O(3)	2.69(2)×2	Sr(4) - O(7)	2.803×2
Sr(1) - O(6)	2.68(3)×1	Re(1) - O(1)	1.90(1)×2
	2.818(3)×2	Re(1) - O(3)	2.00(3)×2
Sr(1) - O(7)	2.862(4)×1	Re(1) – O(5)	1.87(2)×1
Sr(2) - O(1)	2.63(2)×2	Re(1) – O(7)	2.004(2)×1
Sr(2) - O(2)	2.53(2)×2	Re(2) - O(2)	1.92(2)×2
Sr(2) - O(3)	3.08(2)×2	Re(2) - O(3)	2.04(2)×2
Sr(2) - O(4)	2.63(1)×1	Re(2) - O(4)	1.86(2)×1
	2.45(2)×1	Re(2) – O(6)	1.86(2)×1
Sr(2) - O(5)	2.848(5)×2		
Sr(3) - O(2)	2.55(2)×2		
	2.69(2)×2		
Sr(3) - O(3)	2.86(2)×2		
Sr(3) - O(4)	2.846(3)×2		
Sr(3) - O(5)	2.49(3)×1		
	2.61(3)×1		

Table 12: Characteristic interatomic distances (Å) for $Sr_7Re_4O_{19}$.

T (K)	$\alpha(10^{-6}$emu/(gG))	H_0 (G)	σ (G)	H_C (G)	$\int_{loop} MdH$ ((emu G)/g)	$M_{H\to 0}(\mu_B$ per Re(+6)-ion)
5.0	4.082	93860	9900	257	10910	0.0718
6.5	4.224	86700	6630	246	7030	0.0686
7.5	4.361	79950	4450	198	4585	0.0654
8.4	4.575	71010	2500	183	2485	0.0609
9.3	4.871	59930	975	~60	~810	0.0547
10.0	5.521	45710	~260	~12	~195	0.0473

Table 13: The field dependence of magnetisation at different temperatures below T_C for $Sr_{11}Re_4O_{24}$.

T (K)	$\alpha(10^{-8}$emu/(gG))	H_C (G)	$\int_{loop} MdH$ ((emu G)/g)	$M_{H\to 0}(\mu_B$ per Re(+6)-ion)
10.0	9.237(6)	660	278	0.00184
50.0	31.33(3)	586	234	0.00176
110.0	-0.944(3)	372	194	0.00170
150.0	1.807(8)	300	166	0.00168
200.0	2.972(9)	184	114	0.00180
250.0	4.056(6)	175	100	0.00176
300.0	4.498(5)	166	67	0.00168

Table 14: The field dependence of magnetisation at different temperatures below T_C for $Sr_7Re_4O_{19}$.

Atom	Occup. (%)	*x/a*	*y/b*	*z/c*	B(Å^2)
Ca(1)	100	0	0.2646(3)	0.0884(5)	1.49(8)
Ca(2)	100	0.5	0.3772(2)	0.3365(5)	1.80(9)
Ca(3)	100	0	0	0.5578(7)	1.4(1)
Re(1)	100	0.5	0.15988(4)	0.37831*	0.70(2)
Re(2a)	75	0	0	0.0072(2)	0.64(3)
Re(2b)	12,5	0	0.0196(4)	0.0306(9)	0.64(3)
O(1)	100	0.279(2)	0.2491(6)	0.341(1)	1.6(2)
O(2)	100	0.274(2)	0.3824(5)	0.047(1)	1.3(2)
O(3)	100	0.252(2)	0	0.859(2)	1.8(3)
O(4)	100	0.5	0.100(1)	0.180(2)	2.1(3)
O(5)	100	0	0	0.248(4)	3.7(6)
O(6)	87,5	0	0.117(1)	0	2.1(4)

Table 15: The atomic parameters of $Ca_5Re_3O_{14,75}$ from Jeitschko *et al.*.

Table 16: The characteristic interatomic distances of $Ca_5Re_3O_{14,75}$:

Re(2a)-O(5)	1.73	1x
Re(2a)-O(6)	1.84	2x
Re(2a)-O(3)	1.77	2x
Re(2b)-O(5)	1.59	1x
Re(2b)-O(6)	1.54	1x
Re(2b)-O(3)	1.90	2x
Re(1)-O(4)	1.71	1x
Re(1)-O(1)	1.89	2x
Re(1)-O(2)	1.88	2x

Atom	*x/a*	*y/b*	*z/c*	B(Å^2)
Ca(1)	0	0.2569(4)	0.069(2)	1.1(2)
Ca(2)	0.5	0.3774(3)	0.325(2)	0.4(1)
Ca(3)	0	0	0.544(2)	1.2(2)
Re(1)	0.5	0.15951(7)	0.363(2)	0.26(4)
Re(2)	0	0	-0.005(2)	0.35(5)
O(1)	0.292(1)	0.2525(6)	0.338(2)	0.4(1)
O(2)	0.273(2)	0.3880(7)	0.040(3)	0.4(1)
O(3)	0.270(2)	0	0.840(3)	0.4(1)
O(4)	0.5	0.0944(9)	0.185(3)	0.4(1)
O(5)	0	0	0.244(3)	0.4(1)
O(6)	0	0.1167(8)	0	0.4(1)

Table 17: The atomic parameters of the $Ca_5Re_3O_{15}$ crystal structure proposed in this work.

Table 18 The characteristic interatomic distances:

Re(2)-O(5)	1.80(3)1x	
Re(2)-O(6)	1.83(1)2x	<d(Re(2)-O>=1.845 Å
Re(2)-O(3)	1.88(2)2x	
Re(1)-O(4)	1.64(2)1x	
Re(1)-O(1)	1.88(8)2x	<d(Re(1)-O>=1.86 Å
Re(1)-O(2)	1.95(5)2x	

Space group	$Fm\bar{3}m$
a (Å)	8.0847(1)
Cell volume (Å ^{3})	528.43(1)
Z	4
Calculated density (g/cm^3)	7.305
Radiation	Co Kα_1
2θ range, time/step	5-110^o, 90 s
No. of reflections	25
Refined parameters	21
Reliability factors	R_I=0.022, R_P=0.045, R_{WP}=0.059

Table 19: Measurements and refinements parameters for Ba_2MgReO_6.

Atom	x/a	y/b	z/c	B, Å ^{2}
Ba	0.25	0.25	0.25	1.99(4)
Mg	0.5	0.5	0.5	0.7(2)
Re	0)	0	0	1.78(3)
O	0.2425(5)	0	0	1.9(1)

Table 20: Positional and thermal parameters for Ba_2MgReO_6.

Ba - O	2.859×12	Re - O	1.961(4)×6
Mg - O	2.082(4)×6		

Table 21 Characteristic interatomic distances (Å) for Ba_2MgReO_6.

Space group	*I*4/*m*
a (Å)	5.57129(3)
c (Å)	7.92387(8)
Cell volume (Å ^{3})	245.952(3)
Z	2
Calculated density (g/cm^3)	6.505
Radiation	Co Kα_1
2θ range, time/step	5-110^o, 90 s
No. of reflections	74
Refined parameters	23
Reliability factors	R_I=0.023, R_P=0.059, R_{WP}=0.078

Table 22: Measurements and refinements parameters for Sr_2MgReO_6.

Atom	x/a	y/b	z/c	B, Å ^{2}
Sr	0	0.5	0.25	0.95(2)
Mg	0	0	0.5	0.3(2)
Re	0	0	0	0.55(1)
O(1)	0	0	0.2465(9)	2.0(1)
O(2)	0.246(4)	0.248(4)	0	2.0(1)

Table 23: Positional and thermal parameters for Sr_2MgReO_6.

Sr - O(1)	2.786×4	Mg - O(1)	2.009(7)×2
Sr - O(2)	2.79(2)×4	Mg - O(2)	1.99(2)×4
	2.80(2)×4	Re - O(1)	1.953(7)×2
		Re - O(2)	1.85(2)×4

Table 24: Characteristic interatomic distances (Å) for Sr_2MgReO_6.

Space group	$P2_1/n$
a (Å)	5.41320(6)
b (Å)	5.54174(6)
c (Å)	7.70415(8)
β, deg.	90.070(2)
Cell volume ($Å^3$)	231.113(4)
Z	2
Calculated density (g/cm^3)	5.556
Radiation	Co $K\alpha_1$
2θ range, time/step	5-110°, 90 s
No. of reflections	179
Refined parameters	35
Reliability factors	R_I=0.032, R_P=0.052, R_{wP}=0.071

Table 25: Measurements and refinements parameters for Ca_2MgReO_6.

Atom	x/a	y/b	z/c	B, Å ^{2}
Ca(1)	0.503(1)	0.5452(5)	0.7488(3)	0.5
Mg(1)	0.503(1)	0.5452(5)	0.57488(3)	0.5
Ca(2)	0.5	0	0.5	0.5
Mg(2)	0.5	0	0.5	0.5
Re	0.5	0	0	0.53(2)
O(1)	0.216(1)	0.194(1)	0.048(1)	0.4(1)
O(2)	0.305(1)	0.715(1)	0.043(2)	0.4(1)
O(3)	0.413(1)	0.970(2)	0.756(1)	0.4(1)

Table 26: Positional and thermal parameters for Ca_2MgReO_6.

Ca, Mg(1) - O(1)	2.341(8)×1	Ca, Mg(1) - O(3)	2.290(8)×1
	2.618(8)×1		2.41(1)×1
	2.704(8)×1	Ca, Mg(2) - O(1)	2.093(6)×2
Ca, Mg(1) - O(2)	2.39(1)×1	Ca, Mg(2) - O(2)	2.063(6)×2
	2.64(1)×1	Ca, Mg(2) - O(3)	2.035(8)×2
	2.67(1)×1	Re - O(1)	1.912(6)×2
		Re - O(2)	1.928(6)×2
		Re - O(3)	1.945(8)×2

Table 27: Characteristic interatomic distances (Å) for Ca_2MgReO_6.

7 References

1 Krebs B., Mueller A., Beyer H.H., "The Crystal Structure of Rhenium (VII) Oxide", Inorg. Chem., 8, 436-443 (1969).

2 Besse J.P., Baud G., Chevalier R., Zarembowitch J., "Mise en Evidence de l'Ion O_2^- dans l'Apatite au Rhenium $Ba_5(ReO_5)_3O_2$", Mat.Res.Bull., v. 15, 1255-1261 (1980).

3 Vielhaber E., Hoppe R., "Über Perrhenate. 3: Zum Aufbau des Mesoperrhenates Na_3ReO_5", Z.anorg.allg.Chem., 610, 7-14 (1992).

4 Meisel K., "Rheniumtrioxyd III. Mitteilung: Über die Kristallstruktur des Rheniumtrioxyds", Z.anorg.allg.Chem., 207, 121-128 (1932).

5 Abakumov A.M., Shpanchenko R.V., Antipov E.V., Lebedev O.I. and Van Tendeloo G., "The Crystal Structure of Ca_3ReO_6", J.Solid State Chem., 131, 305-309 (1997).

6 Cheetham A.K., Thomas D.M., "An Investigation of the Low Oxidation State Chemistry of Rhenium in the BaO-Re-Re_2O_7 Phase Diagram", J.Solid State Chem., 71, 61-69 (1987).

7 Sleight A.W., Bither T.A., Bierstedt P.E., "", Solid State Comm., 7, 299- (1969).

8 Ferreti A., Rogers D.B., Goodenough J.B., "The Relation of the Electrical Conductivity in Single Crystals of Rhenium Trioxide to the Conductivities of Sr_2MgReO_6 and Na_xWO_3", J. Phys. Chem. Solids, 26, 2007-2011 (1965).

9 Allen Ph.B., Schulz W.W., "Bloch-Boltzmann analysis of electrical transport in intermetallic compounds: ReO_3, $BaPbO_3$, $CoSi_2$ and Pd_2Si", Phys. Rev. B., 47, 1434-1439 (1993).

10 Swanson H.E., Fuyar R.K., "Standard X-ray Diffraction Powder Patterns", National Bureau of Standards (U.S.), Circular 359, 1-65 (1953).

11. Cotton F.A. and Harris C.B., "The Crystal and Molecular Structure of Dipotassium Octachlorodirhenate(III) Dihydrate, $K_2[Re_2Cl_8]\times 2H_2O$", Inorg. Chem., 4, 330-333 (1965).

12. Waltersson K., "The Crystal Structure of $La_4[Re_2]O_{10}$, a Fluorite-Related Structure Containing Rhenium Doublets"Acta Cryst., B32, 1485-1489 (1976).

13. Wentzel I., Fuess H., Bats J.W., Cheetham A.K., "Preparation and Crystal Structure of $PbRe_2O_6$, An Example of the Re_2O_{10} Unit with No Metal-Metal Bonding" Z. anorg. allg. Chem., 528, 48-50 (1985).

14. Wltschek G., Paulus H., Ehrenberg H., Fuess H., "Crystal structure and Magnetic Properties of Sm_2ReO_5", J.Solid State Chem., 132, 196-201 (1997).

15. Besse J.P., Baud G., Chevalier R., Gasperin M., "Structure Cristalline d'Oxydes Doubles de Rhénium. II. L'Oxide de Lanthane-Rhénium $La_6Re_4O_{18}$" Acta Cryst., B34, 3532-3535 (1978).

16. Torardi C.C., Sleight A.W, "Preparation and Crystal Structure of $La_3Re_2O_{10}$: An Example of Metal-Metal Bonding within Re_2O_{10} Units" J. Less-Comm. Met., 116, 293-299 (1985).

17. Wilhelmi K.A., Lagervall E., Muller O., "On the Crystal Structure of $Nd_4Re_2O_{11}$", Acta Chem. Scand., 24, 3406-3408 (1970).

18. Ehrenberg H., Hartmann T., Wltschek G., Fuess H., Morgenroth W., Krane H.-G., "The crystal structure of $Tm_5Re_2O_{12}$", Acta Cryst., B55, 849-852 (1999).

19. Baur W.H., Joswig W., Pieper G., Kassner D., "$CoReO_4$, a New Rutile-Type Derivative with Ordering of Two Cations", J.Solid State Chem., 99, 207-211 (1992).

20. Rae-Smith A.R. and Cheetham A.K., "The Preparation and Crystal Structures of $BiReO_4$ and $BiRe_2O_6$", J.Solid State Chem., 30, 345-352 (1979).

21. Watanabe H., Imoto H., Tanaka H., "Preparation, Crystal Structure, and Electrical Resistivity of $SbRe_2O_6$ with Re-Re bond", J.Solid State Chem., 138, 245-249 (1998).

22. Magnèlli A., "Studies of Rhenium Oxides", Acta Chem. Scand., 11, 28-33 (1957).

23. Longo J.M., Sleight A.W., "Characterization and Structure of $La_4Re_6O_{19}$, a new Metal Cluster Compound", Inorg. Chem., 7, 108-111 (1968).

24. Baud G., Besse J.P., Chevalier R., Chamberland B.L., "Structure d'un Oxyde Double de Rhenium a Charpente de Type $KSbO_3$ Cubique: Sr_xReO_3 ($0.4<x<0.5$)", J.Solid State Chem., 28, 157-162 (1979).

25. Abakumov A.M., Shpanchenko R.V., Antipov E.V., "Synthesis and Structure of the Double Oxide $Pb_6Re_6O_{19}$", Z.anorg.allg.Chem., 624, 750-753 (1998).

26. Abakumov A.M., Shpanchenko R.V., Antipov E.V., Kopnin E.M., Capponi J.J., Marezio M., Lebedev O.I., Van Tendeloo G., Amelinckx S., "Synthesis and Structural Study of $Pb_2Re_2O_{7-x}$ Pyrochlores", J.Solid State Chem., 138, 220-225 (1998).

27 Brusset et al., C. R. Seances Acad. Sci., Ser. C, 275, p. 327 (1972).

28. Donohue P.C., Longo J.M., Rosenstein R.D., Katz L., "The Preparation and Structure of Cadmium Rhenium Oxide, $Cd_2Re_2O_7$", Inorg. Chem., 4, 1152-1153 (1965).

29. Wltschek G., Paulus H., Svoboda I., Ehrenberg H., Fuess H., "Crystal Structure and Magnetic Properties of Sm_3ReO_7", J.Solid State Chem., 125, 1-4 (1996).

30. Hartmann T., Ehrenberg H., Miehe G., Wltschek G., Fuess H., "Preparation and Characterization of Rare Earth Rhenium Oxides Ln_6ReO_{12}, *Ln*=Ho, Er, Tm, Yb, Lu", J.Solid State Chem., 148, 220-223 (1999).

31. Besse J.P., Baud G., Chevalier R., Joubert J.C., "Synthese sous Haute Pression et Structure d'un nouveau Pyrochlore Contenant du Rhenium: $Ca_{1+x}Re_2O_6(OH)_{2x}$ (x = 0.3)", Mat.Res.Bull., 13, 217-220 (1978).

32. Calvo C., Ng H.N., and Chamberland B.L., "Preparation and Structure of a Ternary Oxide of Barium and Rhenium, $Ba_3Re_{2-x}O_9$", Inorg. Chem., 17, 699-701 (1978).

33. Kovba L.M., Lykova L.N., Balashov V.L., Kharlanov A.L., "Crystal Structure of Ba_2WO_5", Koordinatsionnaya Khimiya, 11, 1426-1429 (1985).

34. Mons H.A., Schriewer M.S., Jeitschko W., "The Crystal Structures of the Isotypic Perrhenates $Ca_5Re_2O_{12}$ and $Sr_5Re_2O_{12}$", J. Solid State Chem., 99, 149-157 (1992).

35. Jeitschko W., Mons H.A., Rodewald U.Ch., Möller M.H., "The Crystal Structure of the Potential Ferroelectric Calcium Rhenate (VI, VII) $Ca_{11}Re_4O_{24}$ and its Relation to the Structure of $Sr_{11}Os_4O_{24}$", Z.Naturforsch., 53b, 31-36 (1998).

36 Picard J.P., Besse J.P., Chevalier R., Gasperin M., "Structure cristalline de $Ca(ReO_4)_2 \times 2H_2O$", J.Solid State Chem., 69, 380-384 (1987).

37. Sleight A.W., Longo J., and Ward R., "Compounds of Osmium and Rhenium with the Ordered Perovskite Structure", Inorg. Chem., 1, 245-250 (1962).

38. Chamberland B.L., Levasseur G., “Rhenium Oxides having an Ordered or Related Perovskite-Type Structure”, Mat.Res.Bull., 14, 401-407 (1979).

39. Anderson M.T., Greenwood K.B., Taylor G.A., and Poppelmeier K.R., “*B*-Cation Arrangements in Double Perovskites”, Prog. Solid State Chem., 22, 197-233 (1993).

40. Woodward P.M., “Octahedral Tilting in Perovskites. I.”, Acta Cryst., B53, 32-45 (1997).

41. Randall C.A., Bhalla A.S., Shrout T.R., Cross L.E., “Classification and consequences of complex lead perovskite ferroelectrics with regard to B-site cation order”, J. Mater. Res., 5, 829-834 (1990).

42. Glazer A.M., “The Classification of Tilted Octahedra in Perovskites”, Acta Cryst., B 28, 3384-3392 (1972).

43. Bramnik K.G., Abakumov A.M., Shpanchenko R.V., Antipov E.V., Van Tendeloo G., “Synthesis and Structure of $Ln_4Re_{6-x}O_{19}$ (Ln=Ce, Pr, Nd) Complex Oxides”, J.Alloys and Comp., 278, 98-102 (1998).

44. Jeitschko W., Heumannskämper D.H., Schriewer-Pöttgen M.S., Rodewald U.Ch., “Preparation, Crystal Structures, and Properties of Rhenates with Multiple Re-Re Bonds: Ln_2ReO_5 (*Ln* = Sm, Eu, Gd), $Ln_3Re_2O_9$ (*Ln* = Pr, Nd, Sm), and $Ln_4Re_6O_{19}$ (*Ln* = La-Nd)”, J. Solid State Chem., 147, 218-228 (1999).

45. Jeitschko W., Heumannskämper D.H., Rodewald U.Ch., Schriewer-Pöttgen M.S., “Preparation and Crystal Structure of Rare Earth Rhenates: the Series $Ln_5Re_2O_{12}$ with *Ln* = Y, Gd-Lu, and the Praseodymium Rhenates Pr_3ReO_8, $Pr_3Re_2O_{10}$, and $Pr_4Re_2O_{11}$”, Z.anorg.allg.Chem., 626, 80-88 (2000).

46. Tsuda N., Nasu K., Yanase A., and Siratori K., “Electronic Conduction in Oxides”, Sects. 2.9.3 and 4.7, Springer, Berlin (1991).

47 Abragam A., and Bleaney B., “Electron paramagnetic resonance of transition ions”, Chap. 7. Oxford Univ. Press, Oxford (1970).

48. Chamberland B.L., Hubbard F.C., “The Characterization of $Ba_3Re_2O_9$ and $Sr_3Re_2O_9$”, J. Solid State Chem., 26, 79-82 (1978).

49. Mackintosh A.R., “”, J. Phys. Chem., 38, 1991- (1963).

50. Sienko M.J., Paper 21 in Nonstoichiometric Compounds, Ward R., ed., Advances in Chemistry Series 39, Am. Chem. Soc., Washington, D.C. (1963).

51. Goodenough J.B., The Oxy-Compounds of the Transition Elements in the Solid State, International Colloqium of the Centre de la Recherche Scientifique, Bordeaux, France (1964). Bull. Soc. Chim. Fr., 4, p. 1200 (1965).

52. Bieringer M., Greedan J.E., Luke G.M., "Li_4MgReO_6: An $S = 1/2$ antiferromagnet exhibiting spin-glass behavior", Phys. Rev. B., 62, 6521-6529 (2000).

53. Akselrud L.G., Grin Yu.N., Zavalij P.Yu., Pecharsky V.K., and Fundamentsky V.S., Thes. report on 12-th ECM, p. 155, Moscow (1989).

54. Izumi F., in *"The Rietveld method"* (R.A. Young, Ed.), Chap. 13. Oxford Univ. Press, Oxford (1993).

55 Aksenov V.L., Balagurov A.M., Simkin V.G. Bulkin A.P., Kudryashev V.A., Trounov V.A., Antson O., Hiismäki P. and Tiita A., "Performance of the High Resolution Fourier Diffractometer at the IBR-2 Pulsed Reactor", J. Neutron Research, 5, 181-200 (1997).

56 Colwel J.F., Miller P.H., and Wittemore W.L., Neutron Inelastic Scattering, Conf. Proc., p. 429, Vienna, IAEA (1968).

57 Miehe G., Thes. report on 3-rd DGK, p. 51, Darmstadt (1995).

58. Kessler V.G., Shevelkov A.V., Khvorykh G.V., Seisenbaeva G.A., Turova N.Ja., Drobot D.V., Russ. J. Inorg. Chem., 40, 1477- (1995).

59. Ellingham H.J.T., "Reducibility of Oxides and Sulphides in Metallurgical Processes", J. Soc. Chem. Ind., 63, 125-133 (1944).

60 Shevchenko N., *et. al.,* Russ. J. Inorg. Chem., 19, 528- (1974).

61 Aranda M.A.G., Attfield J.P., "Strukturbestimmung von "$BaCuO_2$" durch kombinierte Röntgen- und Neutronenbeugungsuntersuchungen an Pulvern", Angewandte Chemie, 105, 1511-1513 (1993).

62 Jeitschko W., Mons H.A., Rodewald U.Ch., "Preparation and Crystal Structure of the Calcium Rhenate (VI, VII) $Ca_5Re_3O_{15-x}$", Z. Naturforsch., 54b, 1483-1488 (1999).

63 Bramnik K.G., Miehe G., Ehrenberg H., Fuess H., Abakumov A.M. and Shpanchenko R.V., Pomjakushin V.Yu., Balagurov A.M., "Preparation, Structure, and Magnetic Studies of a New $Sr_{11}Re_4O_{24}$ Double Oxide", J. Solid State Chem., 149, 49-55 (2000).

64 Shannon R.D. and Prewitt C.T., "Effective Ionic Radii in Oxides and Fluorides", Acta Crystallogr., B25, 925-931 (1969).

65 Tomaszewka H., Müller-Buschbaum H.K., "Ein neues gemischtvalentes Oxoosmat (VI, VII): $Sr_{11}Os^{6+}{}_2Os^{7+}{}_2O_{24}$", Z.anorg.allg.Chem., 619, 1738-1742 (1993).

66 Lang C., Müller-Buschbaum H.K., "Über ein neues Oxoiridat (IV): $Ba_7Ir_6O_{19}$", Monatshefte fuer Chemie, 120, 705-710 (1989).

67 Bramnik K.G., Ehrenberg H., Fuess H., "Preparation, Crystal Structure, and Magnetic Studies of a New $Sr_7Re_4O_{19}$ Double Oxide and its Relation to the Structure of $Ba_7Ir_6O_{19}$", J. Solid State Chem., 160, (2001).

68 Dollase W.A., "Correction of Intensities for Preferred Orientation in Powder Diffractometry: Application of the March Model", J. Appl. Crystallogr., 19, 267-272 (1986).

69 Donohue P.C., Katz L., and Ward R., "The Crystal Structure of Barium Ruthenium Oxide and Related Compounds", Inorg. Chem., 4, 306-310 (1965).

70 Thornton G., Jacobson, A.J., "A Neutron Diffraction Determination of the Structures of $Ba_2Sb^{V}Bi^{III}O_6$ and $Ba_2Bi^{V}Bi^{III}O_6$", Acta Crystallogr., B34, 351-354 (1978).

71 Schriewer M.S., Jeitschko W., "Preparation and Crystal Structure of the Isotypic Orthorhombic Strontium Perrhenate Halides $Sr_5(ReO_5)_3X$ (X = Cl, Br, I) and Structure Refinement of the Related Hexagonal Apatite-like Compound $Ba_5(ReO_5)_3Cl$", J. Solid State Chem., 107, 1-11 (1993).

72 Marezio M., Remeika J.P., Dernier P.D., "The Crystal Chemistry of the Rare Earth Orthoferrites", Acta Crystallogr., 26, 2008-2022 (1970).

Die vorliegende Arbeit wurde im Fachbereich Material- und Geowissenschaften, Fachgebiet Strukturforschung der Technischen Universität Darmstadt, auf Anregung und unter Anleitung von Herrn Prof. Dr. H. Fuess in der Zeit von Mai 1997 bis April 2001 durchgeführt.

Herrn Prof. Dr. H. Fuess möchte ich für die interessante Themenstellung, sein Interesse am Fortgang der Arbeit, seine großzügige Unterstützung und Förderung sowie seine Diskussionsbereitschaft danken.

Herrn Dr. H. Ehrenberg danke ich für seine kollegiale und uneingeschränkte Unterstützung, seine Hilfe bei der Auswertung der Magnetisierungsmessungen, seine stete Diskussions- und Hilfsbereitschaft und konstruktive Kritik.

Herrn Dr. G. Miehe und Herrn Dipl.-Ing. J.K. Dehn danke ich für ihre Hilfe bei den durchgeführten TEM Untersuchungen.

Herrn Prof. Dr. E.V. Antipov, Herrn Dr. R.V. Shpanchenko und Herrn Dr. A.M. Abakumov danke ich für konstruktive Kritik und anregende Diskussionen, für ihre ständige Bereitschaft zur Zusammenarbeit bei kniffligen Problemen.

Herrn Dipl.-Ing. R. Theissmann möchte ich für seine ständige Hilfsbereitschaft bei den SQUID Messungen danken.

Herrn Dipl.-Ing. Th. Hartmann, Herrn J.-C. Jaud, Herrn Dipl.-Ing. H. Mohren für ihre Unterstützung und Hilfe bei den verschieden technischen Problemen danken.

Nicht zuletzt sei allen Kollegen, den Mitarbeitern des Institutes, insbesondere den Mitarbeitern des Arbeitskreises Strukturforschung, und all denen gedankt, die zum Gelingen der Arbeit beigetragen haben.

Schließlich danke ich dem Bundesministerium für Bildung und Forschung für die Förderung dieser Arbeit.

Veröffentlichungen

"Synthesis and Structure of $Ln_4Re_{6-x}O_{19}$ (Ln=Ce, Pr, Nd) Complex Oxides", Bramnik K.G., Abakumov A.M., Shpanchenko R.V., Antipov E.V., Van Tendeloo G., J.Alloys and Comp., 278, 98-102 (1998).

"Preparation, Structure, and Magnetic Studies of a New $Sr_{11}Re_4O_{24}$ Double Oxide", Bramnik K.G., Miehe G., Ehrenberg H., Fuess H., Abakumov A.M. and Shpanchenko R.V., Pomjakushin V.Yu., Balagurov A.M., J. Solid State Chem., 149, 49-55 (2000).

"Preparation, Crystal Structure, and Magnetic Studies of a New $Sr_7Re_4O_{19}$ Double Oxide and its Relation to the Structure of $Ba_7Ir_6O_{19}$", Bramnik K.G., Ehrenberg H., Fuess H., J. Solid State Chem., 160, 45-49 (2001).

"Synthesis and crystal structure of the lithium perrhenate monohydrate $LiReO_4 \cdot H_2O$", Abakumov A.M., Rozova M.G., Shpanchenko R.V., Mironov A.V., Antipov E.V., Bramnik K.G., Solid State Sciences, 3, 581-586 (2001).

Tagungsbeiträge

"Structural investigations in the *M*-Re-O system (*M* = Ca, Sr, Ba)", K.G. Bramnik, G. Miehe, R.V. Shpanchenko, H. Fuess, MSU-HTSC-V in Moskau vom 26. bis 31. März 1998

"Preparation, structure investigations and magnetic properties of $M_{11}Re_4O_{24}$ (*M* = Sr, Ba)", K.G. Bramnik, H. Ehrenberg, H. Fuess, A.M. Abakumov and R.V. Shpanchenko, Materialien der 7.Jahrestagung der Deutschen Gesellschaft für Kritallographie (DGK) in Leipzig vom 8. bis 10. März 1999, S.26.

"Preparation, structure investigations and magnetic properties of Sr_3ReO_6", K.G. Bramnik, A.M. Abakumov, H. Fuess, ECM 19 in Nancy vom 24. bis 31. August 2000

"Preparation, structure investigations and magnetic properties of $Sr_7Re_4O_{19}$", K.G. Bramnik, H. Ehrenberg, H. Fuess, Materials Discussion 3 (Inorganic Solids - Properties and Possibilities) in Cambridge 26-29 September 2000

"Synthesis, structure characterization and magnetic properties of $Sr_{11}Re_4O_{24}$; Structure investigation of rhenium dioxide by neutron powder diffraction at ambient and high pressure." K.G. Bramnik, H. Fuess, Second Russian-German User Meeting in Dubna, 21-25 April 2001

Lebenslauf

Zur Person

Name:	Kirill Grigor'jewitsch Bramnik
Adresse:	Noackstr. 15/013 64285 Darmstadt
Geburtsdatum:	08.09.1974
Geburtsort:	Monino, Moskauer Gebiet

Ausbildung

1981-1983	Schule №1 der Stadt Archangel'sk.
1983-1991	Schule №23 der Stadt Archangel'sk.
9/1991-7/1996	Studium der Chemie an der Staatlichen Universität Moskau; Diplomarbeit: "Synthese und Untersuchung ternärer Oxide des Rheniums mit Seltenen Erden" unter Leitung von Herrn Dr. R.V. Shpanchenko.
5/1997-4/2001	Wissenschaftlicher Mitarbeiter im Fachgebiet Strukturforschung.

Eidesstattliche Erklärung

Hiermit erkläre an Eides Statt, dass ich meine Dissertation selbständig und nur mit den angegebenen Hilfsmitteln angefertigt habe und noch keinen Promotionsversuch unternommen habe.

Darmstadt, den 09.05.2001